Office of Naval Research

Contract Nonr-1866 (10) NR-371-[illegible]

ARPA Contract No. 4-66

THE PREPARATION OF THIN FILMS FOR USE IN OPTICAL MEASUREMENTS IN THE VISIBLE AND ULTRAVIOLET

by

Charles E. Moss

October 1968

Technical Report No. HP-18

Technical Report No. ARPA-29

Division of Engineering and Applied Physics

Harvard University • Cambridge, Massachusetts

Office of Naval Research

Contract Nonr-1866(10) NR-017-308

ARPA Contract SD-88

THE PREPARATION OF NiO THIN FILMS FOR USE IN OPTICAL MEASUREMENTS IN THE VISIBLE AND ULTRAVIOLET.

by

Charles E. Rossi

October, 1968.

Technical Report No. HP-18

Technical Report No. ARPA-29

The research reported in this document was made possible through support extended the Division of Engineering and Applied Physics, Harvard University, by the Office of Naval Research, under Contract Nonr-1866(10), and by the Advanced Research Projects Agency under Contract ARPA SD-88.

Division of Engineering and Applied Physics

Harvard University Cambridge, Massachusetts

BLANK PAGE

TABLE OF CONTENTS

TABLE OF CONTENTS	i
LIST OF FIGURES	iii
LIST OF TABLES	ix
ABSTRACT	xi
Chapter One. INTRODUCTION	1-1
A. INCENTIVE FOR NiO FILM RESEARCH	1-1
B. PROPERTIES OF NiO	1-2
1. Magnetic Properties	1-2
2. Transport Properties	1-5
3. Optical Properties	1-20
BIBLIOGRAPHY	1-35
Chapter Two. PREPARATION OF FILMS	2-1
A. EVAPORATION IN A HIGH VACUUM	2-2
B. CHEMICAL TRANSPORT	2-4
C. FLASH EVAPORATION	2-12
D. ELECTRON BEAM EVAPORATION	2-14
E. SPUTTERING	2-18
F. OXIDATION OF NICKEL FILMS	2-21
G. CONCLUSION	2-22
BIBLIOGRAPHY	2-37
Chapter Three. OPTICAL RESULTS	3-1
A. DESCRIPTION OF EQUIPMENT	3-1
B. TRANSMISSION RESULTS	3-3
C. LOW TEMPERATURE MEASUREMENTS	3-16
D. REFLECTIVITY MEASUREMENTS	3-18

E. CONCLUSION 3-22

BIBLIOGRAPHY 3-67

Chapter Four. CONCLUDING STATEMENTS AND SUGGESTED FURTHER WORK ON NiO 4-1

APPENDIX. KRAMERS KRONIG PROGRAM A-1

A. DESCRIPTION OF THE PROGRAM A-1

B. INSTRUCTIONS FOR PREPARATION OF INPUT TO THE KRAMERS KRONIG ANALYSIS PROGRAM A-3

ACKNOWLEDGEMENTS

LIST OF FIGURES

Fig. 1-1 Resistivity, Hall coefficient, and Hall mobility, in NiO (Ref. 36).

Fig. 1-2 Seebeck coefficient, drift and Hall mobility in NiO (Ref. 36).

Fig. 1-3 Absorption spectrum of NiO film as given in Ref. 51.

Fig. 1-4 Absorption spectrum of NiO at 300°K, 77°K. Dashed lines are interpolations, as given in Ref. 39.

Fig. 2-1 Schematic of evaporation equipment.

Fig. 2-2 Schematic of chemical transport apparatus.

Fig. 2-3 Electron diffraction pattern of a NiO film grown by vapor deposition on a MgO substrate.

Fig. 2-4 Electron diffraction pattern of a film grown on LiF by flash evaporating NiO powder in a vacuum of $5 \cdot 10^{-6}$ mm Hg. The evaporation time was twenty-two minutes.

Fig. 2-5 Electron diffraction pattern of a film grown on LiF by flash evaporating NiO powder in an O_2 atmosphere of $2 \cdot 10^{-4}$mm Hg. The evaporation time was forty minutes.

Fig. 2-6 Schematic of electron beam evaporation equipment.

Fig. 2-7 Electron diffraction pattern of a film grown on CaF_2 by electron beam evaporation of Ni in an O_2 atmosphere of $1 \cdot 10^{-4}$mm Hg. The evaporation time was eighteen minutes.

Fig. 2-8 Schematic of sputtering equipment.

Fig. 2-9 Electron diffraction pattern of a film grown on LiF by sputtering Ni in a 20% O_2, 80% A atmosphere of .9 microns. The sputtering time was twenty minutes.

Fig. 2-10 Electron diffraction pattern of a film grown on LiF by sputtering Ni in a 20% O_2, 80% A atmosphere of .9 microns. The sputtering time was forty-five minutes.

Fig. 2-11 Electron diffraction pattern of a film grown on CaF_2 by sputtering Ni in a 20% O_2, 80% A atmosphere of .9 microns. The sputtering time was forty-five minutes.

Fig. 2-12 Electron diffraction pattern of a Ni film grown on LiF by flash evaporating Ni powder in a vacuum. The evaporation time was twenty minutes.

Fig. 3-1 Optical system used with the McPherson model 225 vacuum ultraviolet spectrometer.

Fig. 3-2 Vacuum ultraviolet lamp.

Fig. 3-3 Schematic of electronics used with the vacuum ultraviolet spectrometer.

Fig. 3-4 Transmission spectra of various substrate materials.

Fig. 3-5 Transmission spectrum of NiO film grown by vapor deposition on a MgO substrate.

Fig. 3-6 Transmission spectrum of a NiO film grown by vapor deposition on a MgO substrate.

Fig. 3-7 Transmission spectrum of a film grown on LiF by flash evaporating NiO powder in an 0_2 atmosphere of $2 \cdot 10^{-4}$mm Hg.

Fig. 3-8 Transmission spectrum of a LiF substrate after being exposed to a tungsten boat heated to 1850°C for one hour in 0_2 at $2 \cdot 10^{-4}$mm Hg.

Fig. 3-9 Transmission spectra of several films grown on LiF by flash evaporating Ni powder in a vacuum of $\sim 3 \cdot 10^{-6}$mm Hg.

Fig. 3-9A Absorption coefficient and reflectivity of Ni from Ref. 4.

Fig. 3-10 Transmission spectrum of a film grown on LiF by flash evaporating NiO powder in a vacuum of $3 \cdot 10^{-6}$mm Hg.

Fig. 3-11 Transmission spectra of Samples 1 through 3 of Fig. 3-9 after oxidation. Sample 1 was oxidized for two hours at 550°C in 0_2 at $2 \cdot 10^{-4}$mm Hg and Samples 2 and 3 were oxidized for three hours at 300°C in 0_2 at room pressure.

Fig. 3-12 Transmission spectra showing color center absorption encountered with LiF substrates when using electron beam evaporation.

Fig. 3-13 Transmission spectra of two films grown on CaF_2 by electron beam evaporation of Ni in an 0_2 atmosphere of $1 \cdot 10^{-4}$mm Hg.

Fig. 3-14 Transmission measurements made between successive evaporations onto the same CaF_2 substrate. The evaporations were made using the electron beam to evaporate Ni in an 0_2 atmosphere of $1 \cdot 10^{-4}$mm Hg.

Fig. 3-15 Comparison of transmission spectra of a film grown on MgO by vapor deposition with that of the thickest film of Fig. 3-14.

Fig. 3-16 Transmission spectrum of the NiO edge of the thickest film in Fig. 3-14 plotted on an expanded energy scale.

Fig. 3-17 Transmission spectra of two films grown on glass microscope slides by electron beam evaporation of Ni in an O_2 atmosphere of $1 \cdot 10^{-4}$mm Hg.

Fig. 3-18 The upper curve shows the transmission of a CaF_2 substrate which was heated to 550°C.while the electron beam gun was turned on the Ni source at a low intensity. The lower curve shows the transmission of the same CaF_2 after annealing in O_2 at $1 \cdot 10^{-4}$mm Hg for fifteen minutes.

Fig. 3-19 Transmission spectrum of a film grown on CaF_2 by electron beam evaporation of Ni in a vacuum of $3 \cdot 10^{-6}$mm Hg.

Fig. 3-20 Transmission spectrum of a film grown on glass by electron beam evaporation of Ni in a vacuum of $3 \cdot 10^{-6}$mm Hg.

Fig. 3-21 Transmission spectrum of a film grown on quartz by electron beam evaporation of Ni in an O_2 atmosphere of $1 \cdot 10^{-4}$ mm Hg.

Fig. 3-22 Transmission spectrum of a film grown on BaF_2 by electron beam evaporation of Ni in an O_2 atmosphere of $1 \cdot 10^{-4}$mm Hg.

Fig. 3-23 Transmission spectrum of a film grown on CaF_2 by sputtering of Ni in a 20% O_2, 80% A atmosphere.

Fig. 3-24 Transmission spectrum of a film grown on LiF by sputtering of Ni in a 20% O_2, 80% A atmosphere.

Fig. 3-25 Transmission spectrum of a film grown on quartz by sputtering of Ni in a 20% O_2, 80% A atmosphere.

Fig. 3-26 Transmission spectrum of a film grown on CaF by sputtering of Ni in a 20% O_2, 80% A atmosphere.

Fig. 3-27 Transmission spectrum of a film grown on quartz by sputtering Ni in a 10% O_2, 90% A atmosphere.

Fig. 3-28 Transmission spectrum of a film grown on quartz by sputtering Ni in a 10% O_2, 90% A atmosphere.

Fig. 3-29 Transmission spectrum of a film grown on LiF by sputtering Ni in a 20% O_2, 80% A atmosphere.

Fig. 3-30 Transmission spectrum of a film grown on LiF by sputtering Ni in a 20% O_2, 80% A atmosphere.

Fig. 3-31 Transmission spectrum of a LiF substrate placed in the sputtering unit plasma and held at 550°C for one hour with the target voltage at zero.

Fig. 3-32 Temperature shift of absorption edge of NiO film grown on quartz by sputtering Ni in a 10% O_2, 90% A atmosphere.

Fig. 3-33 Temperature shift of absorption edge of NiO film grown on CaF_2 by electron beam evaporation of Ni in an O_2 atmosphere of $1 \cdot 10^{-4}$mm Hg.

Fig. 3-34 A second measurement of the temperature shift of the film of Figs. 3-14 and 3-33 including a check for hysteresis.

Fig. 3-35 Temperature shifts of the films in Figs. 3-32 and 3-33 shown on an expanded scale.

Fig. 3-36 Reflectivity spectra of three films of NiO grown on MgO substrates by vapor deposition. The measurements were taken with the Jarrell Ash equipment (Ref. 1).

Fig. 3-37 Reflectivity spectrum of a NiO film grown on a MgO substrate by vapor deposition. The measurements were made with the McPherson model 225 vacuum ultraviolet spectrometer (Fig. 3-1).

Fig. 3-38 Reflectivity spectra of bulk NiO. The upper curve shows the reflectivity of a polished sample and the lower curve the reflectivity of a polished and etched sample. The measurements were made with the McPherson model 225 vacuum ultraviolet spectrometer. (Fig. 3-1)

Fig. 3-39 Reflectivity spectrum of bulk NiO over the wavelength range of 1250 to 6000 A. The sample is the same as that of Fig. 3-38 and the surface is the polished and etched surface of Fig. 3-38. The measurements were made with the McPherson model 225 vacuum ultraviolet spectrometer (Fig. 3-1). Different filters were used in different wavelength regions with overlap between the regions. A separate symbol has been used in the figure to designate data obtained with each filter.

Fig. 3-40 Reflectivity data used in the Kramers Kronig analysis of Figs. 3-41 and 3-42. The bulk data is that obtained by drawing a reasonably smooth curve through the values plotted in Fig. 3-39. All gaps in data were filled in by extrapolation to provide values for the computer program used in the analysis. The film data shown between 1800 and 2500 A was obtained by adjusting the values of Fig. 3-37 to agree with the bulk values at $\sim$1800 and $\sim$2500 A.

Fig. 3-41 The absorption constant obtained by a Kramers Kronig analysis of the bulk NiO reflectivity data shown in Fig. 3-40. The absorption constant is shown for three extrapolation parameters, P = 2, 3 and 4 (see Appendix).

Fig. 3-42 The absorption constant obtained by a Kramers Kronig analysis of the bulk NiO reflectivity data modified to agree with NiO film results between 1800 and 2500 A. The data used are shown in Fig. 3-40. The absorption constant is shown for three extrapolation parameters, P = 2, 3, and 4 (see Appendix).

LIST OF TABLES

Table 1-1 Optical spectrum of NiO as given in Ref. 51.

Table 1-2 Optical spectrum of NiO at 300°K as given in Ref. 39.

Table 1-3 Spectrum of NiO as given in Ref. 56.

Table 2-1 Summary of lattice constant measurements.

ABSTRACT

In this report, several methods for producing nickel oxide films for use in optical experiments are discussed including an indication of the significant problems encountered with each method. Electron reflection diffraction measurements indicate that films grown by electron beam evaporation of nickel in an oxygen atmosphere and by reactive sputtering on CaF_2 and LiF have at least some degree of crystalline order. Transmission spectra between 2000 angstroms and 6000 angstroms are presented for films grown by both electron beam evaporation and reactive sputtering. The spectra appear to be consistent with one another as well as with the spectra of epitaxial NiO films grown on MgO by vapor deposition. The spectra are, however, at least in some cases, distorted by color centers introduced in the substrate during film deposition. Two films have been used to provide information on the shift of the NiO absorption edge with temperature, the results being $2.9 \cdot 10^{-4}$ eV/°C and $-4.2 \cdot 10^{-4}$ eV/°C respectively. A Kramers Kronig analysis of the reflectivity of bulk NiO has been made and shows that the absorption of the films is consistent with the absorption constant derived from the reflectivity data.

BLANK PAGE

Chapter One

INTRODUCTION

A. Incentive for NiO Film Research

Many recent papers have indicated that the optical properties of thin epitaxial films of semiconducting materials are the same as those of bulk samples. This allows the use of film transmission to study the optical properties in the region above the fundamental absorption edge where reliable information was previously available only from reflectivity measurements. A number of workers, for example, have reported the use of Ge, PbS, PbSe, PbTe, and Cd-HgTe films to obtain reliable optical data in the transparent and highly absorbing regions.[1-10]

The present work was initiated by the desire to extend the technique of epitaxial thin film growth to the transition metal oxides, NiO being the obvious first step. Since the ultimate goal was to investigate the optical behavior of the materials in the visible and ultraviolet at energies where they are quite absorbing, the deposited films had to be of a good optical quality and have optical properties as nearly as possible identical to the properties of the bulk material.

The experiments described in this report were performed to find a suitable method of preparing epitaxial NiO films of a good optical quality. Much of the work was directed towards determining the consistency of the optical properties of the films, the effects which the film fabrication procedure might have on the film optical properties, and at least a qualitative comparison of the film properties with bulk properties.

B. Properties of NiO

Many of the interesting properties of the transition metal oxides are at least in part due to the fact that the transition metals have only partly filled 3d atomic levels. This fact affects the magnetic, optical, and transport properties of the material. In the periodic system of the elements, the 3d level begins to fill after calcium in which the 4s level is filled as well as the levels up to and including 3p. The element nickel in addition to filled levels through 3p and a filled 4s level contains eight electrons in the 3d level.

Hund's rule[11,12] dictates that with Russell-Saunders coupling the angular momentum ℓ_i of the individual equivalent electrons in an atom or ion combine to form a resultant L, the individual equivalent electron spins s_i combine to form a resultant S, and S and L combine to form a resultant J to yield a ground state in which:

1) The multiplicity 2S+1 is the maximum allowed by the Pauli Principle

2) The resultant L is the maximum allowed by the Pauli Principle and a maximum 2S+1

3) $J = |L - S|$ when the atomic level is half filled and $J=L+S$ when the level is more than half filled.

For a free nickel atom or for a free Ni^{++} ion the ground state is $^3F_4$ (S=1, L=3, J=4).

1. Magnetic Properties

The magnetic moment of a free ion or atom is given by $g[J(J+1)]^{1/2}$ in Bohr magnetons where g is the Lande's g factor and depends on L, S, and J[11,12]. For Ni^{2+} this gives a value of 5.59. A typical experimental value for Ni^{2+} in a crystal is, however, considerably less -- the value

being $\sim$2.83.[12] In a crystal, rotational symmetry no longer exists since the field in which the ion is located has the symmetry of the crystal. The five degenerate 3d orbitals are no longer degenerate since depending upon the orientation of the orbits with respect to the charge distribution of adjacent ions some of the orbitals will have higher energies than others. For O_h symmetry, the five 3d orbitals are split into a doubly degenerate set and a triply degenerate set. The new energy levels are split by an energy conventionally designated as 10 Dq.[14] In NiO six electrons are in the lowest d levels and two are in the upper levels. The magnetic moment of the ion in the crystal is the value of the operator $\mu_B(L+2S)$ in the quantum state of the eight electrons as modified by the crystal field where μ_B is the Bohr magneton. Due to the effects of the crystal field on the orbital levels, the orbital levels contribute considerably less to the moment when the ion is in the crystal than when the ion is free.

The overall eigenstate of the system must be antisymmetric -- this gives the Pauli principle as a consequence and is the origin of the "effect" or "force" generally referred to as exchange. Following Reference 15 let ϕ_a and ϕ_b be two orthogonal space eigenfunctions of the one electron Hamiltonian from which one can construct symmetric and antisymmetric space functions for two electrons. For the antisymmetric space function the electron spins must be parallel and for the symmetric space function the spins must be antiparallel -- this yields overall antisymmetric states which satisfy the Pauli Principle. These space functions can be written as:

$$\Phi_s = \frac{1}{\sqrt{2}} \left(\phi_a(r_1)\, \phi_b(r_2) + \phi_a(r_2)\, \phi_b(r_1)\right), \text{ symmetric function}$$

and $$\Phi_a = \frac{1}{\sqrt{2}} \left(\phi_a(r_1)\, \phi_b(r_2) - \phi_a(r_2)\, \phi_b(r_1)\right), \text{ antisymmetric function}$$

The average of the Coulomb energy $\frac{e^2}{|r_1 - r_2|}$ will be different for these states by an amount

$$2 \iint \phi_a^*(r_1)\, \phi_b^*(r_2)\, \frac{e^2}{|r_1 - r_2|}\, \phi_a(r_2)\, \phi_b(r_1)\, dr_1\, dr_2$$

which is the exchange integral. This difference is frequently written as $2JS_1 \cdot S_2$ for the spins S_1 and S_2 being parallel and antiparallel, respectively. For two electrons on the same atom in an incomplete shell the exchange interaction is such that the spins line up to give the maximum total spin consistent with the number of states to be filled in the shell.[15] This is consistent with Hund's rule. For spins on different ions the exchange interaction is in general negative which favors antiparallel spins on neighboring ions.

In some cases magnetic ions in a crystal may be sufficiently separated that they are not linked by an exchange integral as discussed above. The mechanism of super-exchange may occur in these cases. Here the spins of the magnetic ions may be coupled to electrons in a non-magnetic intervening ion in such a way that the magnetic ion spins are for all practical purposes coupled.

The exchange interaction between spins on neighboring atoms is frequently treated by assuming a spin Hamiltonian written as

$$-\sum_{\ell\, \ell'} J_{\ell\, \ell'}\, S_\ell \cdot S_{\ell'} - \mu_\beta\, 2H \cdot \sum_\ell S_\ell$$

where S_ℓ is the total spin operator for the atom at site ℓ, $J_{\ell\ell'}$ is the exchange integral and is a function of the relative positions of sites ℓ and ℓ', and H is an external magnetic field.

The Ni^{++} magnetic moments in NiO are coupled such that NiO is antiferromagnetic below its Neel temperature T_N of 523°K.[16] Above 523°K NiO is paramagnetic. Above T_N, NiO is cubic and below T_N it is distorted by a contraction along one of the original cubic unit cell<111> axes. The structure is rhombohedral. When antiferromagnetic the moments of Ni^{++} form ferromagnetic sheets in (111) planes along the distorted [111] axis. The spins on adjacent sheets are oriented antiparallel to give the antiferromagnetism.

2. Transport Properties

Since Ni^{++} has an unfilled 3d shell in NiO, one would expect by simple band theory that NiO would be a conductor. This is not, however, the case. Pure NiO has a specific resistivity greater than 10^{10} ohm-cm.[13,17,18] When NiO deviates from stoichiometry or when it is doped with Li the resistivity drops by orders of magnitude.[13,17,18] Considerable effort has been directed towards determining the process by which conductivity occurs in NiO.

Verwey and deBoer[19] have explained the fact that NiO is an insulator by assuming the 3d electrons to be localized on the Ni^{++} ions. Conduction takes place by the presence of Ni^{+++} caused either by Ni vacancies or by the replacement of Ni by Li at some Ni sites. The conduction is due to hopping of holes from Ni^{+++} to Ni^{++}. The holes are attracted to either the Li^+ or Ni vacancies and the activation energy in the conductivity is the energy required to free the holes from the Li^+ or Ni vacancies. Verwey and DeBoer assumed that once the holes

are free no activation energy is required for them to move from Ni^{+++} to Ni^{++}.

Heikes and Johnston[20] and Morin[21,22,23] concluded from experimental results that the activation energy in the conductivity was associated with the mobility and not with the production of carriers. The activation energy for the mobility was explained (Heikes and Johnston) as being the result of the self trapping of holes by the lattice distortion as they move through the lattice. Conductivity then occurs as a thermally activated hopping of the holes. Arguments which apparently confirmed this view are summarized by Bosman and Crevecoeur,[24] who interpret their own results to show that the hopping model is not correct. The arguments were:

1) The activation energy in the conductivity does not disappear at Li concentrations where nearly all Ni ions have Li neighbors. If the activation energy were due to the binding of holes to Li impurities it should disappear at high Li concentrations. Since an activation energy exists at high Li concentrations, it must be due to the mobility.

2) The simplest explanation of the observed proportionality of the conductivity to the Li concentration is that the number of holes equals the Li concentration.[24] This implies that the activation energy is not connected with the creation of carriers.

3) The low values for the mobility which are derived from a hopping model are consistent with the fact that no Hall effect could be detected in early measurements.

4) Measurements of the mechanical and dielectric losses indicated that holes moved around the Li^{+} ions to which they were bound with an activation energy of the same order of magnitude

as that obtained from conductivity measurements.[25,26,27,28]

Mott[29] has proposed an argument which explains the insulating behavior of materials with apparently half-filled bands. The model is also of interest because it predicts a sharp transition between insulating behavior and metallic behavior as the lattice constant is decreased. With large lattice constant and small overlap of the wavefunctions on adjacent atoms, electrons are localized at each atomic site. In order to place two electrons on the same atom, an energy sufficient to overcome the coulomb repulsion would be required. Thus there are no states lying adjacent to the filled states even with only one electron per atomic orbital and the material will be an insulator. As the lattice constant is reduced and the overlap of the wavefunctions increases it becomes easier to excite electrons into higher energy levels and the electrons tend to be less bound. As electrons are freed from their original atomic orbitals they tend to screen other electrons from the coulomb potentials of the atoms and from the coulomb potential between electrons. As more electrons are freed the range of the coulomb potential is decreased by the screening making it easier to free electrons. When the screening becomes sufficient, all electrons will be freed. The transition from bound states to band states according to Mott will be discontinuous with variation in lattice constant.

Slater[30] has proposed an energy gap in materials which are antiferromagnetic even though there may be only one electron per atomic orbital. The argument is that the sites having "up" spins are not

the same as those with "down" spins and thus the lattice constant is effectively doubled. The non-identical lattice sites cause a splitting of what would be one band if the antiferromagnetism were not present. This model appears to predict metallic behavior above the Neel temperature in contrast to the results of experiments on NiO.

S. Van Houten[17] made measurements on pressed samples of NiO fired at high temperatures (1200 to 1550°C). These as well as samples of many early workers were, of course, not single crystals. Van Houten measured the Seebeck effect and the electrical resistivity as a function of temperature and lithium concentration. For the pure NiO, the log ρ/T (where ρ is the resistivity and T the temperature in °K) varied from $\sim$0 to $\sim$8 as $10^4/T°K$ varied from $\sim$8 to $\sim$32. Both the log ρ and the activation energy of the resistivity dropped rapidly as the Li concentration was increased from 0 to $\sim$3 atomic %. As the Li concentration was further increased the log ρ and activation energy fell more slowly. The resistivity of the NiO samples showed an activation energy of $\sim$.5 eV at temperatures below the Neel temperature of 523°K and $\sim$1.0 eV above the Neel temperature. The activation energy in the Li doped samples was $\sim$.1 to $\sim$.2 eV. Statements concerning the way the activation energy varies with temperature made in Reference 17 as well as several other papers discussed in this chapter could in some cases be incorrect. For example, if the gap $E_g = E_g^o - \beta T - \gamma T^2$ where E_g^o, β, and γ are constants then the log of the resistivity versus $\frac{1}{T}$ can have a higher slope at high temperatures than at low temperatures. However, for the above variation of E_g with T the activation energy is in fact less at the higher temperatures.

Van Houten interpreted his results to support the thermally activated hopping hypothesized by Heikes and Johnston.[20] He describes NiO as having full $3d^8$ levels which are localized and which lie about 5.4 eV below the empty $3d^9$ Ni^+ levels which may or may not be localized. He indicates that the oxygen 2p band lies ~5.3 eV below the Ni^{++} levels and yields no contribution to the conductivity. Van Houten's estimates of the energy levels were obtained by starting with the ionization energies of the free ions, combining them with the Madelung potentials and making corrections to account for the lattice polarization and crystal field energies. His estimates imply that the oxygen 2p band lies 10 to 11 eV below the $3d^9$ Ni^+ levels. The small conductivity in pure NiO is stated to be the result of accidental impurities giving acceptor levels at 1 to 2 eV above the Ni^{++} levels. Li addition gives acceptor levels ($Li^+ \cdot Ni^{++}$) about .035 eV above the Ni^{++} filled levels. Annealing NiO in oxygen causes the creation of Ni^{++}-vacancy acceptor levels. The creation of the acceptor levels explains the rapid decrease in activation energy and resistivity when lithium is introduced into NiO samples. At temperatures somewhat above room temperature all of the acceptors are ionized. The mobilities are then assumed to increase exponentially with temperature, the activation energy being a consequence of the self-trapping of holes as described by Heikes and Johnston.[20]

Resistivity and Hall effect measurements on Li doped NiO single crystals were made by Roilos and Nagels.[31] According to hypotheses that conduction is a thermally activated diffusion or hopping process, the mobility in NiO should be quite small. For example, Van Houten[17] has calculated values from his resistivity

measurements which vary from $2 \cdot 10^{-5}$ to $60 \cdot 10^{-5}$ cm^2/V sec. Roilos and Nagels present results for samples with chemical formula $Li_{.002}\ Ni_{.998}0$. The Hall effect measurements indicated p type conduction and a carrier density (assuming one kind of carrier) which increases with temperature. The resistivity varied from $\sim 10^2$ to $\sim 5 \cdot 10^8$ ohm-cm as $10^3/T$ (°K) varied from ~3 to 9.5. The Hall mobility varied from ~.25 cm^2/V-sec to ~.08 cm^2/V-sec as $10^3/T$ (°K) varied from ~3.5 to ~6. The Hall mobility increased with temperature and its value at room temperature was .25 cm^2/V sec. Roilos and Nagels compared their Hall mobilities with the other existing results. The results of Ksendzov, Ansel'm, Vasil'eva and Latysheva (32 as quoted in 31) are shown as having a temperature dependence similar to that found by Roilos and Nagels but having values smaller by a factor of ~10. Roilos and Nagels attribute the difference as due to the fact that Ksendzov et. al. used polycrystalline samples in which grain boundary effects may be important. Other results quoted by Roilos and Nagels are those of Zuhze and Shelykh (33 as quoted in 31) (they found a Hall mobility of .2 cm^2/V sec for NiO single crystals and .08 cm^2/V sec for polycrystalline $Li_{.034}\ Ni_{.966}0$) and Fujime, Murakami, and Hirahara (34 as quoted in 31) ($3.7 \cdot 10^{-4}$ cm^2/V sec at room temperature).

Several workers have observed a change in the activation energy of NiO at a temperature near the Neel temperature. Some have observed a decrease[35,18,36] in the activation energy above the Neel temperature while others have observed an increase.[17,20] Akiyama has measured the paramagnetic susceptibility χ and electrical conductivity of antiferromagnetic $Ni_{1-x}\ Li_x0$ and $Ni_{1-x}\ Mg_x0$ as a function of x for $x < 3$. The samples were sintered. He has plotted χ_N/χ_{max} (χ_N is the value of susceptibility at the Neel temperature and χ_{max} the maximum

susceptibility as a function of temperature) against the log of the conductivity at 500°K and noted a monotonic increase of χ_N/χ_{max} as the log of the conductivity decreases. He hypothesizes a magnetic interaction due to electrical conduction to explain his results.

Koide[18] made a study of the resistivity in NiO as a function of temperature (300 to 1020°K) and lithium content (x = 0 to .065 in $Li_xNi_{(1-x)}0$). His experiments were all made on single crystal thin films grown on MgO by halide decomposition[38] -- crystals grown in this manner are thought to be more stoichiometric than Verneuil crystals[39] and yield samples which should be a considerable improvement over the sintered samples used by numerous early workers. Expressing the resistivity ρ as

$$\rho/T = A_1 \exp [\varepsilon_1/kT] \text{ for } T>T^*$$

$$\rho/T = A_2 \exp [\varepsilon_2/kT] \text{ for } T<T^*$$

where A_1 and A_2 are constants and ε_1 and ε_2 are activation energies (20 as quoted in 18). Koide summarizes his results as follows:

1) ε_1, ε_2, $\varepsilon_2 - \varepsilon_1$ and ρ decrease rapidly as x varies from 0 to .015. A kink appears in the plots of ρ/T at a transition temperature T^* where T^* appears to be near the Neel temperature. As the Li content goes from x = 0 to x = .015, $\rho(300°K)$ varies from $\sim 10^{10}$ ohm-cm to $\sim$10 ohm-cm and $\rho(556°K)$ varies from $\sim 3 \cdot 10^3$ ohm-cm to $\sim$.5 ohm-cm. ε_2 varies from $\sim$.9 to $\sim$.2 eV and ε_1 from $\sim$.68 to $\sim$.14 eV. A_1 and A_2 increase with x for $0<x<.015$.

2) For $x>.015$, ε_1 appears to saturate at .14 eV while ε_2, $\varepsilon_2 - \varepsilon_1$, and ρ continue to decrease slightly. $\varepsilon_2 - \varepsilon_1$ approaches kT* for $x>.025$ and T*, A_1 and A_2 decrease with increasing x. $\rho(300°K)$ falls to $\sim 3 \cdot 10^{-1}$ ohm-cm at $x = .065$.

3) ε_2 is always greater than ε_1 -- this is not in agreement with the results of Heikes and Johnston who used sintered samples (20 as quoted in 18).

4) The rapid decrease of ρ as x goes from 0 to .015 is a result of the decrease in ε_1 and ε_2. For x greater than .015 ρ decreases because A_1 and A_2 decrease.

Koide interprets his results as follows:

1) The decrease in resistivity and activation energies as x varies from 0 to .015 is a result of a decrease in the potential energy which binds a hole on Ni^{+++} to Li^{+} or Ni^{++} vacancies.

2) For Li concentrations x where $x>.015$ the Li^{+} - Li^{+} distance decreases such that the energy required to release carriers is essentially 0. The saturated value of ε_1 is then entirely due to the mobility. This activation energy is a result of the interaction of localized hopping holes with acoustical phonons. Koide indicates that his results appear to be more in agreement with the hopping model of Toyozawa (40 as quoted in 18) than that of Heikes and Johnston (20 as quoted in 18). The two models differ in their prediction of the force range of the interaction between the carriers and the lattice.[18]

3) The difference in activation energy below and above the Neel temperature is qualitatively explained in terms of the change in the elastic constants at the Neel temperature. For $x>.025$ $\varepsilon_2 - \varepsilon_1$ depends upon the antiferromagnetic ordering which Koide[18] indicates might be unfavorable for hopping.

4) The increase in A_1 and A_2 with x for $0<x<.015$ is due to an increase in the number of Li^+ trapping centers.

Koide indicates that his conclusions 3 and 4 above are "rather temporary".

Koide[18] was apparently unable to detect a Hall voltage. Based on the hopping model which he discusses he estimates the mobility at room temperature to be $\sim$.7 to $1.0 \cdot 10^{-4}$ cm^2/volt sec.

Vernon and Lovell[35] have measured the conductivity in single crystal NiO between 293°K and 675°K. They have used crystals which were grown epitaxially on MgO and then removed from the MgO by dissolving the substrates. They have further made measurements on crystals grown in a carbon arc image furnace (41 as quoted in 35). In addition to a decrease in the activation energy above the Neel temperature of 523°K, they report another change in activation energy near 390°K. If ε_1 is the activation energy below $\sim$390°K, ε_2 the activation energy between 390°K and 523°K and ε_3 the activation energy above 523°K, their results show that $\varepsilon_2 > \varepsilon_1$ and ε_3. The relation between ε_1 and ε_3 appears to vary depending upon the sample and the annealing. The change in slope near 390°K decreases with increasing oxygen content in the specimens. Vernon and Lovell attribute the effect near 390°K to be the result of a small Jahn-Teller effect. They further hypothesize that the NiO structure is distorted from cubic to rhombohedral at a

temperature near 400°K (it is cubic at high temperatures and rhombohedral at low temperatures) rather than at the Neel temperature as usually stated. They report further that thermal hysteresis in the change in activation energy at the Neel temperature is a result of strain in the crystal and hypothesize that strain free samples would show no hysteresis.

Bosman and Crevecoeur[24] measured the conductivity and Seebeck effect of Li doped NiO in the temperature range 100 to 1300°K. Their samples were pressed bars of NiO fired at 1300°C in oxygen. The choice of samples is rather unfortunate since errors are probably introduced into the measurements by the non-crystalline samples. They did however measure the a.c. as well as the d.c. conductivity to insure that the values obtained were representative of the bulk material.

Bosman and Crevecoeur found that the thermoelectric power of a sample containing $8.8 \cdot 10^{-2}$ atomic % Li had a maximum at 140°K, decreased rapidly at temperatures below 140°K, and decreased above 140°K to a minimum near 900°K. The resistivity of the same sample changed by a factor of 10^{11} in the temperature range of 100 to 1300°K. Between 140 and 400°K the log of the resistivity varied linearly with the reciprocal of the temperature and showed an activation energy of .30eV. The temperature dependence of the log of the resistivity decreased above 400°K and below 140°K.

The temperature variation of the Seebeck effect indicated that the change in resistivity between 170°K and 400°K was due to the change in free hole concentration with temperature. The maximum in

the thermoelectric power at 140°K was explained by assuming two conductivity mechanisms at low temperatures -- impurity conduction in the $Li^{+}Ni^{+++}$ acceptor levels and a free hole conductivity. Above 140°K, the variation of thermoelectric power was explained assuming a narrow acceptor band having a band width larger than kT with the acceptors partly compensated by donors. The amount of compensation calculated from the analysis of the Seebeck effect appeared to agree reasonably well with the compensation found by chemical analysis. The assumption of the compensation was also consistent with the presence of an impurity band.

Bosman and Crevecoeur[24] have computed mobilities as a function of temperature from their conductivity and Seebeck effect measurements assuming a bandwidth less than kT and assuming a bandwidth narrow but larger than kT. They have compared the mobilities with Hall mobilities measured on pressed, fired NiO doped with $8.8 \cdot 10^{-2}$, $1.1 \cdot 10^{-2}$ and $5 \cdot 10^{-3}$ atomic % of Li (42 as quoted in 24) and with the Hall mobilities measured by several other workers (31, 32, 33 as quoted in 24). The mobilities derived from conductivity and Seebeck measurements were considerably greater than the Hall mobilities -- the difference increased at high temperatures. The value of the mobility was $\sim$.5 to 5 cm^2/V sec at room temperature depending upon the assumption made concerning the band width and shape. The mobility decreased with increasing temperature. Bosman and Crevecoeur conclude from the Seebeck effect, conductivity, and Hall effect measurements that "employment of the band model leads to reasonable results".

Bosman and Crevecoeur[24] hypothesize that other authors have been misled and assumed a hopping model because

1) Grain boundary effects in samples used have given incorrect results.
2) The Seebeck effect has been interpreted without the assumption of acceptor compensation.
3) Workers have attempted to formulate models based only upon conductivity measurements.
4) The results of mechanical and dielectric loss measurements have been erroneously interpreted neglecting the possibility of impurity conduction.

One further point of interest is that Bosman, van Daal, and Knuvers (42 as quoted in 24) found that the Hall mobility showed a change in sign above the Neel point. Van Daal and Bosman[43] measured the Hall effect and resistivity between 200 and 1500°K on ceramic and single crystal NiO. The Hall constant was found to have a sign opposite to that expected for p type materials above the Neel temperature whereas the Seebeck effect has the expected sign. The Hall constant was found to be proportional to the reciprocal of the carrier concentration and the Hall mobility to be less than the drift mobility by $\sim 10^{-2}$. Below T_N, the Hall constant had the sign expected assuming p type conductivity. Van Daal and Bosman hypothesized that the anomalous sign change was due to an interaction between the carriers and the induced magnetic field. Their data indicated that the interaction becomes important above 400°K. They further hypothesized the Hall coefficient to be composed of two components -- the normal Hall effect and a component proportional to the normal component caused by the interaction with the induced magnetic moment. They interpreted their

results as being "inconsistent with the hopping model."

Austin, Springthorpe, Smith, and Turner[36] measured the Hall effect, conductivity, and Seebeck effect of NiO with up to .6 atomic percent lithium in the range 150 to 1100 K. Some of their results are shown in Figures 1-1 and 1-2. Their measurements were performed on single crystals which removes one source of error likely to be present in measurements made on sintered samples. They also investigated the conductivity of single domains of NiO. Between 150 and 400°K they found the resistivity to vary with an activation energy which decreased rapidly with increasing Li content. The activation energy decreased above the Neel temperature as did that of Koide.[18] The activation energy decreased steadily with decreasing temperature below 150°K and was $\sim$.007eV for temperatures less than 40°K. The resistivities measured in single domains with current flow parallel and perpendicular to the (111) spin planes were the same and the temperature variations were the same between 25 and 400°K to within $\sim \pm$ 2%.

Between 250 and 400°K, the Hall constant varied with an activation energy slightly larger than that of the resistivity. The Hall constant activation energy also decreased as the Li content increased. Samples with little or no Li had Hall mobilities which decreased with increasing temperature, the room temperature value being $\sim$.4 cm^2/volt-sec. The Li doped samples had Hall mobilities with a maximum between 200 and and 300°K and the Hall mobility of the most heavily doped crystal was significantly less than the mobilities of the other samples. In the region of overlap with the values measured by Bosman and Crevecoeur (24 as quoted in 36) the agreement was quite good.

The thermoelectric power had a maximum at low temperature which was particularly evident in the undoped, non-stoichiometric samples.[36] The Seebeck measurements showed a change in slope at the Neel temperature and a shallow minimum near 1000°K in the samples containing Li.

Using their resistivity and Seebeck results, Austin et. al. calculated the drift mobility as a function of temperature and found the ratio of drift mobility to Hall mobility to be ∿10 in the temperature range 250 to 400°K. The temperature dependence of the two mobilities was quite similar.

Austin, Springthorpe, Smith, and Turner[36] interpreted their results as indicating conduction in two levels -- am impurity band and a narrow 3d band. This interpretation including the assumption of compensation is consistent with the results and interpretation of Bosman and Crevecoeur.[24] The maximum in the Seebeck measurements on undoped crystals which occurred near 320°K was cited as evidence that impurity conduction is important at room temperature. Austin et. al. discussed the effect of electron-phonon coupling in NiO and concluded that their results suggested small-polaron conduction in a narrow 3d band in the temperature region where impurity conduction is not dominant. The activation energy for holes to get into the band is .16 to 1.2eV depending upon the Li concentration. The isotropy of the conductivity in single domains was stated to indicate that the 3d band conduction depends on indirect overlap through the oxygen ions rather than direct 3d overlap.

Young, Wilson, and Schwartz[44] investigated the effect of pressure on the NiO resistivity and Seebeck coefficient near room temperature and interpreted the results to show that the hole mobility decreased with

pressure up to 60000 atmospheres -- the decreased hole mobility was explained in terms of the early hopping models as due to a decrease in the diffusion rate of self trapped holes with pressure. The main point of interest in their measurement, however, was that no Mott transition was found at pressures up to 200000 atmospheres. Unfortunately, their samples as was the case with many early measurements were not single crystals.

Vaisnys[45] measured the variation of the conductivity and thermoelectric power with pressure and found

$$\frac{d\varepsilon}{dP} = -1.0 - 10^{-6} \text{ eV/bar and } \frac{d(QT)}{dP} = -5 \cdot 10^{-6} \text{ eV/bar}$$

where ε is the activation energy for conductivity and QT the thermoelectric power. The samples were again not crystalline. The results were interpreted in terms of an activated mobility in conflict with most recent interpretations of the Hall effect, conductivity and Seebeck effect.

J. Feinleib[46] has suggested that the band like conduction in NiO suggested by the most recent experimental data and the crystal field type optical spectra (see the following section) are consistent with a model where hole conduction occurs in an oxygen 2p band separated from a Ni 4s band by about 4 eV. The d^8 levels are localized at energies in the gap.

D. Adler[47] has reviewed the theoretical models and experimental results of the transition metal oxides in general. His review contains a very complete list of the references on not only NiO but also the other transition metal oxides. It is worthwhile to reproduce a list

contained in Adler's review which summarizes the properties of NiO as indicated by experimental work to date. As yet a consistent model is not available to explain these properties. The list as contained in Reference 47 is:

(1) The semiconducting nature of NiO at all temperatures.

(2) The antiferromagnetism and low temperature rhombohedral distortion.

(3) The decreasing drift mobility with increasing temperature.

(4) The slowly decreasing Hall mobility with increasing temperature.

(5) The small value of the ratio $\mu_H/\mu_{drift} \sim .01 - .1$.

(6) The change in sign of the Hall coefficient in the vicinity of T_N.

(7) The optical absorption peak at .24 eV which vanishes above T_N (this will be discussed in the following section on optical properties).

(8) The absorption edge and photoconductivity edge at 3.7 eV (this will be discussed in the following section on optical properties).

(9) The activation energies of .25 - .50 eV in the 300-1000°K range.

(10) The discontinuous decrease of this activation energy at T_N.

(11) The activation energy of 1.0 eV above 1000°K, independent of impurity concentration.

References 48, 49 and 50 are of general interest for those studying transport in the transition metal compounds -- particularly those compounds which exhibit a metal to semi-conductor transition with temperature.

3. Optical Properties

One of the earlier measurements of the optical properties of NiO was made by Doyle and Lonergan.[51] They measured the absorption spectra of thin films between 2000 angstroms and one micron and the spectra of pressed potassium bromide discs containing NiO between 3600 angstroms

and one micron. The thin films were oxidized films of nickel, and the potassium bromide discs contained .1, .2 and .5% NiO. The absorption spectrum of a typical NiO film is shown in Figure 1-3 and the results from the pressed discs are summarized in Table 1-1. The thin film spectrum shows a threshold at 6000 angstroms, a broad maximum at 2800 angstroms and a peak at 2400 angstroms.[51] The absorption coefficient at short wavelengths is $\sim 10^6$ cm^{-1}.

Doyle and Lonergan attribute the maximum at 2800 angstroms to an electron transfer from the O_2^{--} to Ni^{++} ion. They eliminate the $3d^8 \rightarrow 3d^7$ 4p transition by arguing that the energy for this process is too high to give agreement with the optical transmission spectrum. In contrast they estimate the energy for the charge transfer process to be approximately that obtained from the optical results. The energy is estimated from the Madelung constant for the lattice, the electron affinity of the O^- ion, the second ionization potential of nickel, and the lattice polarization energy -- the latter was estimated from the refractive index. They also make estimates for the band width of the filled O_2^{--} level. The transition they describe is from the highest filled oxygen band to the first exciton level. The second absorption peak (2400 angstroms) is interpreted as the transition to the conduction band.

Table 1-1 compares the absorption peaks measured by Doyle and Lonergan[51] in pressed potassium bromide discs with those observed by Morin (22 as quoted in 51) in a thick NiO film, by Kroger, Vink and van der Boomgaard (52 as quoted in 51) in the diffuse reflection spectra of NiO+ MgO mixed crystals, and by Orgel (53 as quoted in 51) in the hydrated Ni^{++} ion in aqueous solution. Table 1-1 also lists

TABLE 1-1 Optical spectrum of NiO as given in Ref. 51.

observed maxima				predicted transitions	
NiO film[a]	NiO+MgO[b]	NiO+KBr	Ni^{2+c}_{aq}	frequency[c]	assignment[c]
8,070 cm^{-1} (1.00 eV)			8,500 cm^{-1} (1.05 eV)	8,500 cm^{-1} (1.05 eV)	$^3A_{2g}$-$^3T_{2g}$
	13,900 cm^{-1} (1.72 eV)	14,500 cm^{-1} (1.80 eV)	14,000 (1.74)	14,000 (1.74)	$^3A_{2g}$-$^3T_{1g}$
15,400 (1.91)	14,900 (1.85)			15,000 (1.86)	$^3A_{2g}$-^1E_g
	21,500 (2.67)	22,200 (2.75)	22,500 (2.79)	22,500 (2.79)	$^3A_{2g}$-$^1T_{2g}$
	25,000 (3.10)	25,000 (3.10)		25,600 (3.17)	$^3A_{2g}$-$^1A_{1g}$
		26,600 (3.30)	26,000 (3.22)	27,000 (3.35)	$^3A_{2g}$-$^3T_{1g}$

[a] Ref. 22 as quoted in Ref. 51

[b] Ref. 52 as quoted in Ref. 51.

[c] Ref. 53 as quoted in Ref. 51.

the assigned crystal field theory transitions of Reference 53 as quoted in 51. Doyle and Lonergan[51] therefore interpret the spectra of the pressed discs as due to transitions in the Ni^{++} ion octahedrally surrounded by O_2^{--}.

Newman and Chrenko[39] measured the optical properties of single crystal NiO between .025 and 10 eV. The crystals were grown in two different ways -- flame fusion and the vapor deposition method described by Cech and Alessandrini in reference 38. Thin films of oxidized nickel were also used for transmission measurements over part of the wavelength spectrum.

The absorption spectrum is shown in Figure 1-4. Between 1.0 eV and 3.5 eV there are several narrow absorption bands which Newman and Chrenko assign to transitions in Ni^{++} as modified by the crystal field. Table 1-2 summarizes the energies of the lines observed and indicates the assignment of each. The table further gives the values of transitions observed in Ni^{++} in MgO (Reference 54 as quoted in Reference 39). The observed transitions are forbidden by the selection rules and only occur due to the interaction with lattice vibrations. From the width of the observed absorption bands Newman and Chrenko estimate the 3d band in NiO to be less than .25 eV wide. The absorption of the observed lines was measured at temperatures between 20°K and 700°K which include temperatures above the Neel point. Newman and Chrenko found slight increases in the intensities of the absorptions and small shifts of the peaks to lower energies as the temperature was increased. They conclude that the absorptions between 1 and 3.5 eV are not affected by the antiferromagnetic ordering in NiO.

At ∿4 eV the NiO absorption increases rapidly to a plateau at higher energies. The measurements shown between 4 and 5.8 eV

TABLE 1-2. Optical Spectrum of NiO at 300°K as given in Ref. 39.

Assignment and crystal symmetry representations of excited states[a]	Observed absorption lines[b] (electron volts)		Calculated absorption lines (electron volts)	Absorption coefficient (cm^{-1})
$\Gamma_5(^3F)$ $^3T_{2g}$	1.13	(1.07)		380
$\Gamma_3(^1D)$ ^1E_g	1.75	(1.68)	1.62[c]	950
$\Gamma_4(^3F)$ $^3T_{1g}$	1.95	(1.83)	1.85[c]	450
? ?	2.15			230
$\Gamma_5(^1D)$ $^1T_{2g}$	2.75	(2.69)		950
$\Gamma_4(^3P)$ $^3T_{1g}$	2.95	(3.04)		1900
$\Gamma_1(^1G)$ $^1A_{1g}$	3.25	(3.21)		9000
$\Gamma_4(^1G)$ $^1T_{1g}$	3.52	(3.50)		12000

[a] The ground state has $\Gamma_2(^3F)$, $^3A_{2g}$ representation.

[b] Values in parenthesis are Ni^{2+} in MgO (Ref. 54 as quoted in Ref. 39).

[c] Calculated using energy level parameters which were obtained from other observed lines.

in Figure 1-4 were made on polycrystalline films of oxidized nickel and showed no fine structure. Using arguments similar to those of Doyle and Lonergan[51] to estimate the energy of transitions in Ni^{++}, Newman and Chrenko hypothesize that the absorption at high energies is due to a charge transfer from O^{--} to Ni^{++}.

Newman and Chrenko show (see Figure 1-4) a continuous background absorption below 4 eV. By measuring the absorption of crystals containing excess oxygen, they demonstrated that the continuous background absorption increased as the O/Ni ratio increased. The positions of the absorption maxima were not changed as the stoichiometry was varied and the intensity of the peaks varied only a small amount.

Figure 1-4 shows an absorption at .24 eV which Newman and Chrenko observed in flame fused crystals grown in their laboratory, in flame fused crystals grown in other laboratories, and in crystals grown by vapor deposition. In all cases the absorption had the same intensity. The above plus the fact that flame fused crystals of MnO and CoO do not have an absorption band at .24 eV led Newman and Chrenko to the conclusion that the absorption is not due to impurities. The peak at .24 eV changes little with temperature below 300°K but becomes less intense and moves to lower energies with increasing temperature above 300°K. At the Neel temperature the absorption is almost gone. The conclusion reached in Reference 39 is that the absorption is associated with the antiferromagnetic ordering in NiO.

Newman and Chrenko measured the reflectivity of single crystal NiO between .025 eV and 10 eV. In the energy range .1 to 10 eV they observed only a single peak at 4 eV corresponding to the rapid increase in absorption at about this energy. Below .1 eV they observed the

structure due to absorption by optical mode lattice vibrations. From the reflectivity they determined the static dielectric constant to be 12 and the high frequency dielectric constant to be 5.4. The transverse optical mode energy is given as .044 eV and the longitudinal optical mode energy as .076 eV.

Ksendzov and Drobkin[55] measured the photocurrent in NiO as a function of wavelength and the electrical conductivity and thermoelectric power as a function of temperature between 700 and 1200°K. The samples were single crystals grown by vapor deposition as described in Reference 38. They found the photocurrent to be small below 3 eV and to increase sharply between 3.5 and 4.0 eV. They state that much transport data has been interpreted ignoring changes in the Ni^{+++} concentration which occur with temperature due to the equilibrium reached between the oxygen content of the samples and the oxygen in the atmosphere surrounding the samples. Ignoring changes in the sample oxygen content with temperature leads to incorrect interpretations concerning the relation of the activation energy to the forbidden band width of intrinsic NiO. Ksendzov and Drobkin measured the conductivity and thermoelectric power in a 10^{-4} mm Hg vacuum where at the temperatures used the changes in NiO oxygen content could be neglected. From the variation of the conductivity with temperature, they determined the forbidden band width to be 3.7 eV. They interpreted their measured thermoelectric power to indicate mixed conduction with a hole mobility greater than the electron mobility. They further state that the forbidden band width is determined by the transition from Ni^{++} $(3d^8)$ to $Ni^{+}(3d^9)$.

Marshall, Mitra, Gielisse, and Plendl[56] have discussed the results of reflection and transmission measurements on NiO, CoO and their mixed crystals. By measuring the reflectivity in the lattice vibration region of NiO, $(Ni_{.75}Co_{.25})O$, $(Ni_{.50}Co_{.50})O$, $(Ni_{.25}Co_{.75})O$ and CoO they determined that the maxima vary from ~475 cm^{-1} in NiO to ~355 cm^{-1} in CoO whereas the minima due to the longitudinal optical mode near k=0 vary from ~625 cm^{-1} in NiO to ~603 cm^{-1} in CoO. They found secondary maxima in the reflectivities which are barely resolved in NiO but are well separated in CoO. They show the absorption of $(Ni_xCo_{1-x})O$ between 1000 and 2400 cm^{-1} including the band at 1935 cm^{-1} (.24 eV) in NiO which Newman and Chrenko have hypothesized to be connected with the antiferromagnetic order in the crystal. Marshall et. al. state that the position of the peak and the absorption coefficient are approximately a linear function of Co content.

The absorption spectrum at higher energies is summarized in Table 1-3 and is attributed to transitions between the Ni^{++} d levels as modified by the crystal field and at the high energies where the bands have not been identified possibly to excitons. Marshall et. al. do not indicate the method of preparation for their samples making it somewhat difficult to determine how reliably their results represent the optical properties of single crystal NiO. They do not show an absorption curve between 3 and 6 eV making it impossible to determine whether they detected the large apparent absorption edge seen by other workers.

Gielisse, Plendl, Mansur, Marshall, Mitra, Mykolajewyez, and Smakula[57] measured the optical properties in the lattice vibrational region of single crystal NiO, CoO and intermediate solid solutions. The samples were

Table 1-3 Spectrum of NiO as given in Ref. 56

Ni^{2+}					
Observed			Tentative Assignment[b]	Estimated[a]	
9020 cm^{-1}	(1.118 eV)		$^3T_2(^3F)$	9280 cm^{-1}	(1.150 eV)
10200	(1.264	)	?		
14560	(1.805	)	$^1E(^1D)$	14880	(1.845)
15620	(1.936	)	$^3T_1(^3F)$	15820	(1.961)
18200	(2.256	)	?		
21220	(2.631	)	?		
28400	(3.521	)	$^3T_1(^3P)$	28700	(3.558)
30900	(3.831	)	$^1T_1(^1G)$	30550	(3.787)
32160	(3.987	)	?		
33900	(4.202	)	$^1E(^1G)$	35550	(4.407)
40700	(5.045	)	?		
44400	(5.504	)	?		

[a] For 10 Dq = 9500 cm^{-1}

[b] The ground state is $^3A_{2g}$.

grown by flame fusion. The reflectivity of NiO had a peak reflectivity of 90.7% at 465 cm^{-1}, a minimum at 625 cm^{-1} and a sideband at 570 cm^{-1}. There were broad maxima at 1000 and 760 cm^{-1}. Transmission measurements revealed absorption bands at 700, 727, 775, 810, 825, 925, 1050, and 1170 cm^{-1} in addition to the band at 1940 cm^{-1} discussed in References 39 and 56. The reflectivity of CoO had a peak of 80.3% at 373 cm^{-1}, a minimum at 613 cm^{-1}, and a secondary peak at 490 cm^{-1}. "Shallow" maxima were found at 800, 1200, 2200, and 2900 cm^{-1}. A transmission minimum was present at 750 cm^{-1} with evidence for structure at 816, 870, and 922 cm^{-1}. The studies of the alloys indicated a linear variation of all major optical and physical parameters (infrared results only are presented) when Co replaces Ni. Gielisse et. al. also derived values for the optical constants, di-electric constants, effective ionic charges, and characteristic frequencies from their results and the values are presented in Reference 57.

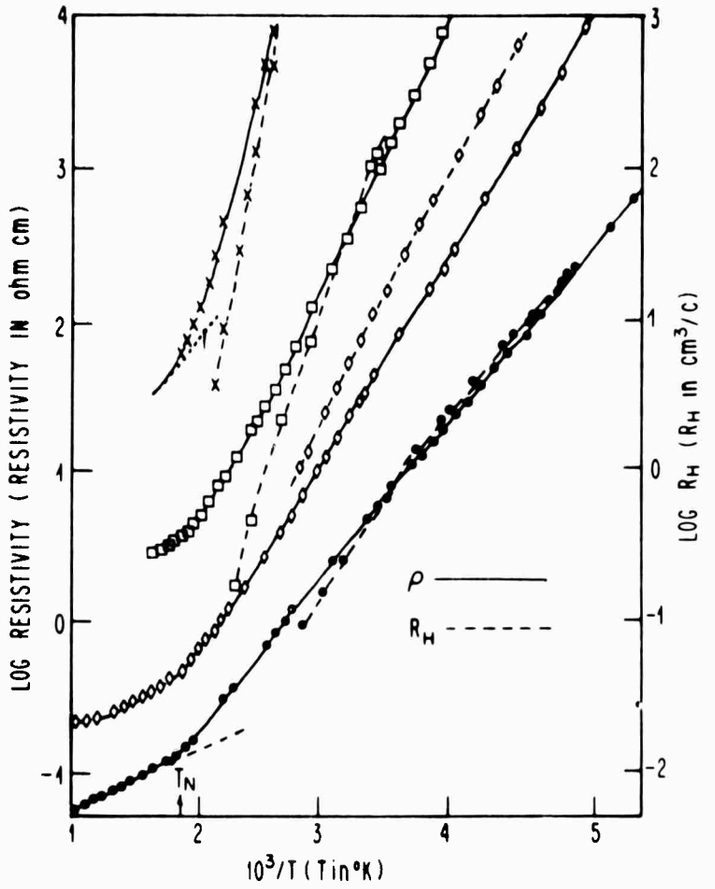

TEMPERATURE DEPENDENCE OF THE RESISTIVITY ρ AND HALL COEFFICIENT R_H IN VARIOUS NiO CRYSTALS.

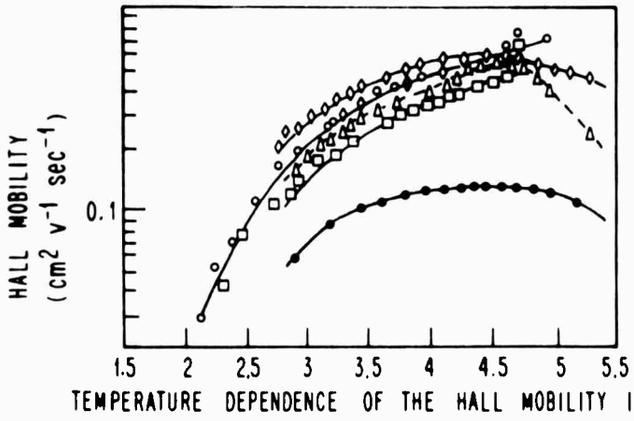

FIG. 1-1 RESISTIVITY, HALL COEFFICIENT, AND HALL MOBILITY IN NiO (REF. 36). AT % LITHIUM: x • 0, ○ • .032, □ • .029, △ • .144, ◇ • .202, ■ • .211, ● • .537.

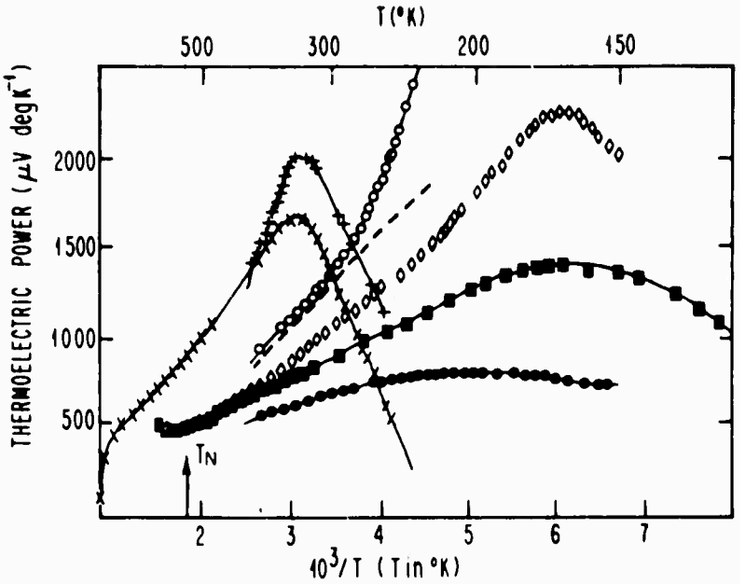

SEEBECK COEFFICIENT IN VARIOUS NiO CRYSTALS. AT. % LITHIUM: +-0, x-0, ○-0.032, ◇-0.202, ■-0.211, ●-0.537

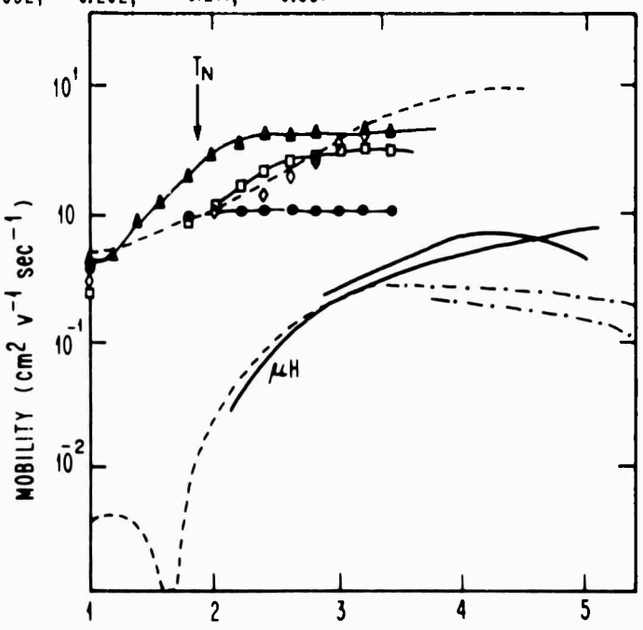

COMPARISON OF THE DRIFT AND HALL MOBILITY IN NiO
—— REF. 36, - - - - REF. 24 AS QUOTED IN 36, — · — · — REF. 31 AS QUOTED IN 36. AT. % LITHIUM: ▲~0.03, □-0.21, ◇-0.202 ●-0.537

FIG. 1-2 SEEBECK COEFFICIENT, DRIFT AND HALL MOBILITY IN NiO (REF. 36).

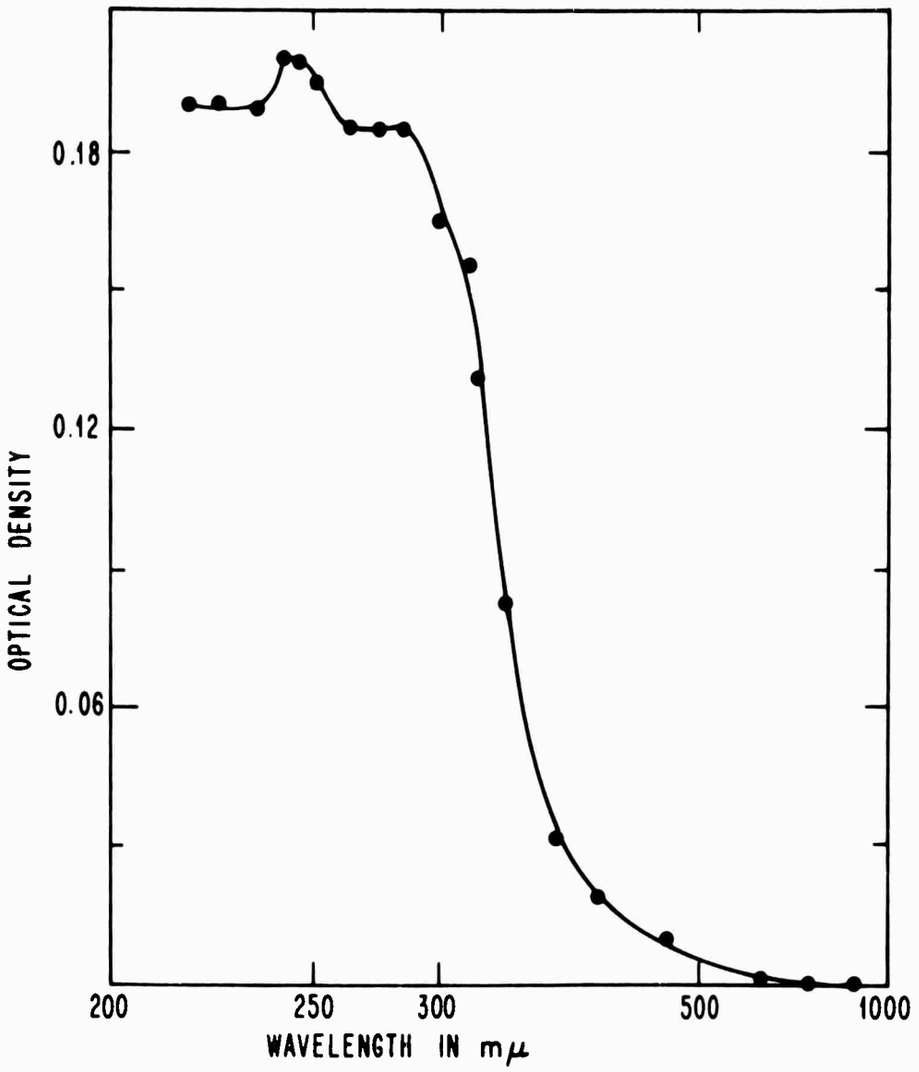

FIG. 1-3 ABSORPTION SPECTRUM OF NiO FILM AS GIVEN IN REF. 51.

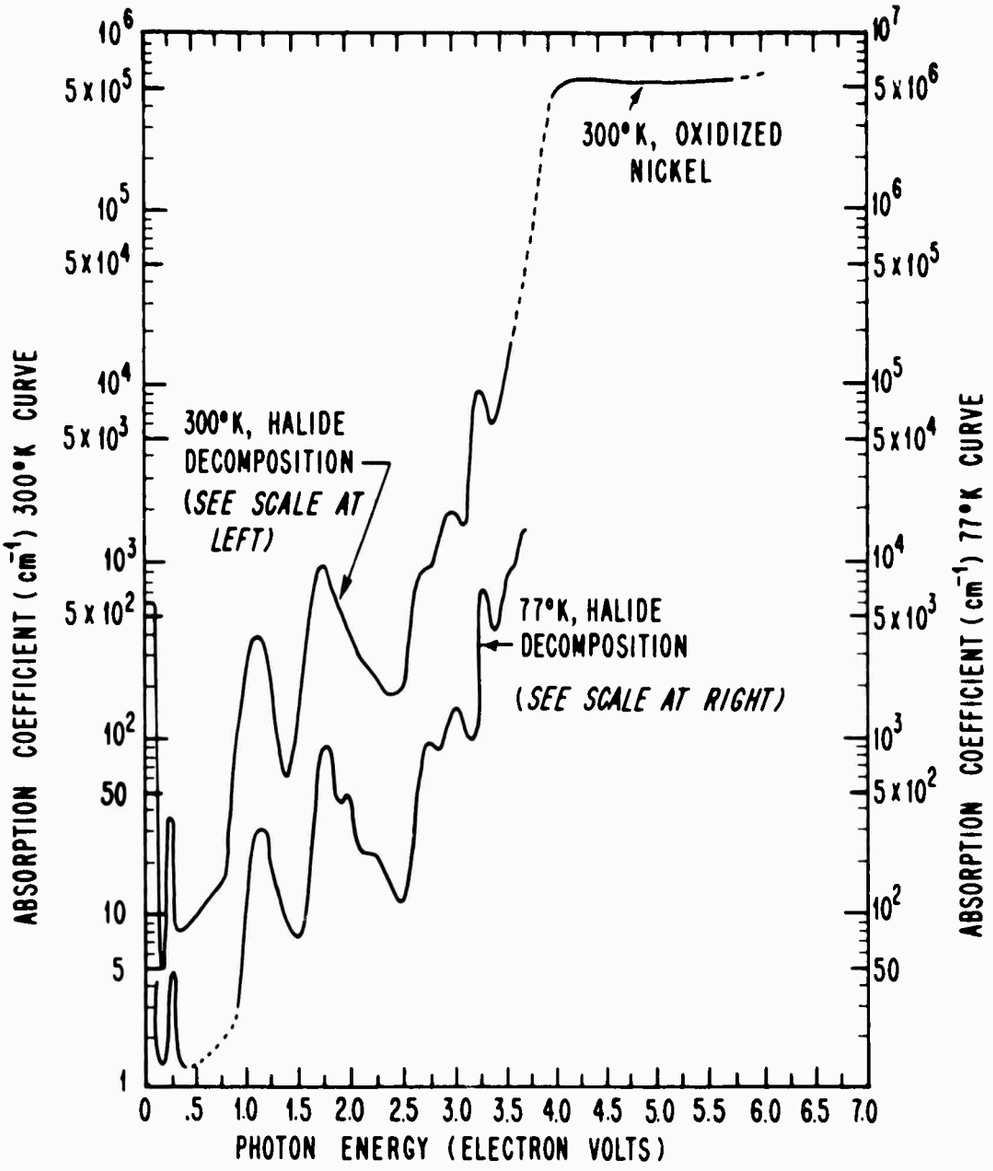

FIG. 1-4 ABSORPTION SPECTRUM OF NiO AT 300°K, 77°K. DASHED LINES ARE INTERPOLATIONS, AS GIVEN IN REF. 39.

Chapter One

BIBLIOGRAPHY

(1) R. B. Schoolar, Bull. Am. Phys. Soc., Ser. II, 8, 516 (1963).

(2) P. R. Wessel, J. R. Dixon, J. N. Zemel, R. B. Schoolar, and J. D. Jensen, Bull. Am. Phys. Soc. Ser. II, 8, 517 (1963).

(3) H. R. Riedl and R. B. Schoolar, Phys. Rev. 131, 2082 (1963).

(4) D. L. Mitchell, E. D. Palik, and J. N. Zemel, Phys. Rev. 135, A 763 (1964).

(5) R. B. Schoolar and J. R. Dixon, Phys. Rev. 137, A667 (1965).

(6) P. R. Wessel, Phys. Rev. 153, 836 (1967).

(7) C. E. Rossi and William Paul, Journal of Applied Physics 38, 1803 (1967).

(8) P. M. Grant and W. Paul, Journal of Applied Physics 37, 3110 (1966).

(9) R. Lüdeke and W. Paul, Journal of Applied Physics 37, 3499 (1966).

(10) S. A. Semiletov, I. P. Voronina, and E. I. Kortukova, Soviet Phys. Cryst 10, 429 (1966).

(11) G. Herzberg, Atomic Spectra and Atomic Structure, Dover Publications, New York (1940).

(12) C. Kittel, Introduction to Solid State Physics, John Wiley and Sons, New York and London (1962).

(13) J. Feinleib, Technical Report No. HP-11, Gordon McKay Laboratory, Division of Engineering and Applied Physics, Harvard University (1963).

(14) D. S. McClure, Solid State Physics, Vol. 9, F. Seitz and D. Turnbull, eds. Academic Press, N.Y. (1959).

(15) J. M. Ziman, Principles of the Theory of Solids, The University Press, Cambridge (1964).

(16) G. A. Slack, Journal of Applied Physics 31, 1571 (1960).

(17) S. Van Houten, J. Phys. Chem. Solids 17, 7 (1960).

(18) S. Koide, J. Phys. Soc. Japan 20, 123 (1965).

(19) J. H. deBoer and E. J. W. Verwey, Proc. Phys. Soc. (London) 49, 59(1937).

(20) R. R. Heikes and W. D. Johnston, J. Chem. Phys. 26, 582 (1957).

(21) F. J. Morin, Phys. Rev. 83, 1005 (1951).

(22) F. J. Morin, Phys. Rev. 93, 1195 and 1199 (1954).

(23) F. J. Morin, Bell Syst. Tech. J. 37, 1047 (1958).

(24) A. J. Bosman and C. Crevecoeur, Phys. Rev. 144, 763 (1966).

(25) R. G. Miller and R. R. Heikes, J. Chem. Phys. 28, 348 (1958).

(26) S. Van Houten, J. Phys. Chem. Solids 23, 1045 (1962).

(27) S. Van Houten and A. J. Bosman, in Informal Proceedings of the Buhl International Conference on Materials, Pittsburgh, 1963, edited by E. R. Schatz (Gordon and Breach Science Publishers, Inc., New York, 1966).

(28) A. J. Bosman and S. Van Houten, in Proceedings of the Seventh International Conference on the Physics of Semiconductors, Paris, 1964 (Academic Press Inc., New York, 1965) p. 1203.

(29) N. F. Mott, Proc. Phys. Soc. (London) A62, 416 (1949).

(30) J. C. Slater, Phys. Rev. 82, 538 (1951).

(31) M. Roilos and P. Nagels, Solid State Communications 2, 285 (1964).

(32) M. Ya. Ksendzov, N. L. Ansel'm, L. L. Vasil'eva, and V. M. Latysheva, Fiz. Tverdvago Tela 5, 1537 (1963); English Translation, Sov. Phys. Solid State 5, 1278 (1963).

(33) P. V. Zhuze and I. A. Shelykh, Fiz. Tverdogo Tela 5, 1756(1963); English Translation, Sov. Phys. - Solid State 5, 1278 (1963).

(34) S. Fujime, M. Murakami, and E. Hirahara, J. Phys. Soc. Japan 16, 183 (1961).

(35) M. W. Vernon and M. C. Lovell, J. Phys. Chem. Solids 27, 1125 (1966).

(36) I. G. Austin, A. J. Springthorpe, B. A. Smith, and C. E. Turner, Proc. Phys. Soc. 90, 157 (1967).

(37) M. Akiyama, J. Phys. Soc. Japan 20, 182 (1965).

(38) R. E. Cech and E. I. Alessandrini, Trans. A. S. M. 51, 150 (1959).

(39) R. Newman and R. M. Chrenko, Phys. Rev. 114, 1507 (1959).

(40) Y. Toyozawa, Prog. Theor. Phys., edited by C. G. Kuper and G. D. Whitfield (Oliver and Boyd, 1963), 26, p. 211.

(41) C. Kooy and H. J. Couwenberg, Phillips Tech. Rev. 23, 161 (1962).

(42) A. J. Bosman, H. J. van Daal, and G. F. Knuvers, Phys. Letters 19, 372 (1965).

(43) H. J. van Daal and A. J. Bosman, Phys. Rev. 158, 736 (1967).

(44) A. P. Young, W. B. Wilson, and C. M. Schwartz, Phys. Rev. 121, 77 (1961).

(45) J. Rimas Vaisnys, Journal of Applied Physics 38, 2153 (1967).

(46) J. Feinleib, Berkeley APS (1968).

(47) D. Adler (to be published).

(48) D. Adler and H. Brooks, Phys. Rev. 155, 826 (1967).

(49) J. Feinleib and W. Paul, Phys. Rev. 155, 841 (1967).

(50) D. Adler, J. Feinleib, H. Brooks, and W. Paul, Phys. Rev. 155, 851 (1967).

(51) W. P. Doyle and G. A. Lonergan, Trans. Faraday Soc. 26 27 (1958).

(52) Kroger, Vink and van der Boomgaard, Physica 18, 77 (1952).

(53) J. Orgel, J. Chem. Physics 23, 1004 (1955).

(54) W. Low, Phys. Rev. 109, 247 (1958).

(55) Ta. M. Ksendzov and I. A. Drobkin, Soviet Physics - Solid State 7, 1519 (1965).

(56) R. Marshall, S. S. Mitra, P. J. Gielisse, and J. N. Plendl, Proceedings of the International Conference on the Physics of Semiconductors, Paris 1964.

(57) P. J. Gielisse, J. N. Plendl, L. C. Mansur, R. Marshall, S. S. Mitra, R. Mykolajewyez, and A. Smakula, Journal of Applied Physics 36, 2446 (1965).

Chapter Two

PREPARATION OF FILMS

There are several methods of depositing films on substrates of either the same material or of some different material. The particular method used in a given case depends upon the substance one wishes to deposit and, to some extent, on the substrate one wishes to use. It was our desire to deposit nickel oxide epitaxially onto a substrate which was transparent far into the ultraviolet. In order to deposit the film epitaxially it was desirable to use a substrate of the same crystal structure as nickel oxide and having a lattice constant reasonably near that of nickel oxide. The ideal substrate material for our purposes was LiF which has the NaCl crystal structure and has a lattice constant of 4.01 angstroms.[1] NiO is nearly cubic (it is distorted slightly along what would be a (111) direction of a cubic structure) and has a lattice constant of 4.18 angstroms.[1] LiF is transparent to about 1040 angstroms in the vacuum ultraviolet.[2] Two other materials which are also transparent into the vacuum ultraviolet might also do -- CaF_2 with a lattice constant of 5.45 angstroms (transparent to 1250 angstroms[2]) and BaF_2 with a lattice constant of 6.18 angstroms (transparent to 1300 angstroms[2]). These substances are both of the fluorite structure and cleave along (111) planes rather than (100). Nevertheless, it should be possible to grow NiO epitaxially on these materials.

In depositing nickel oxide for use in optical experiments, we have investigated six essentially different techniques:

A. Evaporation of NiO in a high vacuum

B. Chemical transport and reaction via a gas

C. Flash evaporation

D. Electron beam evaporation of nickel in an O_2 atmosphere

E. Sputtering of nickel in an atmosphere containing O_2

F. Oxidation of nickel films

In the sections to follow we will discuss each of these methods and indicate their relative merits and disadvantages. Many of the procedures used here are discussed in the general references on evaporation techniques and thin films. References 3, 4, 5, and 6 are particularly useful.

A. Evaporation in a High Vacuum

Probably the simplest and most commonly used method of depositing films (particularly metals) is evaporation in a vacuum. The material to be deposited is heated in a vacuum usually of the order of 10^{-6} mm Hg until it evaporates. The substrate is placed such that the evaporating material strikes it. The prime requirement necessary for this technique is that one be able to hold the material in a boat or crucible which can be heated and which neither evaporates nor reacts with the material to be deposited at the temperatures required. Furthermore, if one is depositing a compound, the compound must either not dissociate or all constituents of the compound must evaporate at approximately the same temperature. Among the materials for which evaporation has been used are metals such as aluminum and silver[3] and semiconductors such as germanium[6,7,8,9] and PbS[10,11,12,13,14].

The schematic of the equipment which we used in our attempts at evaporation is shown in Figure 2-1. The substrate was attached to a tantalum plate which was heated by a tantalum wire heater located just above it. The NiO was heated in a tungsten boat. The source to substrate

distance was approximately 25 cm. and the vacuum was $2\text{-}3 \cdot 10^{-6}$ mm Hg. A shutter was placed between the source and the substrate in order that the source could be brought to temperature for a short period before evaporating anything onto the substrate.

With most materials, it is necessary to heat the substrate in order to obtain an epitaxial film. The temperature required however, varies with both film material and substrate material. A thermocouple was attached to the tantalum plate in order to monitor the substrate temperature during evaporation.

Nickel oxide evaporates at temperatures of the order of 1600°C. We found that it was difficult to heat the NiO in a tungsten boat sufficiently to evaporate it. The NiO appeared to decompose and leave nickel behind to subsequently evaporate. In addition the nickel tended to alloy with the boat and cause it to burn out. In view of these difficulties we concluded that straightforward evaporation of NiO films was not possible and that other deposition techniques would have to be used.

It should be noted that regardless of the material used as an evaporation boat, evaporation by resistance heating always results in the production of considerable heat in the boat which can be transmitted by conduction and radiation to the electrical leads used and to other adjacent materials. The method is, thus, quite likely to cause impurities to be evaporated along with the source material when the source material evaporates at high temperatures. We did make attempts to evaporate using graphite resistance heated boats but found that the electrical contacts used with the graphite became quite hot.

B. Chemical Transport

Cech and Alessandrini[15] have shown that epitaxial thin films of nickel oxide can be grown on MgO by decomposition of a nickel halide in an atmosphere of water vapor at a temperature of about 700°C. Optical measurements and electrical measurements[16,17] indicate that crystals grown by this method are at least as good as those grown by flame fusion techniques. Furthermore, there are indications[16,17] that the films may have better stoichiometry than crystals grown by flame fusion.

Our apparatus used to grow NiO by the method of Cech and Alessandrini is shown in Figure 2-2. The MgO substrate and a small quartz boat containing the nickel halide were placed within a piece of quartz tubing about one inch in diameter and three feet long. Vacuum tubing and rubber stoppers were used to connect the quartz tubing to a water aspirator at one end and a small flask containing water at the other end. A closed piece of glass tubing was used to allow a thermocouple to be placed near the substrate. The section of tubing containing the MgO and nickel halide was heated by a cylindrical furnace. By pumping on the tubing with a water aspirator the pressure can be lowered sufficiently to cause the water in the flask to boil at room temperature. The water vapor passes over the nickel halide and reacts with the halide vapor forming NiO on the MgO substrate. The reaction is as follows:

$$NiX_2 + H_2O \rightarrow NiO + 2HX$$

where X is one of the halogens. Cech and Alessandrini indicate that the MgO may act as a catalyst for the reaction.

Several films were made on MgO using the halide nickel bromide. The procedure was to bring the oven to ∿800°C with a valve at the flask closed so that the quartz tubing was shut off from the water vapor supply. Furthermore, during the time required for the oven to heat, the portion of the tubing containing the substrate and the nickel bromide was not in the oven. After the oven had reached a temperature of ∿800°C, the section of tubing containing the substrate and nickel bromide was placed in the oven and the water vapor was allowed to enter the tubing. By putting several pieces of MgO in the reaction chamber at one time several films could be made during one run. We made four or five films on MgO in two runs taking about two hours each. In preliminary runs we found that the nickel bromide tended to "pop" out of the quartz boat and by landing on the substrate cause the films to look spotted when observed. Thus, we put a piece of quartz over the quartz boat to prevent chunks of $NiBr_2$ from popping out. The temperatures given above are approximate only as the thermocouple was never actually in the vapor stream. For the MgO films, we placed the thermocouple outside the quartz tube between the tube and the oven wall. In our later attempts to grow films on other substrates, we located the thermocouple as shown in Figure 2-2.

Films obtained in the manner described above were epitaxial (see Figure 2-3 and Table 2-1) and had optical spectra similar to that measured by Newman and Chrenko between 3500 angstroms and 6000 angstroms (see the following chapter). At wavelengths shorter than 3500 angstroms, the MgO substrate material is not transparent. Thus, films on this material are not appropriate for transmission work in the ultraviolet or vacuum ultraviolet.

TABLE 2-1 SUMMARY OF LATTICE CONSTANT MEASUREMENTS

The following table gives, for the purpose of comparison, the relative spacing of the dots in Laue patterns for films of PbS, Ni, and NiO deposited in different ways. 5% would probably be a good estimate of the accuracy of the measurements. The theoretical values of the ratios of the spacing, based on the accepted lattice constants for the materials are:

$$\frac{NiO}{Ni} = .842 \qquad \frac{PbS}{Ni} = .590 \qquad \frac{PbS}{NiO} = .700$$

The table has been divided into four sections -- Section 1 gives the Laue pattern measurements for known PbS films (the method of deposition is described in Reference 14), Section 2 for known Ni Films, Section 3 for NiO films with lattice constants near that of NiO, and Section 4 for NiO films which have lattice constants near that of Ni. Several of the films in Section 3 have Laue pattern measurements somewhat on the small side in comparison with the theoretical value for NiO. A small Laue spacing would mean a large lattice constant. This and the scatter in the data are probably due to variations in electron microscope alignment on different days -- in particular voltage variations from day to day will give scatter in the data.

Material & Substrate	Method of Deposition	Relative Laue Spacing	Comparison to avg. Ni Spacing	Comparison to avg. PbS Spacing	Date of Electron Diffraction
PbS(CaF_2)	Evap.	5.05	$\frac{PbS}{Ni} = .602$	----------	
PbS (KCl)	Evap.	5.00	$\frac{PbS}{Ni} = .596$	----------	8/14/65
PbS (NaCl)	Evap.	5.07	$\frac{PbS}{Ni} = .604$	----------	9/1/65
PbS (NaCl)	Evap.	4.97	$\frac{PbS}{Ni} = .592$	----------	
Avg. PbS		5.02	$\frac{PbS\ avg}{Ni\ avg} = .598$		

Material & Substrate	Method of Deposition	Relative Laue Spacing	Comparison to avg. Ni Spacing	Comparison to avg. PbS Spacing	Date of Electron Diffraction
Ni(LiF)	Evap.	8.33	----------	$\frac{PbS}{Ni}$ = .603	6/14/65
Ni (LiF)	Evap.	8.50	----------	$\frac{PbS}{Ni}$ = .592	6/14/65
Ni (LiF)	Flash Evap. in Vacuum	8.35	----------	$\frac{PbS}{Ni}$ = .602	4/30/66
Ni (LiF)	Flash Evap. in Vacuum	8.38	----------	$\frac{PbS}{Ni}$ = .600	4/29/66
Avg. Ni		8.39	----------	$\frac{PbS}{Ni\ avg}$ = .598	
NiO (MgO)	Vapor Deposition	7.17	$\frac{NiO}{Ni}$ = .854	$\frac{PbS}{NiO}$ = .715	7/1/65
NiO (CaF_2)	Sput.	6.84	$\frac{NiO}{Ni}$ = .816	$\frac{PbS}{NiO}$ = .735	7/14/66
NiO (CaF_2)	Elec. beam in O_2	6.72	$\frac{NiO}{Ni}$ = .802	$\frac{PbS}{NiO}$ = .748	7/14/66
NiO (CaF_2)	Elec. beam in O_2	7.00	$\frac{NiO}{Ni}$ = .835	$\frac{PbS}{NiO}$ = .718	7/14/66
NiO (CaF_2)	Elec. beam in O_2	6.80-7.00	$\frac{NiO}{Ni}$ = .823	$\frac{PbS}{NiO}$ = .728	7/14/66
NiO (LiF)	Sput.	6.83	$\frac{NiO}{Ni}$ = .815	$\frac{PbS}{NiO}$ = .735	7/14/66
NiO (LiF)	Sput.	7.07	$\frac{NiO}{Ni}$ = .843	$\frac{PbS}{NiO}$ = .712	7/14/66

Material & Substrate	Method of Deposition	Relative Laue Spacing	Comparison to avg. Ni Spacing	Comparison to avg. PbS Spacing	Date of Electron Diffraction
NiO (LiF)	Flash Evap. in O_2 $2 \cdot 10^{-4}$ mm Hg	6.50	$\frac{NiO}{Ni} = .776$	$\frac{PbS}{NiO} = .773$	10/11/65
NiO (LiF)	Flash Evap. in O_2 $2 \cdot 10^{-4}$ mm Hg	6.57	$\frac{NiO}{Ni} = .783$	$\frac{PbS}{NiO} = .765$	10/11/65
NiO (LiF)	Flash Evap. in O_2 $2 \cdot 10^{-4}$ mm Hg	7.10	$\frac{NiO}{Ni} = .847$	$\frac{PbS}{NiO} = .707$	9/14/65
NiO (LiF)	Flash Evap. in air $2 \cdot 10^{-4}$ mm Hg	7.10	$\frac{NiO}{Ni} = .847$	$\frac{PbS}{NiO} = .707$	1/12/66
NiO (LiF)	Flash Evap. in air $2 \cdot 10^{-4}$ mm Hg	7.00	$\frac{NiO}{Ni} = .835$	$\frac{PbS}{NiO} = .718$	1/7/66
NiO (LiF)	Flash Evap. in O_2 $2 \cdot 10^{-4}$ mm Hg	6.50	$\frac{NiO}{Ni} = .776$	$\frac{PbS}{NiO} = .772$	10/11/65
NiO (LiF)	Flash Evap. in O_2 $2 \cdot 10^{-4}$ mm Hg	6.60	$\frac{NiO}{Ni} = .787$	$\frac{PbS}{NiO} = .762$	10/11/65

Material & Substrate	Method of Deposition	Relative Laue Spacing	Comparison to avg. Ni Spacing	Comparison to avg. PbS Spacing	Date of Electron Diffraction
NiO (LiF)	Flash Evap. in O_2 $2 \cdot 10^{-4}$ mm Hg	7.05	$\frac{NiO}{Ni}$ = .842	$\frac{PbS}{NiO}$ = .713	9/16/65
NiO (LiF)	Flash Evap. in air $2 \cdot 10^{-4}$ mm Hg	7.00	$\frac{NiO}{Ni}$ = .835	$\frac{PbS}{NiO}$ = .718	1/12/66
NiO (LiF)	Flash Evap. in Vac.	8.35	$\frac{NiO}{Ni}$ = .996	$\frac{PbS}{NiO}$ = .602	9/1/65
NiO (LiF)	Flash Evap in O_2 $5 \cdot 10^{-5}$ mm Hg	8.44	$\frac{NiO}{Ni}$ = 1.01	$\frac{PbS}{NiO}$ = .595	9/14/65
NiO (LiF)	Flash Evap. in Vac.	8.35	$\frac{NiO}{Ni}$ = .996	$\frac{PbS}{NiO}$ = .602	9/1/65
NiO (LiF)	Flash Evap. in Vac.	8.27	$\frac{NiO}{Ni}$ = .985	$\frac{PbS}{NiO}$ = .607	9/1/65
NiO (LiF)	Flash Evap. in Vac.	8.40	$\frac{NiO}{Ni}$ = 1.00	$\frac{PbS}{NiO}$ = .598	9/14/65
NiO (LiF)	Flash Evap. in Vac.	8.33	$\frac{NiO}{Ni}$ = .993	$\frac{PbS}{NiO}$ = .603	9/14/65

Material & Substrate	Method of Deposition	Relative Laue Spacing	Comparison to avg. Ni Spacing	Comparison to avg. PbS Spacing	Date of Electron Diffraction
NiO (LiF)	Flash Evap. in O_2 $2 \cdot 10^{-4}$ mm Hg	8.50	$\frac{NiO}{Ni} = 1.01$	$\frac{PbS}{NiO} = .592$	9/10/65
NiO (LiF)	Flash Evap.	8.40	$\frac{NiO}{Ni} = 1.00$	$\frac{PbS}{NiO} = .598$	9/14/65

We made numerous attempts to extend the above method to lithium fluoride substrates. Our first efforts were to use the identical procedure as used with the MgO. We found that the LiF either evaporated or reacted with HBr vapor given off in the chemical reaction of $NiBr_2$ and H_2O. Between 700°C and 800°C as measured on the thermocouple the LiF appeared in some cases to be etched on the surface and in others it actually left a deposit on the quartz tubing. NaF did not appear to give any better results.

We next used a separate heater around the portion of the quartz tube containing the substrate in order that the substrate could be kept at a lower temperature than the $NiBr_2$. In runs carried out with the substrate at about 300°C, there was no visible film formed on the LiF. No optical scans of these were made.

Runs made using NiI_2 instead of $NiBr_2$ were also unsuccessful. No film was formed in the runs at 550-600°C and the substrate was slightly etched at 650°C.

From our experiments, we concluded that the method of Cech and Alessandrini could not be extended to substrates of LiF. It should be pointed out, however, that there are undoubtedly many combinations of parameters which we did not use. Furthermore, in the cases where we indicate no film was formed there is the possibility that there was a very thin film present which was sufficiently transparent that it was not visible. This would be the case if films grew on LiF at a considerably slower rate than on MgO. We did not see sufficient indications that the method might work on LiF, however, to warrant any additional refinements to attempt to grow films with this method.

C. Flash Evaporation

One of the problems in the ordinary evaporation of compounds is that one or more elements may evaporate from the compound more readily than the others giving a film containing an excess of the element or elements which evaporate first. In flash evaporation one attempts to solve this problem by dropping small particles of the compound onto a surface held at a temperature sufficiently high to quickly evaporate all constituents.

Our flash evaporation equipment consisted of a modification of the scheme shown in Figure 2-1 whereby NiO powder was dropped continuously onto the heated tungsten boat. The tungsten boat was held at a temperature between 1800° and 2000°C as measured by an optical pyrometer. We fed the nickel oxide down a tantalum sluice into either a boron nitride or carbon cylinder which rested on the tungsten boat. The cylinder was 3/4 inch high with a hole about 3/8 inch in diameter and was about 1/32 inch thick. The purpose of the cylinder was to keep the NiO from bouncing off the tungsten boat. Some films were also made by merely dropping the NiO down a tantalum sluice directly onto the boat. This appeared to work reasonably well, although a moderate amount of NiO did bounce off the tungsten. The flash evaporation procedure worked very well for evaporating epitaxial nickel films as will be discussed later.

The NiO evaporations were carried out by dropping 200 mg of powder onto the hot tungsten boat over a period of twenty minutes. In some cases two or even three evaporations onto the same substrate were made to obtain thicker films. A few films were also made by dropping 500 mg of NiO powder onto the heated tungsten over a twenty minute

period. It should be noted that not all of the NiO evaporated since some bounced out of the tungsten boat even when the carbon cylinder was used.

Several nickel films were deposited on LiF with the substrates held at 450°C. Usually these films were epitaxial, and photographs of the electron diffraction patterns were used as standards to give the spacing of the diffraction pattern for nickel. Similarly, photographs of the electron diffraction patterns of NiO films on MgO and PbS films on NaCl, KCl and CaF_2 (Reference 14) were used as standards giving the spacing of the diffraction patterns for these materials. The diffraction patterns of films grown by flash evaporation were compared with known patterns of Ni, NiO and PbS to determine whether the films were nickel or nickel oxide. Table 1 summarizes the results.

From the electron diffraction patterns of films obtained by flash evaporating NiO powder in a vacuum of $5 \cdot 10^{-6}$mm Hg, we concluded that the flash evaporation of NiO powder, in general, yields nickel films. Three films deposited at $5 \cdot 10^{-6}$mm Hg on substrates of LiF held at 450°C had Laue patterns with nickel spacing. One additional film showed a Laue pattern with NiO spacing. One film made at a higher substrate temperature (650°C) also had the lattice constant of nickel. A typical electron diffraction pattern of a film made by flash evaporating NiO powder in a vacuum is shown in Figure 2-4.

Flash evaporation of NiO powder in either air or O_2 at $\sim 2 \cdot 10^{-4}$mm Hg with LiF substrates at 500 to 550°C in general yields films with at least a faint Laue pattern having the spacing of NiO. Usually, the diffraction patterns also contain rings. The intensity of the Laue pattern as

compared with that of the rings varied from film to film even though the evaporation conditions were nominally the same. A typical electron diffraction result is shown in Figure 2-5. The diffraction patterns indicate that the NiO films are not of as high a crystalline quality as the films of other materials deposited in this laboratory (for example, the PbS films discussed in Part One and Reference 14). Furthermore, the rings in the electron diffraction patterns may be due to impurities in the films. Annealing the films in either vacuum or air did not significantly improve the diffraction patterns.

From the optical transmission measurements of the flash evaporated films which are discussed in the next chapter and the electron diffraction patterns discussed above we concluded that the films obtained by flash evaporating nickel oxide in an oxygen atmosphere were probably oriented films of nickel oxide. However, other oxides (probably tungsten oxide) were evaporated and distorted the transmission curves.

D. Electron Beam Evaporation in O_2 Atmosphere

The main problem with the flash evaporation appeared to be that impurities were introduced in the films from the tungsten boat and related high temperature materials used in heating the NiO to its evaporation point. The electron microscope patterns indicated that films of NiO were probably being formed, however, when the flash evaporation was carried out in an O_2 atmosphere. Alessandrini[18] has removed epitaxial nickel films from NaCl substrates and converted the unsupported films to NiO by annealing at 450°C in air at about $1 \cdot 10^{-4}$ mm Hg. Furthermore Collins and Heavens[19] report that oriented NiO can be produced on oriented Ni

films at temperatures above 450°C. The above facts suggest that one might be able to grow NiO films by evaporating nickel in an O_2 atmosphere.

Evaporation by an electron beam has the advantage that the beam in striking the material to be evaporated heats it directly, thus reducing the possiblity of evaporating impurities. The apparatus which we used is shown schematically in Figure 2-6. A Veeco Model VeB-6 electron beam gun was used at 11 KV. A nickel plate was used as a shield on top of the cooled copper block to minimize the possibility of evaporating even small amounts of copper. Both alumina and carbon crucibles were used to hold globules of nickel metal. The beam was adjusted such that the crucible remained as cool as possible -- in any event the nickel could be heated considerably hotter than the crucible. The same substrate heater as used with the direct evaporation and flash evaporation was again used here.

The substrates were heated to 550°C in a vacuum of $5 \cdot 10^{-6}$mm Hg and O_2 was then continuously bled into the system to maintain a pressure of $1 \cdot 10^{-4}$mm Hg. The electron beam was adjusted to the desired intensity, and a shutter between the source and substrate opened to begin the evaporation. The evaporation rate was controlled with the electron beam intensity by watching the molten pool of nickel formed and keeping just below the point at which molten nickel began to pop out of the crucible.

We first used electron beam evaporation with LiF substrates and observed that the substrate surfaces became orange colored during the evaporation. To determine the cause of the coloring we next evaporated

onto LiF, KCl, NaCl, and glass substrates simultaneously. The LiF substrates were colored orange, whereas the other substrate materials appeared not to be colored. These tests eliminated the possibility that the coloring was due to some impurity being evaporated with the nickel.

A LiF substrate was heated to 550°C and the electron beam gun turned on the nickel source at a sufficiently low intensity that no nickel was evaporated. The LiF substrate was again colored. This test indicated that the effect was not associated with the evaporation of the nickel but rather was in some way associated with the use of the electron beam. Further tests showed that the coloring was neither due to O_2 nor N_2 in the vacuum system and that the coloring was more intense when the substrate was heated than when it was cold. A check of a piece of LiF used in the x-ray facility at Harvard in adjusting the x-ray beam indicated that the LiF did become orange colored after prolonged exposure to x-rays. This piece, of course, was cold when irradiated and the x-ray energy was undoubtedly different from that of any x-rays produced in the electron beam evaporation. The above tests all indicate that the coloring of the LiF is probably due to color centers produced in the LiF by x-rays created when the electron beam hits the nickel source. The optical spectra of the irradiated LiF will be discussed in the next chapter.

CaF_2 substrates were also affected by x-rays produced by the electron beam, however the effect was not as great when evaporations were made in an O_2 atmosphere as with the LiF substrates. The coloring, however, was fairly intense when nickel films (no O_2 atmosphere) were

evaporated. No visible coloring occurred with BaF_2 or quartz substrates. Again the optical spectra will be shown in the next chapter.

Several films grown on CaF_2 with the substrate at 550°C in O_2 at $1 \cdot 10^{-4}$mm Hg had Laue patterns with rings. The Laue patterns had the spacing of NiO (Table 2-1). The electron diffraction pattern of one such film is shown in Figure 2-7. The evaporation time for this film was eighteen minutes. By making consecutive evaporations onto the same substrate we produced one film with a total cumulative evaporation time of three hours and forty minutes with each separate evaporation lasting between twenty and sixty minutes. We took optical scans in between each evaporation. It was not possible to make one evaporation lasting this long because the vacuum system bell jar began to get quite hot after about one hour. The electron diffraction pattern of this film as well as those on quartz and the one on BaF_2 showed only rings. As will be discussed later, the optical spectra indicate that the films were all NiO. The incorsistencies which we found in the spectra can all be explained in terms of color centers in the substrates and variations in stoichiometry between different films.

In our procedure, the nickel was apparently oxidized at the source rather than at the substrate. After each evaporation we noted green nickel oxide powder around the region where the electron beam struck the nickel. Furthermore the optical spectra of films grown on glass microscope slides placed in the vacuum system but not heated to the substrate temperature indicated that the films were nickel oxide not nickel. The surface of the nickel where the electron beam strikes is probably oxidized and then the oxide subsequently evaporates.

E. Sputtering

In sputtering, the source material for the film is bombarded by positive ions which cause material to be emitted by the source with energies of the order of 10 to 30 eV.[20,21] The molecules removed from the source subsequently strike the substrate which is placed nearby, thus forming a film. Since the method does not require the source to be heated, it is applicable to materials with high as well as low evaporation temperatures, and, as in electron beam evaporation, contamination from materials required to heat the source is not a problem. The applicability of sputtering to a given material depends on the conductivity of the material rather than on its vapor pressure versus temperature. With the use of high frequency sputtering, however, even good insulators can be sputtered. Sputtered films are frequently epitaxial at lower substrate temperatures than are evaporated films, since the molecules hit the substrate with more energy and hence have a higher surface mobility than is the case with evaporation.[20]

For sputtering we used the R. D. Mathis Model SP210A sputtering module modified to contain a substrate heater and to allow the use of a smaller source target area. We used a Welch model 3101A turbomolecular pumping unit to evacuate the sputtering module. A schematic of the sputtering equipment is shown in Figure 2-8. The sputtering module was first pumped down to about $5 \cdot 10^{-5}$ mm Hg. The substrate heater was turned on and the substrate brought to temperature as determined by a thermocouple attached to the nickel plate holding the substrate and heated from beneath by a tantalum wire coil. The current to the tungsten filament was adjusted to about 7.4 amps, and the voltage to the primary

anode was set to about 150 volts. The sputtering gas which was a mixture of argon and oxygen was then introduced through the controlled leak valve until an arc appeared getween the filament and the primary anode. The anode current which we used was 1.8 amps, and the gas pressure during sputtering was .9 microns. Two magnetic coils as shown in the schematic were provided to confine the plasma and increase the plasma density. The target voltage used was about 1500 volts.

Our films were made by d.c. reactive sputtering. The gas which contains oxygen is ionized and the ions are drawn to the nickel source target by the negative 1500 volts applied to it. The oxygen molecules react with the nickel probably at the source and NiO is then sputtered onto the substrate. We made the plate holding the substrate out of nickel to minimize the possibility of contamination by other materials.

Sputtering colored the substrates in a manner similar to electron beam evaporation. Apparently color centers are created by the high energy ions and electrons striking the substrate material. LiF, for example, became reddish brown when placed in the unit with the gas discharge on but the target voltage set at zero to avoid sputtering any of the source.

Several films were epitaxial and had the lattice constant of nickel oxide (Table 2-1). Figures 2-9, 2-10, and 2-11 show the diffraction patterns of three of the films. The film in Figure 2-9 is on a LiF substrate and was made by sputtering for twenty minutes in a gas atmosphere of 20% 0_2 and 80% A at .9 microns (the gas was purchased premixed). The substrate was unheated. The film in Figure 2-10 was grown by sputtering for forty-five minutes in 20% 0_2 and 80% A at .9 microns but

with the substrate heated to 550°C. The films in Figures 2-9 and 2-10 are both on (100) faces of the LiF but the electron beam in Figure 2-9 is along a (100) direction whereas in Figure 2-10 it is along a (110) direction -- this is the reason the patterns look different. Figure 2-11 shows a film grown on a (111) face of CaF_2. The sputtering parameters for the film in Figure 2-11 were the same as for the film in Figure 2-10. In Figure 2-11 the electron beam is along a (110) direction in a (111) face. We would like to point out that our method of determining the lattice constant could not differentiate between the lattice constant of LiF and NiO. We, however, consider it very unlikely that the patterns in Figures 2-9 and 2-10 are due to the LiF rather than a film on the LiF. The lattice constant measurement can easily differentiate between CaF_2 and NiO, however, and thus there is very little doubt that the pattern shown in Figure 2-11 is due to a NiO film. It should be noted that this film has a very clear distinct Laue pattern with very few rings.

We sputtered three films on quartz -- one in a gas of 20% O_2 and 80% A and the other two in 10% O_2 and 90% A. Only one of these films was examined in the electron microscope, and its diffraction pattern showed broken rings.

In addition to the coloring of the substrates reported above, we found that the substrate surfaces and film surfaces looked quite poor on films sputtered for periods of around three hours. We did not investigate the effect of moving the substrate further away from the source where, perhaps, it might be struck by fewer ions and electrons. This could reduce both the coloring and apparent surface damage.

Our optical measurements indicated that the films had spectra very similar to the spectra of the NiO films made by electron beam evaporation. Our measurements on the films on quartz further indicated that the films grown in 10% O_2 and 90% A were more stoichiometric than the films grown in 20% O_2 and 80% A. Two films sputtered in pure O_2 (during the same sputtering run but on different substrates) did not have sharp edges at 3500 angstroms. The optical spectra will be discussed in detail in the next chapter.

F. Oxidation of Nickel Films

One common way of obtaining metallic oxides for physical measurements is to deposit a film of the metal and then oxidize this film by heating in an O_2 or air atmosphere. Optical measurements made on NiO films produced in this manner have been reported in References 16 and 22. The films were on quartz substrates and were polycrystalline.

We oxidized several films of nickel on LiF, starting with oriented nickel films rather than amorphous or polycrystalline ones. We deposited the nickel films both by direct evaporation and by flash evaporation. The substrate temperature in each case was 450°C. In the ordinary evaporations we wrapped nickel foil around tungsten filaments. We deposited several films in this manner, however we had considerable difficulty with the nickel alloying with the tungsten and causing the filaments to melt. We found that flash evaporation worked much better. In this we dropped 300 mg. of nickel powder onto a tungsten boat heated to 1650°C as measured by an optical pyrometer. The evaporation time was twenty minutes. We found only a slight tendency of the nickel to alloy with the

tungsten boats. Usually a tungsten boat could be used for several evaporations before burning out. A typical electron diffraction pattern of a nickel film is shown in Figure 2-12. This pattern shows some ring structure in addition to the Laue pattern. We also had some films with a considerably less intense ring pattern.

We oxidized one film in O_2 at approximately 300°C for three hours and a second in O_2 at approximately 500°C for eight hours. The diffraction patterns of these films showed only rings after oxidation.

We made optical scans of films oxidized at atmospheric pressure and of one oxidized at $2 \cdot 10^{-4}$ mm Hg. The optical results indicated that the oxidized films varied considerably in stoichiometry.

Our somewhat cursory attempts at oxidizing nickel films did not indicate much promise that epitaxial films could be made by any improvements of the method. One could, however, by studying the effects of various oxidation parameters in more detail probably find parameters which would give reasonably stoichiometric films. The films would probably be polycrystalline and contain considerable local strain.

G. Conclusion

In this chapter we have discussed several methods which we have investigated for producing epitaxial nickel oxide films, indicating the significant problems encountered with each. Again, we would like to point out that there remain many variations which we did not attempt. Our discussion, however, should give a good indication of the effects of at least some of the important parameters. Our work indicates that evaporation of nickel in an oxygen atmosphere and reactive sputtering are the most promising methods for depositing films on LiF and CaF_2. Either method

should give good optical quality films if the problems caused by color centers can be solved. One possibility is the use of either a laser beam or induction heating to evaporate the nickel in an O_2 atmosphere.

Our work further indicates the importance of careful control of deposition parameters and care in not introducing impurities onto the films. In order to get reliable optical measurements, as many checks as possible should be made to insure the spectra are not affected by impurities, lack of stoichiometry poor crystalline quality, or absorption bands in the substrate.

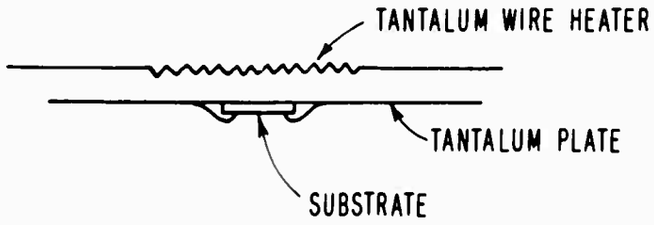

SOURCE TO SUBSTRATE DISTANCE ~10"

RESISTANCE HEATED
BOAT

FIG. 2-1 SCHEMATIC OF EVAPORATION EQUIPMENT

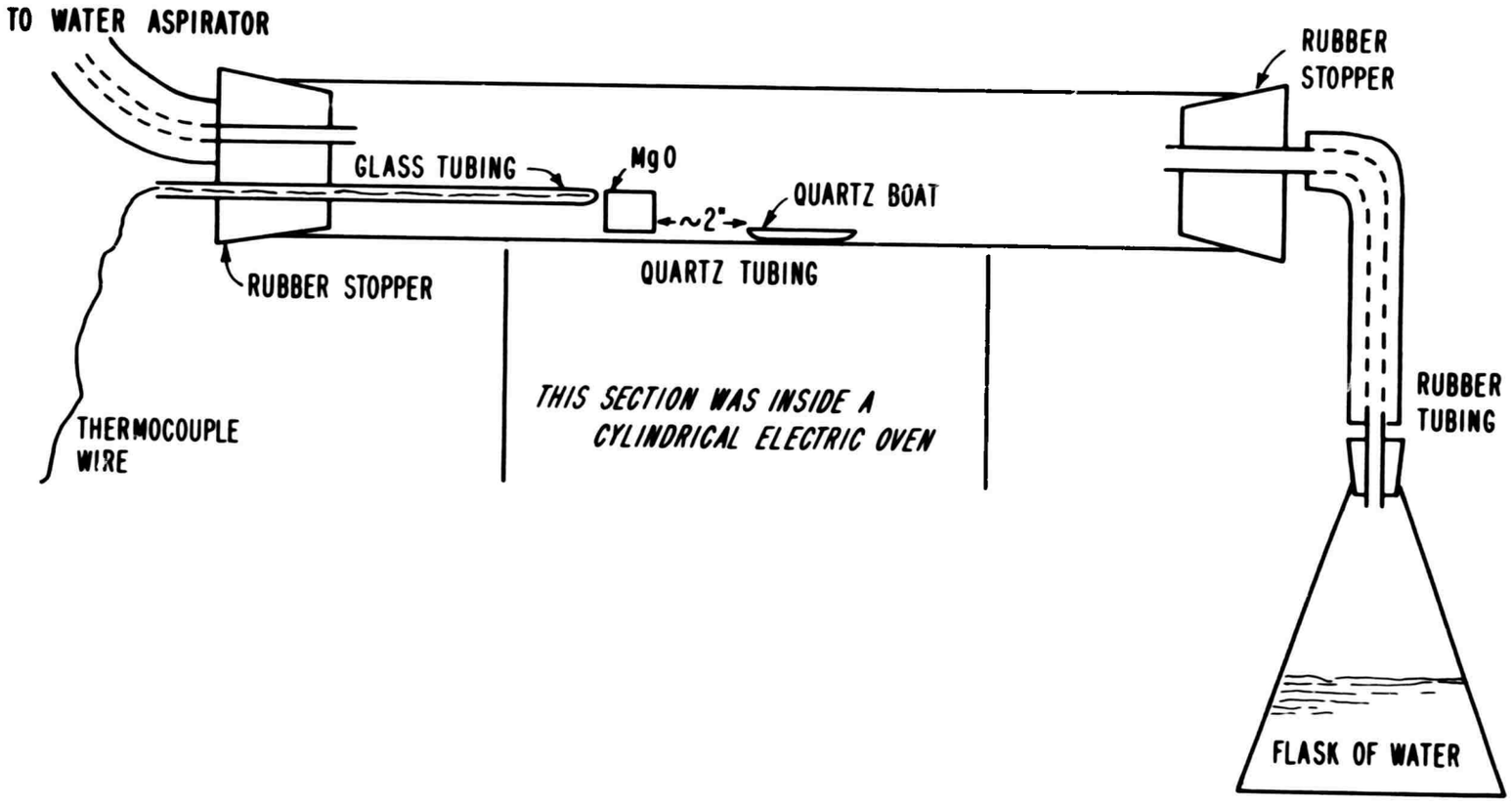

FIG. 2-2 SCHEMATIC OF CHEMICAL TRANSPORT APPARATUS

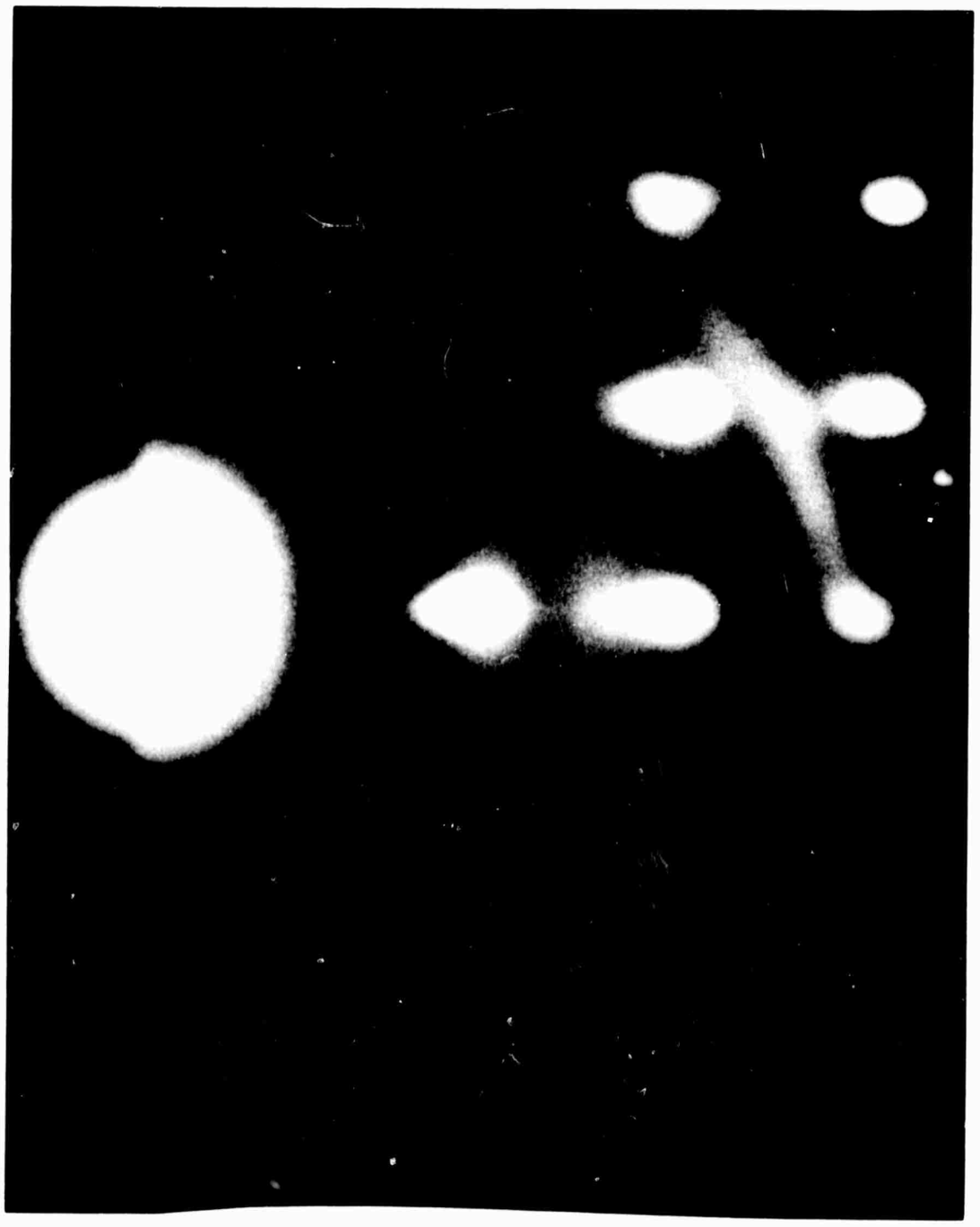

FIG. 2-3 ELECTRON DIFFRACTION PATTERN OF A NiO FILM GROWN BY VAPOR DEPOSITION ON A MgO SUBSTRATE.

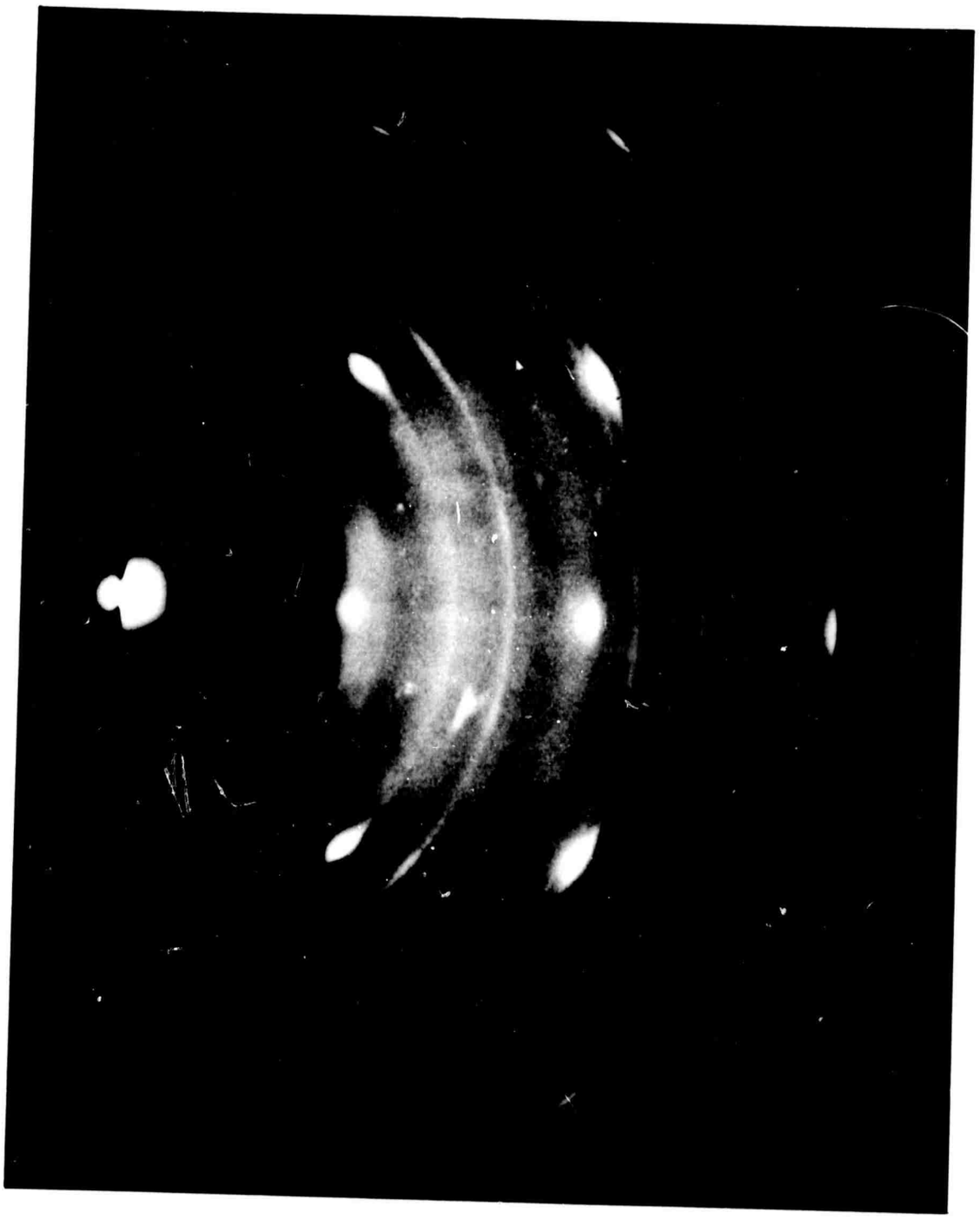

FIG. 2-4 ELECTRON DIFFRACTION PATTERN OF A FILM GROWN ON LiF BY FLASH EVAPORATING NiO POWDER IN A VACUUM OF 5.10^{-6} mm Hg. THE EVAPORATION TIME WAS TWENTY-TWO MINUTES.

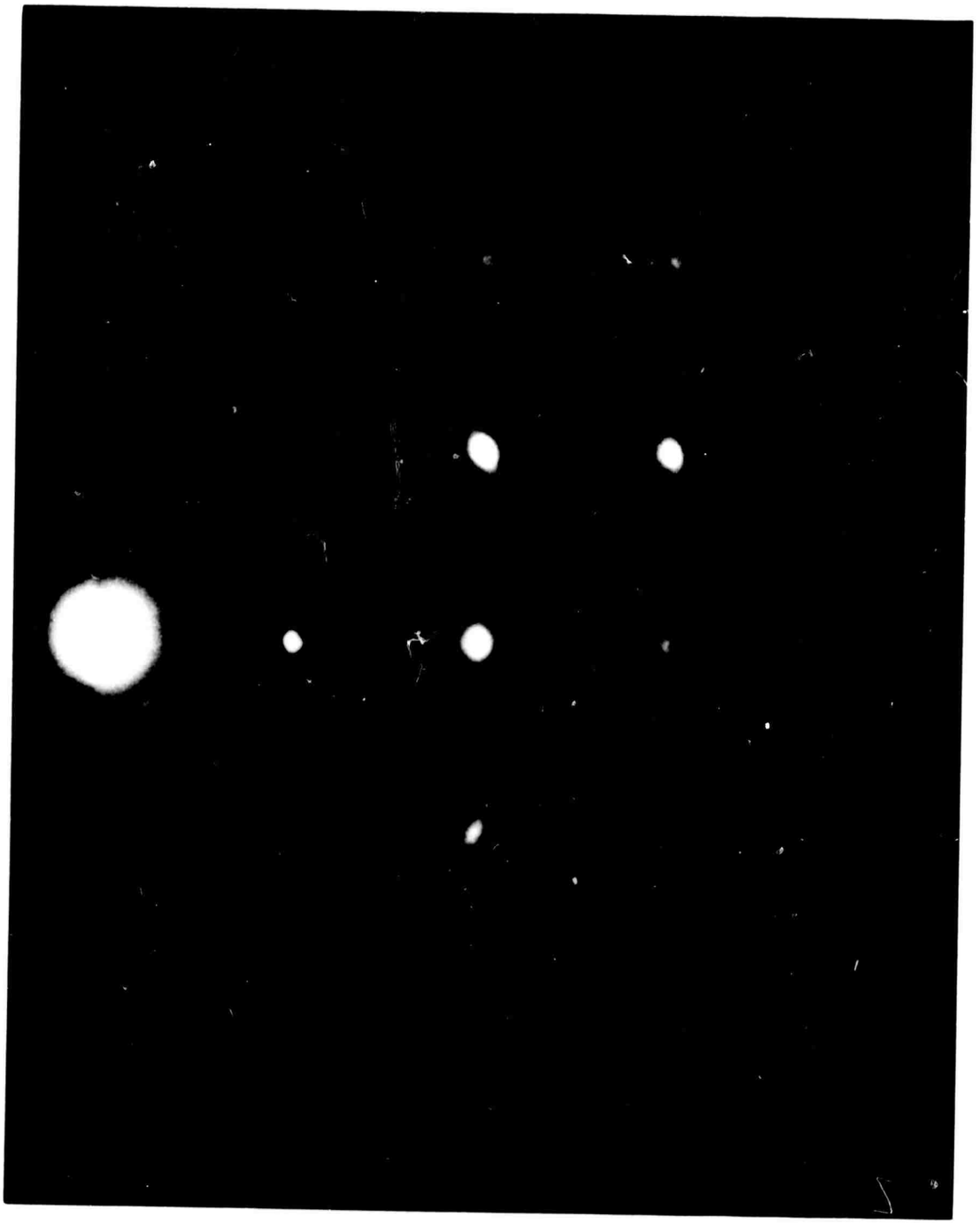

FIG. 2-5 ELECTRON DIFFRACTION PATTERN OF A FILM GROWN ON LiF BY FLASH EVAPORATING NiO POWDER IN AN O_2 ATMOSPHERE OF 2.10^{-4} mm Hg. THE EVAPORATION TIME WAS FORTY MINUTES.

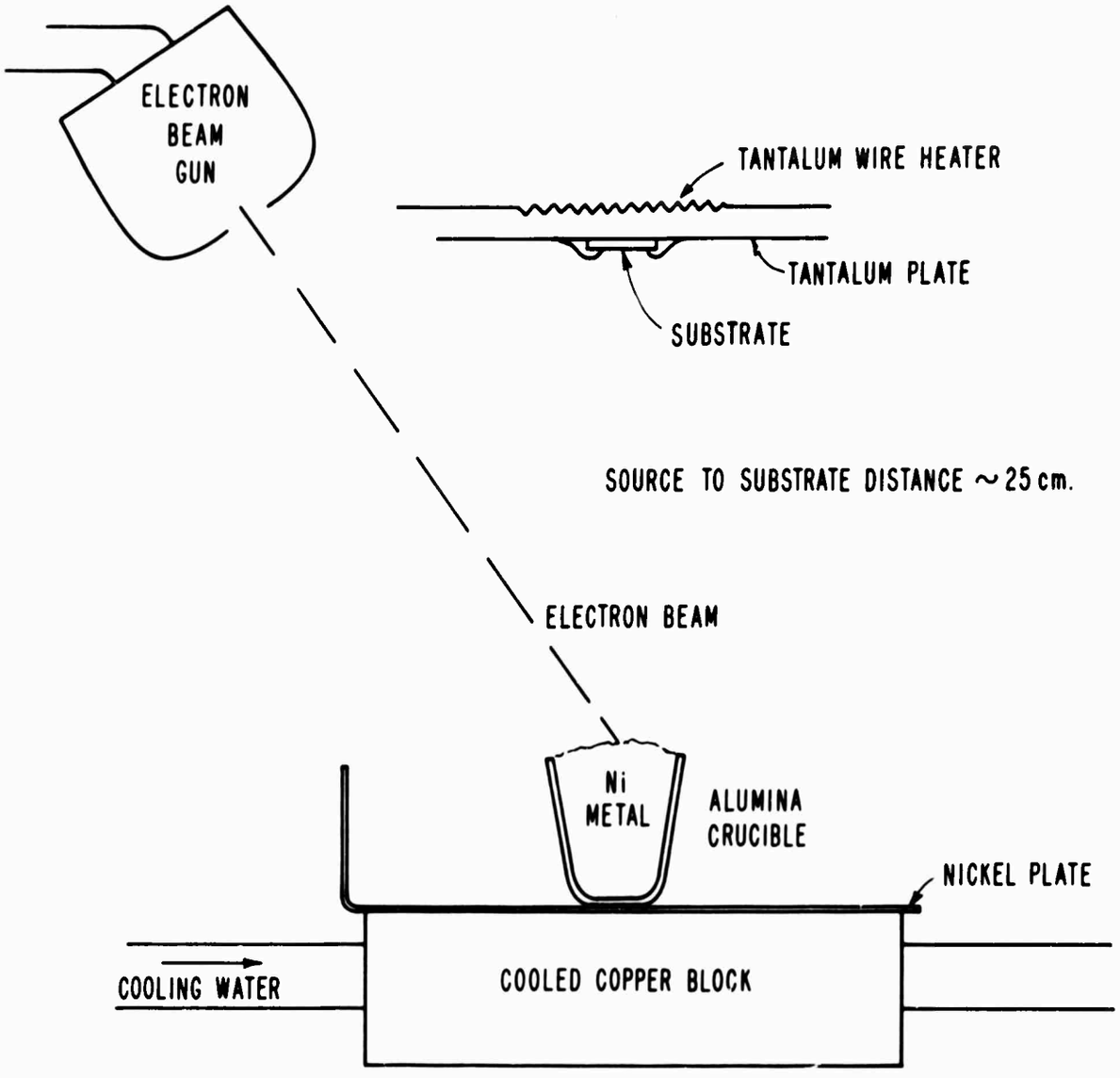

FIG. 2-6 SCHEMATIC OF ELECTRON BEAM EVAPORATION EQUIPMENT

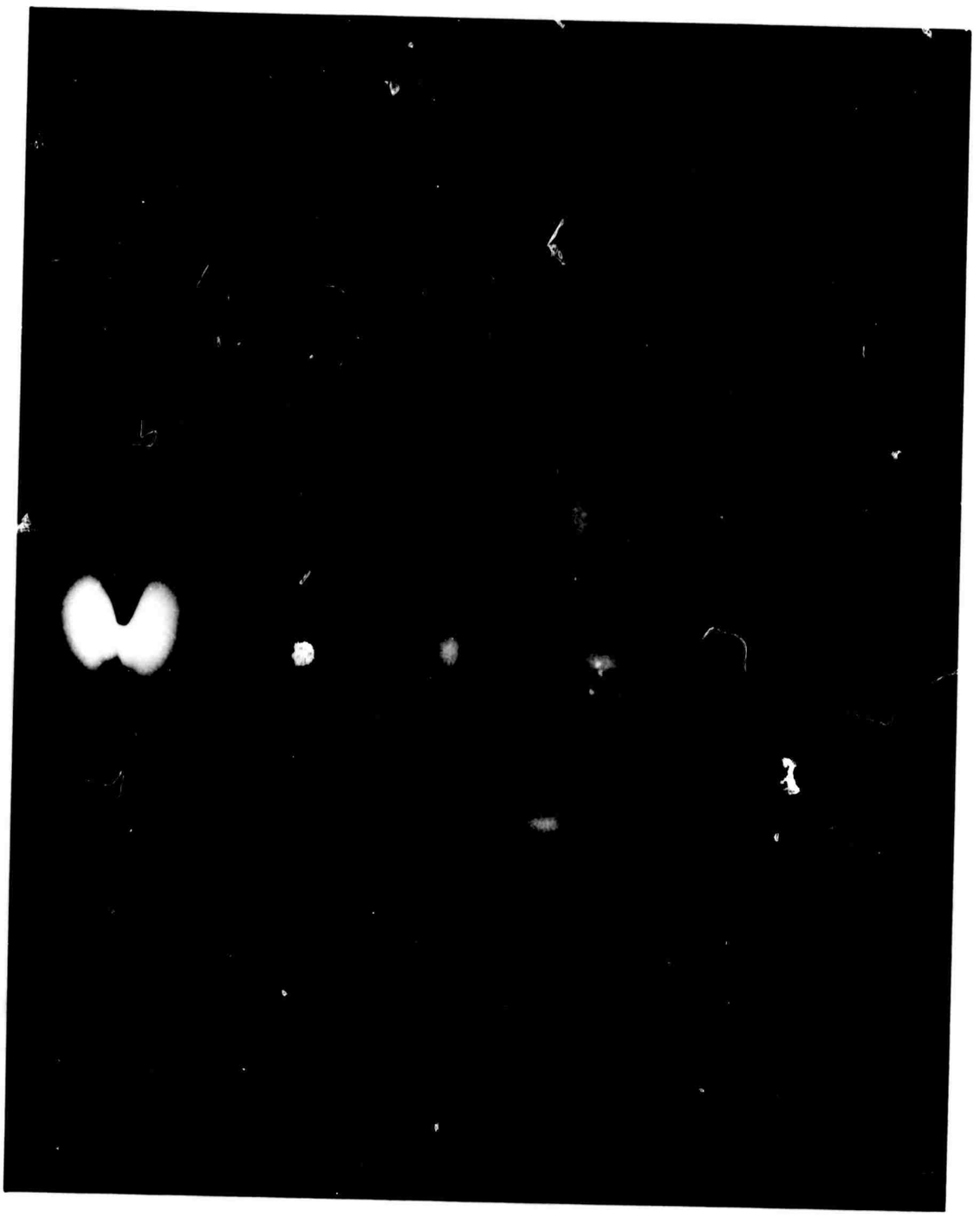

FIG. 2-7 ELECTRON DIFFRACTION PATTERN OF A FILM GROWN ON CaF_2 BY ELECTRON BEAM EVAPORATION OF Ni IN AN O_2 ATMOSPHERE OF 1.10^{-4} mm Hg. THE EVAPORATION TIME WAS EIGHTEEN MINUTES.

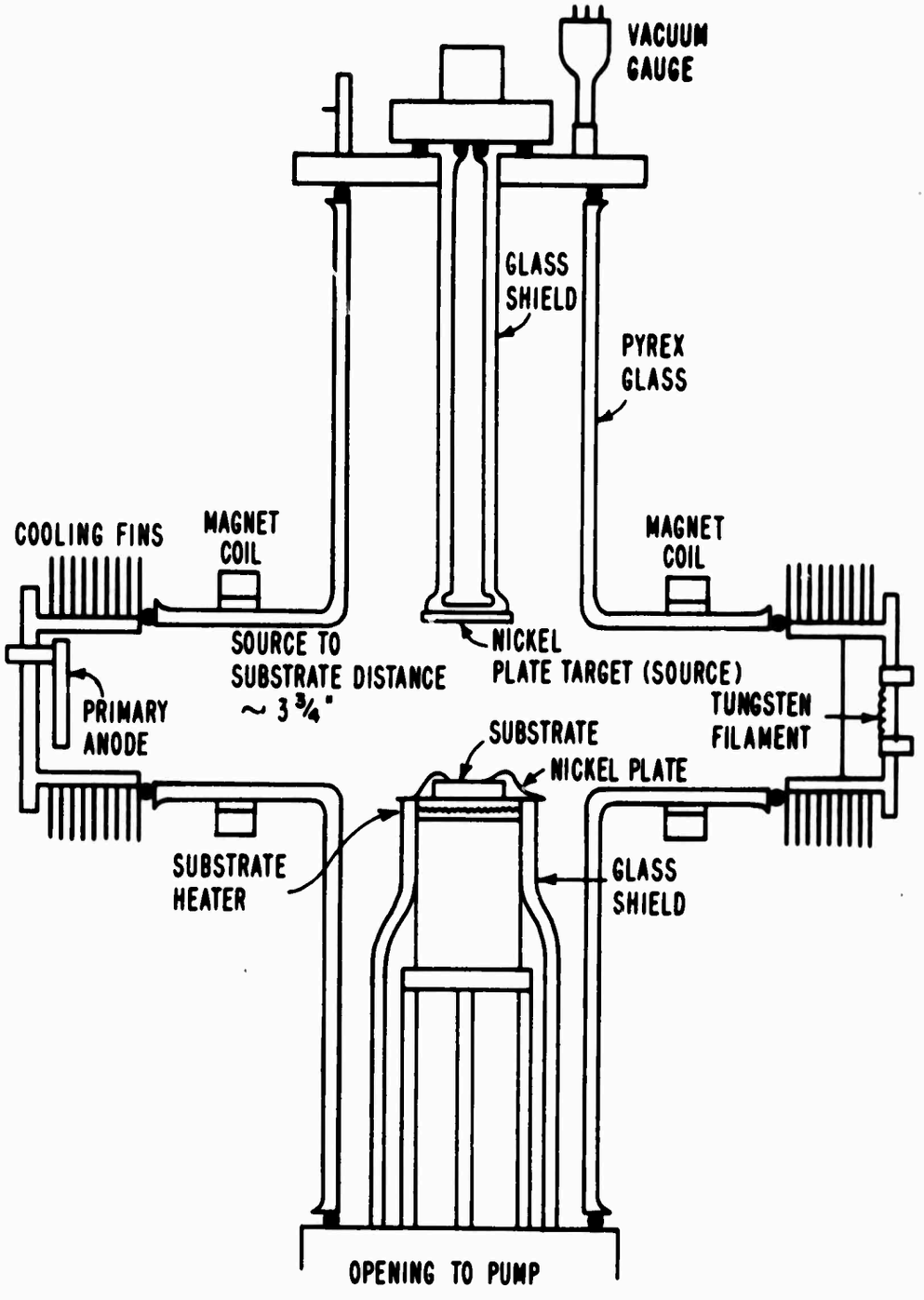

FIG. 2-8 SCHEMATIC OF SPUTTERING EQUIPMENT

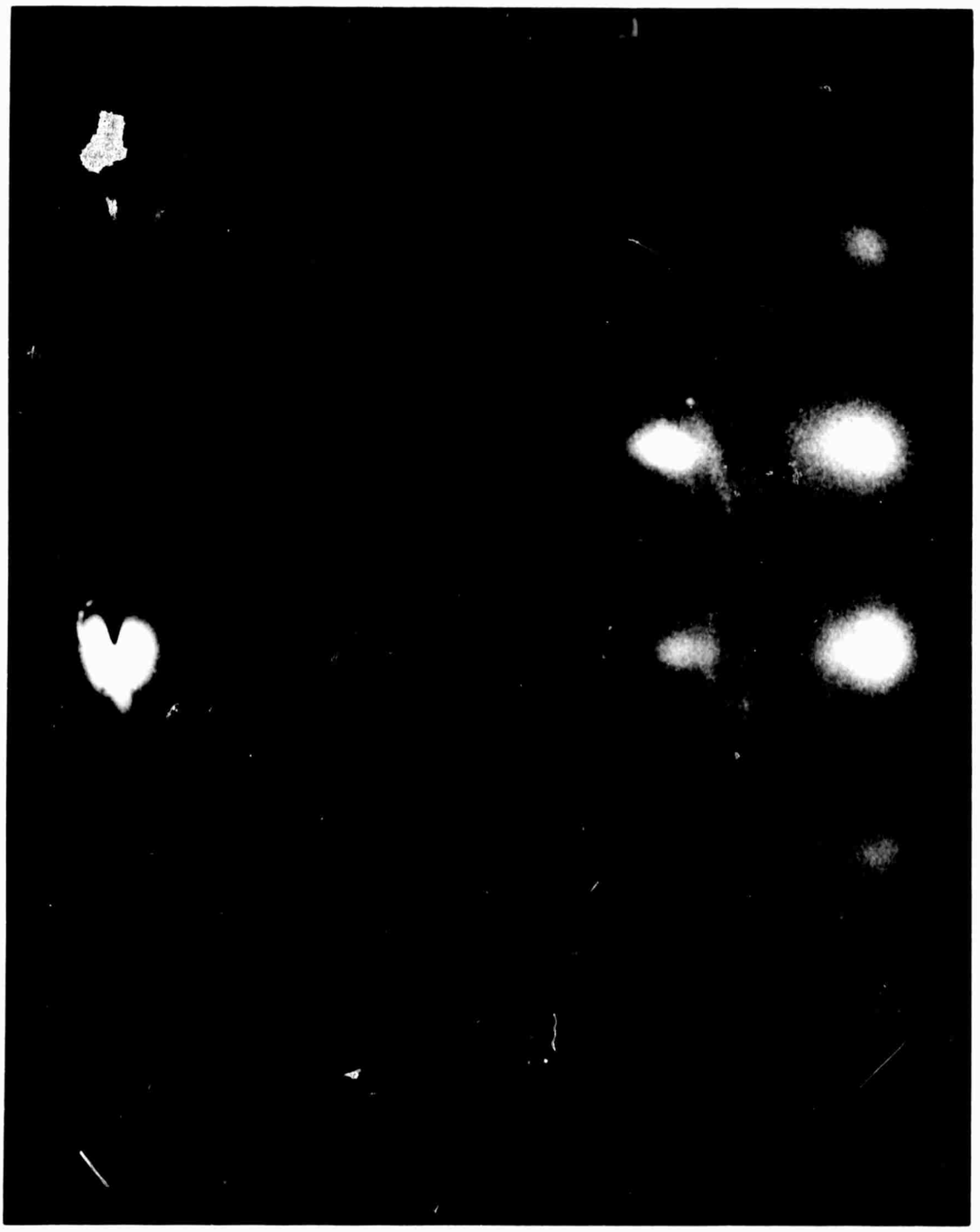

FIG. 2-9 ELECTRON DIFFRACTION PATTERN OF A FILM GROWN ON LiF BY SPUTTERING Ni IN A 20% O_2, 80% A ATMOSPHERE OF .9 MICRONS. THE SPUTTERING TIME WAS TWENTY MINUTES.

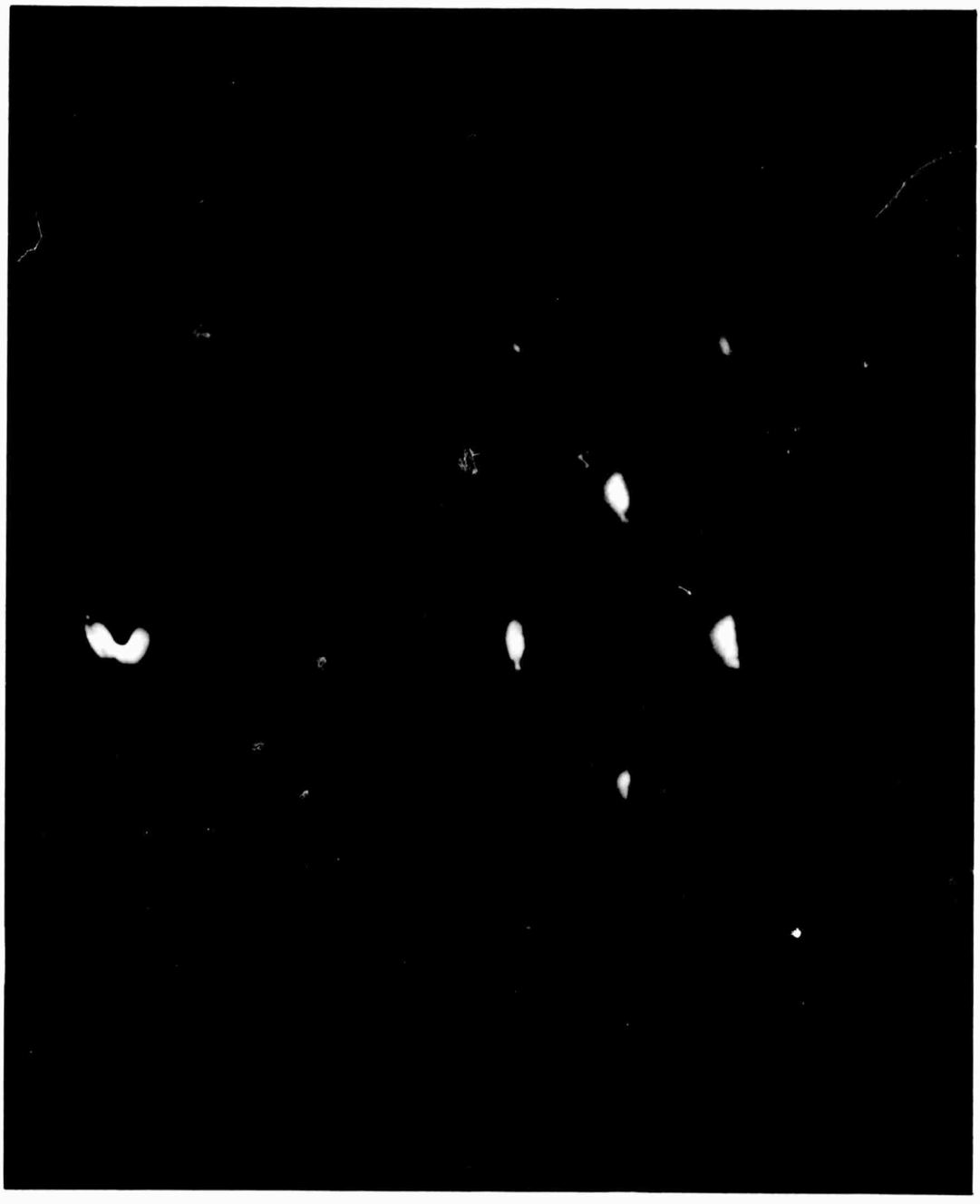

FIG. 2-10 ELECTRON DIFFRACTION PATTERN OF A FILM GROWN ON LiF BY SPUTTERING Ni IN A 20% O_2, 80% A ATMOSPHERE OF .9 MICRONS. THE SPUTTERING TIME WAS FORTY-FIVE MINUTES.

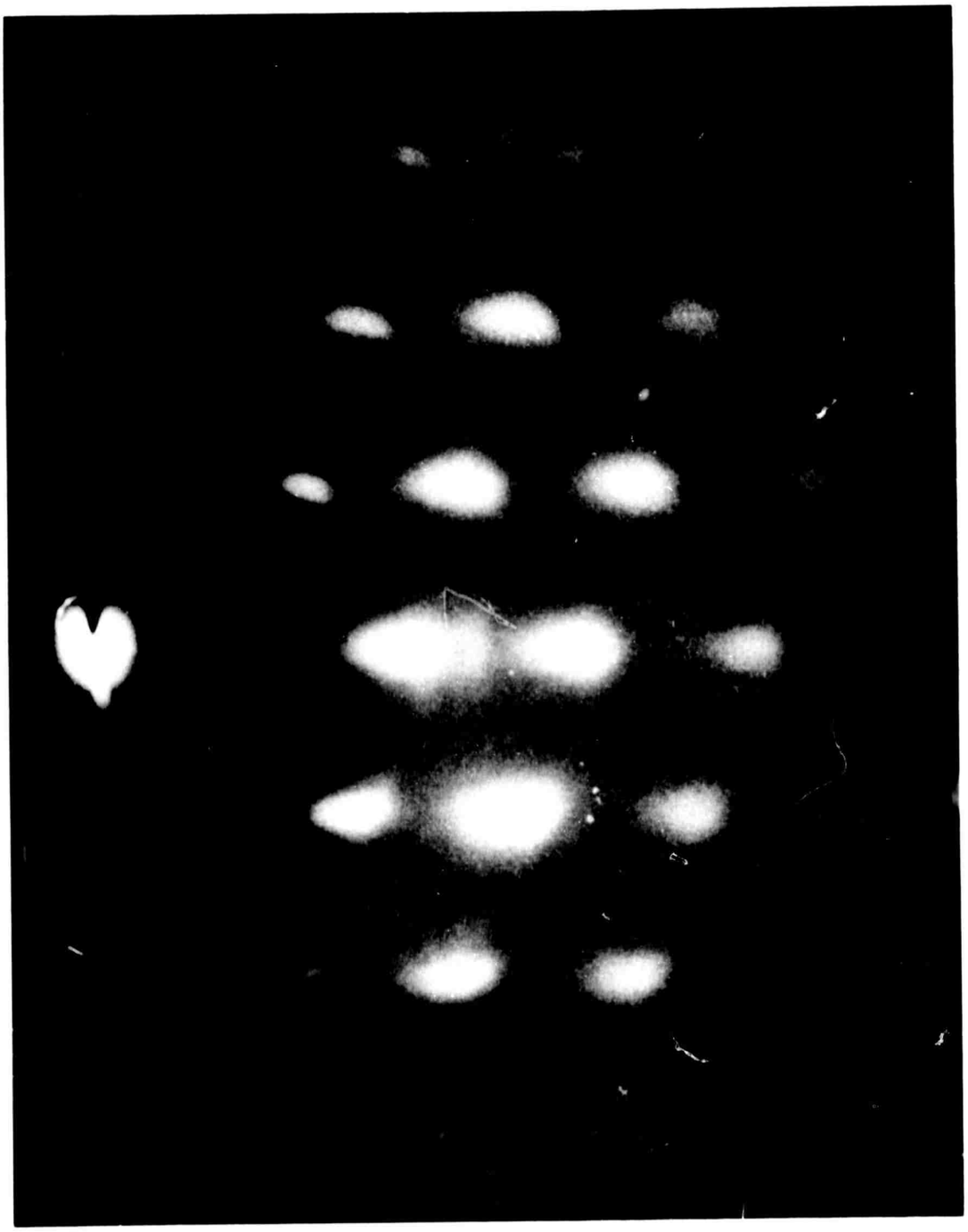

FIG. 2-11 ELECTRON DIFFRACTION PATTERN OF A FILM GROWN ON CaF_2 BY SPUTTERING Ni IN A 20% O_2, 80% A ATMOSPHERE OF .9 MICRONS. THE SPUTTERING TIME WAS FORTY-FIVE MINUTES.

FIG. 2-12 ELECTRON DIFFRACTION PATTERN OF A Ni FILM GROWN ON LiF BY FLASH EVAPORATING Ni POWDER IN A VACUUM. THE EVAPORATION TIME WAS TWENTY MINUTES.

BLANK PAGE

Chapter Two

BIBLIOGRAPHY

(1) Handbook of Chemistry and Physics (Chemical Rubber Publishing Company, Cleveland, 1955).

(2) Optovac Optical Crystals Bulletin No. 50, (Optovac Inc., North Brookfield, Mass., Jan. 1964).

(3) L. Holland, Vacuum Deposition of Thin Films (John Wiley and Sons, Inc., New York, 1960).

(4) O. S. Heavens, Optical Properties of Thin Solid Films (Butterworths Scientific Publications, London, 1953).

(5) M. H. Francombe and H. Soto, Single Crystal Films (MacMillan, New York, 1964).

(6) P. M. Grant, Technical Report No. HP-14, Gordon McKay Laboratory, Division of Engineering and Applied Physics, Harvard University, 1965.

(7) G. G. Via and R. E. Thun, Natl. Symposium on Vacuum Technol. Trans. 8, 950 (1962).

(8) J. Marucchi and A. Nifontoff, Compt. Rend. 249, 435 (1959).

(9) B. W. Sloope and C. O. Tiller, J. Appl. Phys. 33, 3458 (1962).

(10) R. B. Schoolar, J. D. Jensen, and J. N. Zemel, Bull. Am. Phys. Soc. Ser. II, 8, 63 (1963).

(11) R. B. Schoolar and J. N. Zemel, J. Appl. Phys. 35, 1848 (1964).

(12) R. B. Schoolar and J. R. Dixon, Phys. Rev. 137, A667 (1965).

(13) P. R. Wessel (to be published).

(14) C. E. Rossi and William Paul, J. Appl. Phys. 38, 1803 (1967).

(15) R. E. Cech and E. I. Alessandrini, Trans. A.S.M. 51 150 (1959).

(16) R. Newman and R. M. Chrenko, Phys. Rev. 114, 1507 (1959).

(17) S. Koide, Journal of the Phys. Soc. of Japan, 20 123 (1965).

(18) E. I. Alessandrini, J. Appl. Phys. 35, 1606 (1964).

(19) L. E. Collins and O. S. Heavens, Proc. Phys. Soc. (London) B70, 265 (1957).

(20) E. H. Blevis, "Hot Cathode and Radio Frequency Sputtering", distributed by R. D. Mathis Co., Long Beach, California.

(21) G. K. Wehner, Phys. Rev. 114, 1270 (1959).

(22) W. P. Doyle and G. A. Lonergan, Disc. Faraday Soc. No. 26 27-33 (1958).

Chapter Three

OPTICAL RESULTS

A. Description of Equipment

Both reflectivity and transmission measurements were made on films. For these, three different optical systems were used -- a Cary 14 spectrometer, a Jarrel Ash 82-000 Ebert Monochrometer, and a McPherson model 225 vacuum spectrometer.

The majority of the transmission measurements were made with the use of the Cary 14. A sample holder was fabricated to hold the 1 cm. by 1 cm. film samples in the normal Cary 14 sample cell chamber. The sample always was placed where the beam was smallest, however, even then the beam covered an area about .2 cm on a side. We always attempted to position the sample such that the transmission measurements were made on the best portion of the film surface. The sample holder arrangement did not allow for a great deal of freedom in adjusting the position of the sample in the beam, thus, one would expect pinholes and cleavage planes to have had some effect on the measurements. Since the slit width and thus, the beam size varies with wavelength in the Cary instrument there is the possibility that the structure of the transmission can be distorted somewhat as the beam moves on to or off of areas of the film having pinholes or cleavage planes.

The optical system using the Jarrel Ash 82-000 instrument was used for both reflectivity and transmission measurements. This system is fully described in References 1 and 2 as well as Part one and will not be discussed further here.

At wavelengths smaller than about 2200 angstroms the McPherson Model 225 vacuum spectrometer was used in conjunction with the optics shown in Figure 3-1. The system shown was enclosed in a vacuum tight container

which was pumped out through the McPherson. The phototube was an RCA 1P21 with a sodium salycilate coated glass microscope slide in front of the cathode. The tube was rotated in front of the sample for reflectivity measurements and behind the sample for transmission measurements. The sample was moved out of the beam when detecting I_o. The sample was near the beam focus and thus the beam area was quite small ($\sim$1 mm. on a side). The position of the sample could be adjusted such that the beam struck the best portion of the sample surface.

A hydrogen lamp (Figure 3-2) with a LiF window was attached to the entrance slit assembly of the spectrometer. The arc was maintained between two aluminum electrodes separated by a hollow ceramic insulator. The electrode nearest the entrance slit was hollow thus allowing the light to pass on to the slit. The lamp was operated at about 3 mm Hg with a continuous flow of hydrogen gas. The power source was a voltage regulated D.C. supply delivering about 300 ma at about 2200 volts across a ballast resistor in series with the lamp. The light source and optical system were designed by Larry Ladd of this laboratory.

The recording electronics used with the McPherson are shown in Figure 3-3. The chopper, positioned at the exit slit, was an electrically driven tuning fork with attached shutters and was manufactured by American Time Products. The unit was designed for 200 c.p.s. and had a reference signal which could be directly applied to the P.A.R. Lock-In Amplifier. This type of chopper was small and compact and was placed inside the vacuum chamber. The remaining phase sensitive detection equipment and recorder are fairly standard.

We originally detected the light by recording the d.c. output of the phototube directly on the Brush Recorder. This worked reasonably well except that it was necessary to subtract the dark current from the total signal. The addition of the chopper eliminated the dark current problem and allowed higher amplifications. The higher amplifications in turn permitted smaller slit widths. The light source drifted continually downward apparently due to the accumulation of aluminum on the LiF window. Our measurements were made taking an I_o run before and after the I_t (or I_r) run. The two I_o runs were then averaged to correct for the drift. We found it necessary to use slit widths of up to 1 mm.

B. Transmission Results

Figure 3-4 shows the transmission spectra of several substrates chosen randomly from the substrate material used in growing the films. The curves indicate quite clearly that neither glass or MgO is usable at wavelengths much below 3500 angstroms. The MgO (obtained from Norton Co.) transmits only about 70% in the wavelength region where it is nominally transparent. The CaF_2 shows negligible structure in the region where measurements were made and the quartz is quite good to 2500 angstroms, showing only a slight fall off at 2200 angstroms.

Two LiF substrates, one cleaved and the other polished, were scanned down to ~1250 angstroms. Both pieces showed a considerable drop in transmission in the vacuum ultraviolet. The polished piece also showed structure near 2000 angstroms. Apparently some of the LiF which we obtained had impurities in it since the third piece scanned

only to 2000 angstroms also showed a dip at this wavelength. Some (not all) of the films grown by flash evaporation which were scanned into the vacuum ultraviolet showed structure at 2000 angstroms which we believe to be due to the substrate material.

Figures 3-5 and 3-6 show the spectra of two films of different thickness grown on MgO by the chemical transport method described in Chapter 2. The structure is due to transitions between the crystal field split d levels and agrees quite well with the results of Newman and Chrenko.[3] (See also Figure 1-4, which shows the results of Newman and Chrenko). Both films were epitaxial having the cubic pattern shown in Figure 2-3. These films on MgO, of course, are useless for measurements at wavelengths less than 3500 angstroms as can be seen from Figure 3-4. They do serve as a standard of comparison for some of the results to be discussed later.

Figure 3-7 shows a transmission spectrum of a film grown on LiF by flash evaporating NiO in an 0_2 atmosphere. Three separate evaporations lasting twenty minutes each were used. The 0_2 pressure was $2 \cdot 10^{-4}$mm Hg and the substrate temperature was 575°C. The film is transparent in the visible and absorbs in the ultraviolet as one expects for NiO. However, Figure 3-8 shows the transmission of a film madeby heating a tungsten boat to 1850°C (50°C above the temperature used in the flash evaporations) for one hour in 0_2 at $2 \cdot 10^{-4}$mm Hg. One can see that the transmission falls in the same general manner as that of the film in Figure 3-7. From this we concluded that other materials (probably tungsten oxide) were being evaporated in sufficient quantities to significantly affect the optical measurements.

Figure 3-9 shows the optical spectra of four nickel films on LiF.

The films were grown by flash evaporation with substrate temperatures of 450°C. In most cases this appeared to give epitaxial films (see Figure 2-12 in Chapter 2), however, in some cases films grown in this manner were polycrystalline. Only one of the films in Figure 3-9 (the thinnest) was checked with the electron microscope and this one happened to be polycrystalline. We later oxidized the films in Figure 3-9 and were concerned that use of the electron microscope might color the LiF substrates thus interfering with the optical measurements of the oxidized films. During our work we did not investigate the effect of the sample crystallinity on the transmission spectra of the nickel films. Our main interest in these films was to demonstrate the distinct difference of the spectra of Ni films with our NiO films. One sample in Figure 3-9 shows a somewhat different shape from the other three. This difference may be due to some oxide impurity in the film. The shift in the minimum at 2300 angstroms could also be due to the dip in transmission near 2000 angstroms which appeared in some of the LiF substrates (see Figure 3-4). The absorption coefficient of nickel derived by Ehrenreich, Philipp, and Olechna[4] from a Kramers Kronig analysis of the reflectivity of nickel is shown in Figure 3-9A along with the measured reflectivity. The transmission of the films in Figure 3-9 agrees well with the absorption constant shown in Figure 3-9A except at wavelengths less than 1500 angstroms. The disagreement at short wavelengths is undoubtedly due to the fall off of the transmission of the LiF substrate (see Figure 3-4).

Figure 3-10 shows the ultraviolet and vacuum ultraviolet transmission spectrum of one of the films grown by flash evaporating NiO in a vacuum of $3 \cdot 10^{-6}$ mm Hg. The electron diffraction pattern of this

film had the spacing of nickel. The spectrum appears to be similar to that of the nickel films except near 2500 angstroms where second order grating reflections distort the measurements. It should be noted that the film made by flash evaporating NiO in 0_2 as well as all the films of NiO which will be discussed shortly have transmissions which fall as one goes from 2500 angstroms to 2000 angstroms in contrast to the film of Figure 3-10.

Figure 3-11 shows the transmission spectra of three of the films in Figure 3-9 after they were oxidized. The sample numbers in Figures 3-9 and 3-11 are the same. Sample 1 was oxidized at 550°C for two hours in 0_2 at $2 \cdot 10^{-4}$ mm Hg, and Samples 2 and 3 were oxidized for three hours in a stream of oxygen at 300°C and room pressure. The three samples show an absorption edge beginning at 3500 to 3800 angstroms and a further onset of absorption at 2200 to 2500 angstroms. The oxidized films have spectra considerably different from those of the nickel films -- in particular they are considerably more transparent between 3500 and 6500 angstroms and show quite different behavior between 2000 and 2500 angstroms. The film made by flash evaporating NiO in an 0_2 atmosphere has a transmission spectrum (Figure 3-7) similar to that of Sample 2 in Figure 3-11 except that the change in slope at 3000 angstroms is much less evident in the film made by flash evaporation. The differences in the three spectra of Figure 3-11 indicate that the optical properties of films made by oxidizing a metal depend considerably on the method of oxidation. The differences are probably due to variations in stoichiometry and imply that oxidized metal films can probably not be used to obtain accurate optical data for the metallic oxide. The use of oxidized metal films to obtain optical information has been fairly

common -- for example, References 3 and 5 report transmission measurements made on oxidized nickel films and Reference 6 reports measurements for oxidized magnesium films.

Figure 3-12 demonstrates the color center problem encountered with the LiF when we used the electron beam gun for evaporation. Sample 5 is a film made by evaporating nickel in an atmosphere of oxygen at $2 \cdot 10^{-4}$ mm Hg for ten minutes onto a substrate at 550°C. This was one of the first films we made using the electron beam gun and the evaporation rate was quite low compared to what we used later, thus, very little nickel was evaporated. The substrate looked as if an orange film had been deposited. As described in Chapter 2, we next deposited simultaneously on LiF, KCl and glass and found that only the LiF became colored. Sample 6 in Figure 3-12 is a LiF substrate which was held at 550°C in a vacuum of $3 \cdot 10^{-6}$ mm Hg while the electron beam gun was operated at an intensity lower than that necessary to evaporate the nickel source. The electron beam gun was on for thirty minutes while the shutter in the evaporation apparatus was open. Again the substrate surface was orange colored -- apparently due to either x-rays created when the beam hit the nickel source or due to electrons scattered onto the substrate by the source.

Samples 7 and 8 in Figure 3-13 are films made by evaporating nickel in an atmosphere of O_2 at $1 \cdot 10^{-4}$ mm Hg onto substrates of CaF_2. The evaporation times were twenty and ten minutes respectively and the substrate temperatures were 550°C. It should be noted that the evaporation rate varied both during a run and between runs since it was controlled only by keeping the electron beam intensity such that a small pool of molten nickel existed around the point where the beam struck the nickel

source. Films grown in this manner had diffraction patterns showing Laue spots (with NiO spacing) in combination with rings or twinning. The pattern of one such film is shown in Figure 2-7.

The films in Figure 3-13 show the edge typical of NiO beginning in the region near 3750 angstroms. They also show the fall in transmission beginning at ~2300 angstroms which we found in almost all other NiO films. The minimum at 3000 angstroms is probably due to the minimum in $(1-R)^2$ which occurs in NiO at 3100 angstroms (see Figures 3-36 and 3-39) in combination with the increasing absorption constant as one goes to shorter wavelengths. A minimum in transmission would be expected only in the very thin films where the transmission depends more on $(1-R)^2$ than on the absorption.

Figure 3-14 shows the results of transmission measurements made between successive evaporations onto the same CaF_2 substrate. The evaporations were again made using the electron beam gun on a nickel metal source in O_2 at $1 \cdot 10^{-4}$ mm Hg. The substrate temperature was 550°C and the cumulative evaporation time (lowest transmission in Figure 3-14) was three hours and forty minutes. The transmission spectra show a sharp edge beginning between 3750 and 3700 angstroms which shifts with thickness due to interference. The two thinnest films showed small dips in the transmission near 3800 angstroms which could be due to the d level absorption seen at this wavelength in films grown on MgO by vapor deposition. Unfortunately the interference fringes made it impossible to determine whether there was an absorption at 3800 angstroms in the thicker films. It should be noted that the film remains quite transparent at wavelengths greater than 4000 angstroms as the film thickness

is increased. Newman and Chrenko (Reference 3) have shown that the transparency of NiO at wavelengths less than ∿4000 angstroms is associated with good stoichiometry.

Figure 3-15 compares the transmission spectrum of a film grown on MgO by vapor deposition with that of the thickest film of Figure 3-14. Aside from the interference fringes in the film grown by electron beam evaporation the transmission spectra are very similar. The interference fringes make it impossible to determine whether any faint d level absorptions are present in the film on CaF_2. The only electron diffraction measurement made on the thick film on CaF_2 was made after the last evaporation. This pattern showed sharp rings. Other thinner films grown by the same method showed a Laue pattern with NiO spacing and rings. We feel that the electron diffraction results and the spectra, shown in Figures 3-14 and 3-15 indicate that the films grown by evaporating Ni in an O_2 atmosphere are NiO of reasonably good quality.

Figure 3-16 shows the NiO edge of the thickest film in Figure 3-14 plotted against energy on an expanded scale. These data were taken on the Cary 14. As indicated previously some distortion of the edge shape may occur when using the Cary 14 as a result of the beam size changing with wavelength. The possibility of distortion of the transmission curve occurs because the beam can move on to or off of areas of the film having either pinholes or cleavage planes.

When making evaporations using the electron beam gun we frequently placed a glass microscope slide on the evaporation apparatus such that material being deposited on the ordinary heated substrate would also be deposited on the glass slide. The glass slides were not intentionally heated, but their location was such that they received some heat from

the substrate heater. Their temperature was probably of the order of 100°C. The transmission spectra of films deposited on two such slides are shown in Figure 3-17. The evaporations were in 0_2 at $1 \cdot 10^{-4}$mm Hg. These films again show breaks at 3750 angstroms and have the same general shape as the NiO films on MgO. This fact indicates that the deposition of NiO does not depend upon the substrate being heated to 550°C. As we indicated in Chapter 2, we noted after each evaporation that a good deal of green NiO powder was left on the nickel source around the area where the electron beam struck the source. We feel that this and the fact that NiO was apparently deposited on the glass slides at temperatures much lower than the 550°C used for the substrates are consistent with a hypothesis that NiO is formed at the source and then evaporated. Our experiments, we should point out, are by no means conclusive on this point. We saw no evidence of d level absorption in the films on glass. This could be due to either the films being too thin or due to lack of order in the films. We strongly suspect it is the latter.

The upper part of Figure 3-18 shows the transmission of a CaF_2 substrate which was heated to 550°C while the electron beam gun was turned on to the nickel source at an intensity below that required for evaporation. The electron beam gun was left on in this manner for two hours. Upon removing the substrate material from the vacuum system we observed that it had a faint bluish tinge. The CaF_2 is apparently colored slightly by either x-rays or scattered electrons from the electron beam gun. Several other CaF_2 pieces were also observed to become bluish when the electron beam gun was held at a low intensity -- only the

one in Figure 3-18 was scanned, however. We feel that in the other cases at least some nickel was evaporated. We do not think that nickel was evaporated in the case of the CaF_2 in Figure 3-18, although, of course, trace amounts could have reached the CaF_2.

We were somewhat puzzled by the fact that the CaF_2 used when evaporating Ni in O_2 apparently did not become colored. We thus annealed the CaF_2 in Figure 3-18 at 550°C for fifteen minutes in O_2 at $1 \cdot 10^{-4}$ mm Hg. An optical scan of the substrate material after annealing in the O_2 is shown in the lower part of Figure 3-18. As can be seen it appears that the absorption near 5700 angstroms was reduced by annealing in the O_2.

Figure 3-19 shows a film made by evaporating nickel onto CaF_2 at 450°C in a vacuum of $3 \cdot 10^{-6}$ mm Hg using the electron beam gun. This film shows a very strong absorption near 5500 angstroms which is not present in the nickel films made by flash evaporation on LiF (Figure 3-9). The film shown in Figure 3-20 on glass (also made by electron beam evaporation) does not show a dip at 5500 angstroms but shows the same behavior as the films in Figure 3-9. The glass was not heated to 550°C but was probably more nearly at 100°C. We did not attempt to isolate the cause of the structure in Figure 3-19 although several further observations were made. The film in Figure 3-19 as well as one other film evaporated onto CaF_2 at 550°C with the electron beam gun looked slightly violet to the eye -- one looked bluish violet and the other more reddish violet. Another film evaporated onto CaF_2 at room temperature did not appear at all colored. This latter film still did not appear colored even after it was heated to 550°C for thirty minutes in a vacuum. It is unlikely that the coloring and

structure in Figure 3-19 are due to an impurity present only during one or two runs and not other runs made with the electron beam gun. The effect is apparently not due solely to x-rays since it does not appear in the films made by evaporations of nickel in O_2. We hypothesize that it is due to nickel contamination of the heated CaF_2 in combination with the radiation from the electron beam gun.

Figures 3-18 and 3-19 again indicate that the substrate can have an effect on the optical results. The effect on the results when nickel is evaporated in O_2 appears to be rather small, but the effect on the one film of nickel deposited in vacuum which was scanned is quite large.

Figures 3-21 and 3-22 show the transmission results for two films made by evaporating nickel onto substrates at 550°C in O_2 at $1 \cdot 10^{-4}$ mm Hg. The film in Figure 3-21 is on quartz and that in Figure 3-22 is on BaF_2. The structure in the two transmission curves agrees quite well and appears to be quite similar to that of the majority of the films made by reactive sputtering which will be discussed shortly. The minimum near 3000 angstroms seen in the results shown in Figure 3-13 is not present in Figures 3-21 and 3-22 probably due to the fact that the absorption in the thicker films of Figures 3-21 and 3-22 dominates the $(1-R)^2$ in determining the shape of the transmission. The films made by oxidizing nickel (Figure 3-11) do not have structure very different from that of Figures 3-21 and 3-22 considering the differences among the films in Figure 3-11.

The films in Figures 3-21 and 3-22 are both polycrystalline whereas some of the sputtered films appeared to be epitaxial. However, judging from the "sharpness" of the absorption beginning near 3750 angstroms

and the transparency at long wavelengths, the films are probably reasonably stoichiometric. The film on quartz appears to be quite transparent at long wavelengths, however, the greater absorption at long wavelengths of the film on BaF_2 may be due in part to irradiation of the substrate material rather than to the film. The transmission of the films on quartz was not corrected for the small drop in transmission of the substrate occurring at short wavelengths and shown in Figure 4. This drop in transmission is considerably less than that shown for the films on quartz.

In the films grown by electron beam evaporation, we did not see any modification of structure in transmission curves which could be attributed to impurities being evaporated with the nickel. As pointed out in Chapter 2, the nickel was always hotter than the crucible holding it since the beam heated the nickel directly. A carbon crucible was used to hold the nickel when the film in the upper part of Figure 3-13 was evaporated and during the first evaporation on the film shown in Figure 3-14. For the other evaporations, an alumina crucible was used. During the third and fifth evaporations on the film in Figure 3-14, the alumina became quite hot. We see no modifications of structure in the transmission curves which could have been caused by alumina evaporation, however Holland [7] gives the evaporation temperatures of the materials of interest as follows:

Ni	1510°C
NiO	1586°C
Carbon	2681°C
Alumina	1781°C

Both nickel and nickel oxide evaporate at temperatures considerably below either carbon or alumina. The vacuum systems used for the NiO

film depositions were available for use by other workers in the laboratory which made impurity control difficult when evaporating a high temperature material such as NiO. Again, we see nothing in the spectra to cause us to believe that impurities had any optical effect.

Figures 3-23 through 3-30 show the transmission spectra of several films made by reactive sputtering. The structure shown in Figures 3-23 through 3-28 looks quite similar to that of the films made by electron beam evaporation in Figures 3-21 and 3-22. LiF substrates appeared to become colored when used for sputtering -- Figure 3-31 shows the spectrum of one substrate placed in the sputtering unit plasma and held at 550°C for one hour with the target voltage set at zero. This film looked reddish-brown to the eye. The absorption near 5000 angstroms in the film grown on LiF at 550°C shown in Figure 3-24 is probably due to color centers in the LiF since it does not appear in films on other substrates.

The color center spectrum of LiF is apparently different depending upon whether the LiF is or is not heated during sputtering. The transmission spectra of two films grown on LiF at room temperature showed sharp absorption dips near 2500 angstroms which we again believe to be due to the LiF. These dips were not present in any of the other films including films grown on LiF at 550°C and the film grown on CaF_2 at room temperature (Figure 3-23). This latter film was made during the same sputtering run as the film shown in Figure 3-29.

The electron diffraction patterns of several of the sputtered films showed the Laue pattern with NiO spacing. The patterns of the films in Figures 3-24, 3-26, and 3-29 are shown in Figures 2-10, 2-11, and 2-9, respectively. There is a slight possibility that the patterns

of the films on LiF could be due to the underlying substrate since our measurements of lattice constant were not accurate enough to differentiate between LiF and NiO. We consider this unlikely, since in all our work on films we have never had reason to believe that any electron diffraction patterns were due to the substrates rather than the films. Our lattice constant measurements were generally on the high side of NiO which is in the wrong direction to be either LiF or Ni. The electron diffraction pattern of the film in Figure 3-26 on CaF_2 shown in Figure 2-11 could not be due to the substrate since the CaF_2 lattice constant is quite different from that of NiO.

The films in Figures 3-23, 3-24, 3-25, 3-26, 3-29, and 3-30 were all grown in 20% O_2 and 80% A mixtures at ~.9 microns. We grew two films on quartz in a 10% O_2 and 90% A mixture. These films appeared to be more transparent at long wavelengths and have sharper absorption edges than the other films. In particular a comparison of the two films on quartz shown in Figures 3-25 and 3-27 shows that the film in Figure 3-27 is more transparent at long wavelengths and more absorbing at short wavelengths than the film in Figure 3-25. These results indicate that films sputtered in 10% O_2, 90% A, may be more stoichiometric than films grown in 20% O_2 and 80% A.

Some of the films grown on quartz both by sputtering and by electron beam evaporation have absorption edges which start at somewhat longer wavelengths than those on the other substrate materials. This can be seen by comparing the spectra of Figures 3-21, 3-27, and 3-28 with those of Figures 3-22, 3-26, 3-14, and 3-17. Figures 3-25 and 3-26, however appear to have edges beginning at almost the same

wavelength. The variations are probably due to varying amount of stress and crystalline order in the films.

The fact that the structure of the sputtered films is essentially identical with the structure of the films grown by electron beam evaporation is an indication that the optical properties are probably not being affected by impurities introduced during film deposition. One would not expect the same impurities to be introduced into films made by the two different processes.

C. Low Temperature Measurements

Two films were scanned at liquid nitrogen temperature using the Cary 14. The samples were attached to the cold finger of a vacuum dewar using teflon clips and a room temperature scan was made. The vacuum chamber of the dewar was then evacuated and the dewar filled with liquid nitrogen. About an hour was allowed for equilibrium to be attained and then a second optical scan was made. The contact between the cold finger and the sample was maintained by the pressure of the teflon clips. The temperature of the sample was not measured in any of the runs. Scans of one of the films were repeated several months following the first scans. In this repeat measurement, the results were essentially the same as those of the first. In the last measurements, a third scan was made when the sample had returned to room temperature to check for hysteresis.

Both samples showed a shift of the absorption edge to higher energies at liquid nitrogen temperature. Figure 3-32 shows the room temperature and liquid nitrogen results for the film of Figure 3-27 which was grown on quartz by sputtering. The edge is shifted by

approximately 62 angstroms which is .065 electron volts. No additional structure was observed in the film at low temperature. A second room temperature scan to check for hysteresis was not made. Figure 3-33 shows the room temperature and liquid nitrogen results for the film of Figure 3-14 grown on CaF_2 using the electron beam gun. The edge is shifted about 90 angstroms or .094 electron volts. This film has an additional bump near 3500 angstroms which could be due to structure or interference -- it is difficult to tell which. A check for hysteresis was not made in the measurement of Figure 3-33. Another measurement of the temperature shift of the edge in the film of Figures 3-14 and 3-33 was made several months later.* In this measurement a room temperature scan was made before and after the scan at liquid nitrogen temperature. Figure 3-34 shows the results. Measurements were made using two different light sources referred to as the visible source and u.v. source in Figure 3-34. In the room temperature scan made after the liquid nitrogen scan, the edge appears to be $\sim$10 angstroms higher in wavelength. It is, however, unlikely that this is hysteresis -- it is probably due to a small shift in the sample position in the light beam during the various runs. Figure 3-35 shows the results from the measurements made in Figures 3-32 and 3-33 on an expanded scale. Three scans of the edge of the film on CaF_2 near 3400 angstroms are shown. These were taken during the same low temperature run (that of Figure 3-33) but were made using different lamps and screen arrangements. The same lamp and screen arrangement was used for the two curves composing each pair in Figure 3-34,

---

* The measurement was performed by Dr. Peter Melz.

of course. The good agreement between the results of Figure 3-34 and those of Figures 3-33 and 3-35 for the film on CaF_2 leads one to believe that the experimental errors in measuring the temperature shift are probably small. Shifts of the sample in the beam as the dewar is cooled and reheated can cause errors by shifting the light beam onto either a thinner or thicker area of the film or onto more or fewer pinholes. It should be remembered that our results are based on only two films and that only one measurement of the temperature shift was made on one of these. The films have the following temperature coefficients:

$$\text{Film on quartz,} \quad \frac{dE_g}{dT} = -2.9 \cdot 10^{-4} \text{ eV/}^oC$$

$$\text{Film on } CaF_2, \quad \frac{dE_g}{dT} = -4.2 \cdot 10^{-4} \text{ eV/}^oC$$

The disagreement between the two results is probably due to different stresses in the film resulting from the fact that they are on different substrates.

D. Reflectivity Measurements

Figure 3-36 shows the reflectivity of three different films of NiO grown on MgO substrates by vapor deposition. The data were taken on the Jarrell Ash instrument described in References 1 and 2. The measurements give relative values of the reflectivity only, as we did not investigate or attempt to correct for effects due to interchanging mirrors or rotating the phototube. As indicated in Reference 2, errors from the mirrors or phototube can, in addition to affecting the reflectivity

magnitude, distort the spectra somewhat and can cause shifts of peaks from their true values. The errors are almost certainly largest at short wavelengths.

The reflectivity spectra of Figure 3-36 all show a fairly sharp peak at 3100 angstroms. This peak has previously been seen by Newman and Chrenko (Reference 3) in both films and bulk samples. The structure in reflectivity is probably the cause of the minimum in transmission seen in the two thin films of Figure 3-13. The reflectivity measurements also showed small structure near 3900 angstroms and a sharp break near 2350 angstroms. The latter structure could be due to the equipment although the bump near 3900 angstroms does correspond to structure in the transmission (see Figure 3-5). The values near 2000 angstroms are undoubtedly affected by scattered light in the Jarrell Ash instrument.

Figure 3-37 shows the reflectivity of one NiO film on MgO measured with the McPherson Model 225 vacuum ultraviolet spectrometer (see Figure 3-1). In contrast to the Jarrell Ash equipment described in References 1 and 2, this equipment does not require the reflected beam and I_o beam to strike different mirrors, thus eliminating one source of error. The largest source of error, as in the case of the Jarrell Ash system, is due to the fact that the reflected beam is reversed from the I_o beam, causing the reflected beam intensity to be spread over the light detection surface in a different way from the I_o beam. Since in the optics used with the McPherson instruments, the beam strikes the sodium salycilate coated microscope slide in front of the phototube at near normal incidence, the intensity of the beam is spread more uniformly across the light detecting surface than is the case with the Jarrell Ash system. Errors caused by the reversed beam image can still exist, but they should be smaller with the McPherson optics design. Scattered light

in the McPherson at short wavelengths less than ~2300 angstroms should be considerably less than in the Jarrell Ash equipment.

The film in Figure 3-37 shows a peak in reflectivity at 2100 angstroms. The reflectivity of a bulk sample in the ultraviolet (measured with the McPherson) is shown in Figure 3-38. The spectrum shown in the upper part of Figure 3-38 was taken after the sample surface was polished but before any attempt to etch it. The spectrum in the bottom part of Figure 3-38 was taken after the sample was polished and etched for twenty minutes in HCl diluted with water to half strength. Both spectra show structure near 2000 angstroms. The structure in the bulk sample reflectivities is not as sharp as that in the film, probably because the polished sample surface is not of as high a crystalline quality as the film surface. The structure in the bulk is sufficiently similar to that in the film to indicate that structure is present at 2000 angstroms - 2100 angstroms. The spectrum of the film differs enough from that of the bulk to indicate that the structure is probably really in the samples and not an anomaly of the optical equipment. Figure 3-39 shows the spectrum of the same bulk sample over the wavelength range 1250 to 6000 angstroms measured on the McPherson*. Measurements using several filters are shown. The agreement between these measurements as well as the agreement in structure with the measurements in Figures 3-36, 3-37, and 3-38 is quite good.

Figure 3-40 shows the average of the various measurements of Figure 3-39. The values of Figure 3-40 were used in a Kramers Kronig analysis (discussed in the Appendix) to derive the absorption constant. Figure 3-40 shows the results of the bulk sample (Figure 3-39)

---

* This measurement was performed by Fred Kahn.

and the results of the film of Figure 3-37 near 2000 angstroms. The film results which had sharper structure near 2000 angstroms were adjusted to agree with the bulk at ∿1800 angstroms and ∿2500 angstroms. A Kramers Kronig analysis was made of both the bulk results and the bulk results modified to agree with the film results between 1800 and 2500 angstroms. The absorption constants derived from the Kramers Kronig analysis are shown in Figures 3-41 and 3-42. The absorption constant is shown for three extrapolation parameters P = 2, 3, and 4 (see the Appendix) to indicate the sensitivity to the extrapolation at high energy. The general shape of the absorption constant appears to be consistent with the film transmission results although the Kramers Kronig results show a peak in the absorption constant at a somewhat longer wavelength than the minimum in the transmision of the films. This is probably because the crystallinity of the polished bulk surface is not particularly good. Also, the quality of the films is undoubtedly not perfect. We did not attempt to determine the accuracy of the absolute magnitude of the reflectivity measurements made on the McPherson by rotating the phototube, etc. We were mainly interested in determining the shape of the absorption constant as a function of wavelength rather than the absolute magnitude. The structure and shape of the spectrum used in the Kramers Kronig analysis (Figure 3-40) does appear to agree well with the shape of the other spectra measured--the results near 2000 angstroms in Figure 3-36 do not appear to agree but this is undoubtedly due to scattered light in the Jarrell-Ash equipment. The reflectivities used in the Kramers Kronig analysis were all measured on the McPherson between 1250 angstroms and 6000

angstroms and should thus give the correct shape in this region. At wavelengths shorter than 1250 angstroms the extrapolations discussed above and in the Appendix were used. At long wavelengths the reflectivity was assumed constant -- the value at 6000 angstroms was used.

The structure near 2100 angstroms was not reported by Newman and Chrenko (Reference 3) but this could be because they did not take measurements at small enough energy intervals. Certainly additional measurements on more samples using different spectrometers would be in order before the existence of the structure is established with certainty.

E. Conclusion

The optical results discussed in this chapter indicate that nickel oxide films can be made by evaporating nickel in an O_2 atmosphere or by sputtering nickel in an O_2-A mixture. We have indicated the problems associated with obtaining accurate optical data from the films -- the most significant being color centers and variations in the absorption edge which are apparently due to variations in stoichiometry. The effects of the deposition parameters on the optical spectra, particularly the sharpness of the absorption edge, have been discussed.

We have presented transmission spectra of films grown by both the electron beam technique and by sputtering which appear to be consistent w th one another as well as with the spectra of films grown on MgO by vapor deposition. Two of the films have been used to provide information on the shift of the NiO absorption edge with temperature, the results being -2.9 and $-4.2 \cdot 10^{-4}$ eV/o_C.

Measurements of the reflectivity of a bulk sample and a film on MgO have provided strong evidence that additional structure is present in the NiO reflectivity spectrum near 2000 angstroms. The absorption constant derived from bulk reflectivity measurements by a Kramers Kronig analysis has a shape which agrees well qualitatively with the shape of the transmission of the films.

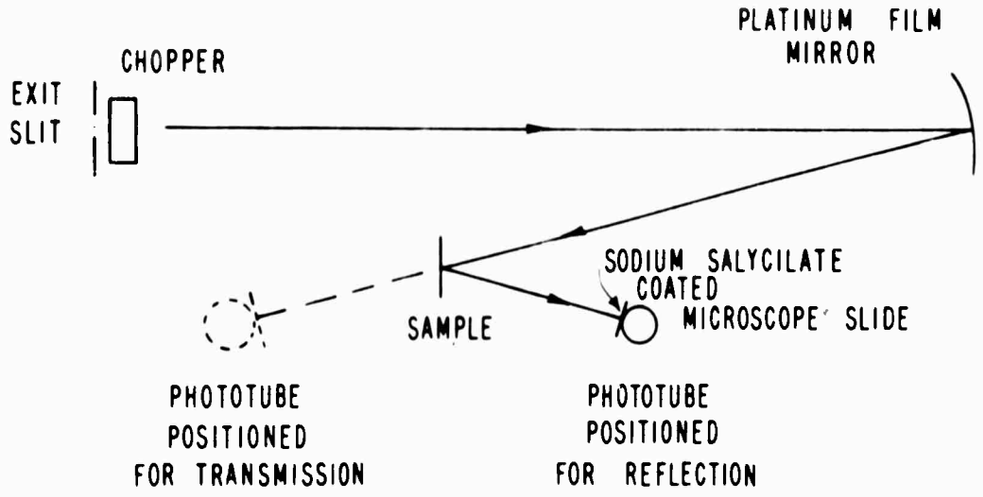

FIG. 3-1 OPTICAL SYSTEM USED WITH THE MCPHERSON MODEL 225 VACUUM ULTRAVIOLET SPECTROMETER.

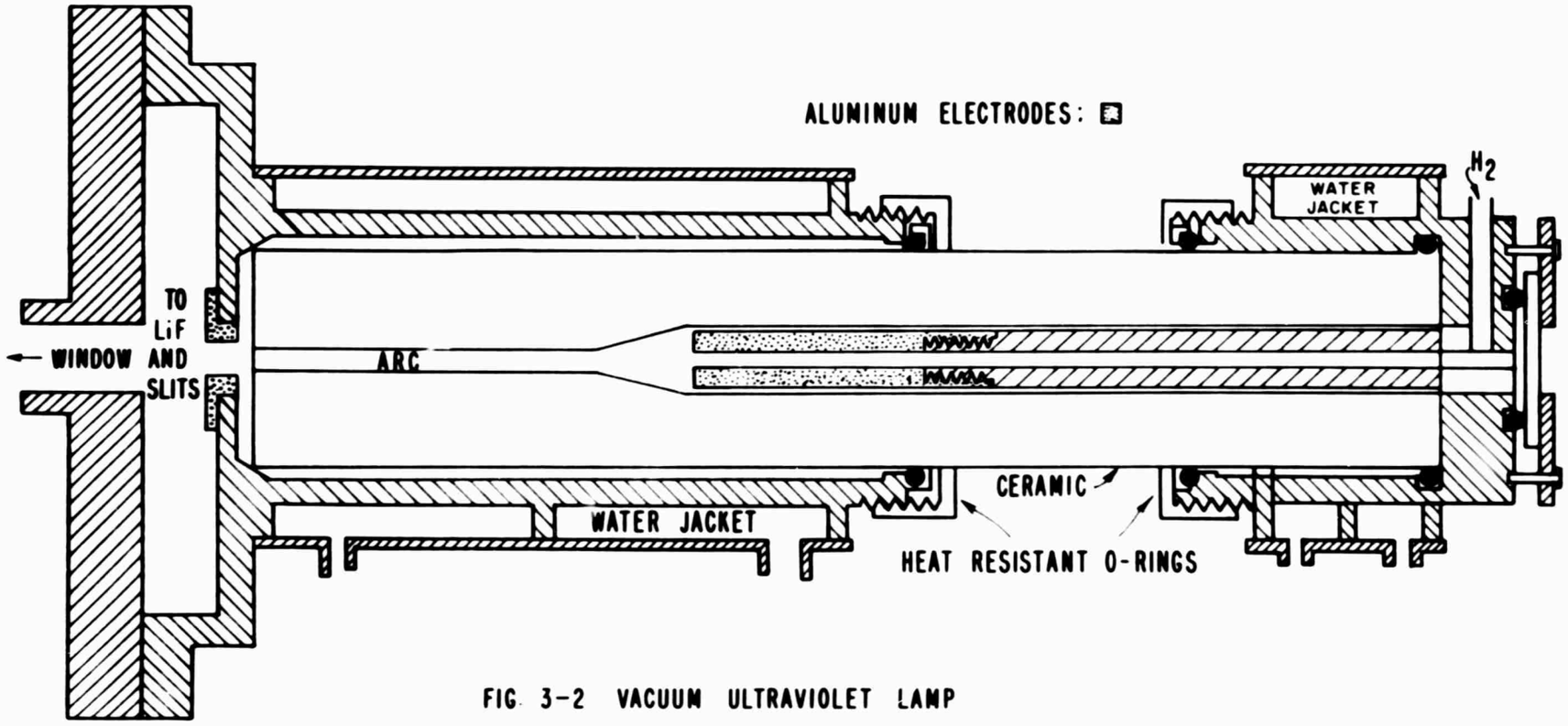

FIG. 3-2 VACUUM ULTRAVIOLET LAMP

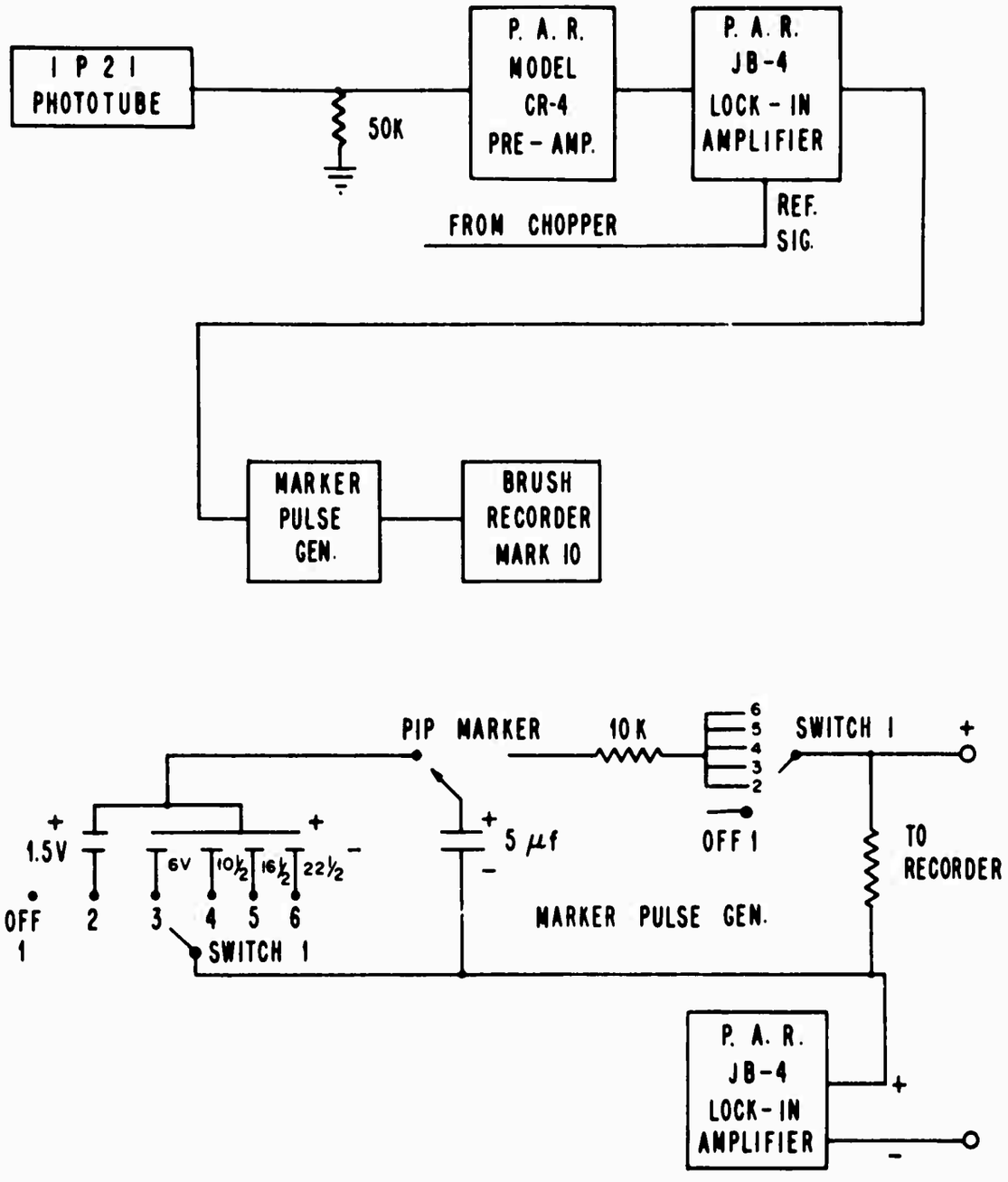

FIG. 3-3 SCHEMATIC OF ELECTRONICS USED WITH THE VACUUM ULTRAVIOLET SPECTROMETER.

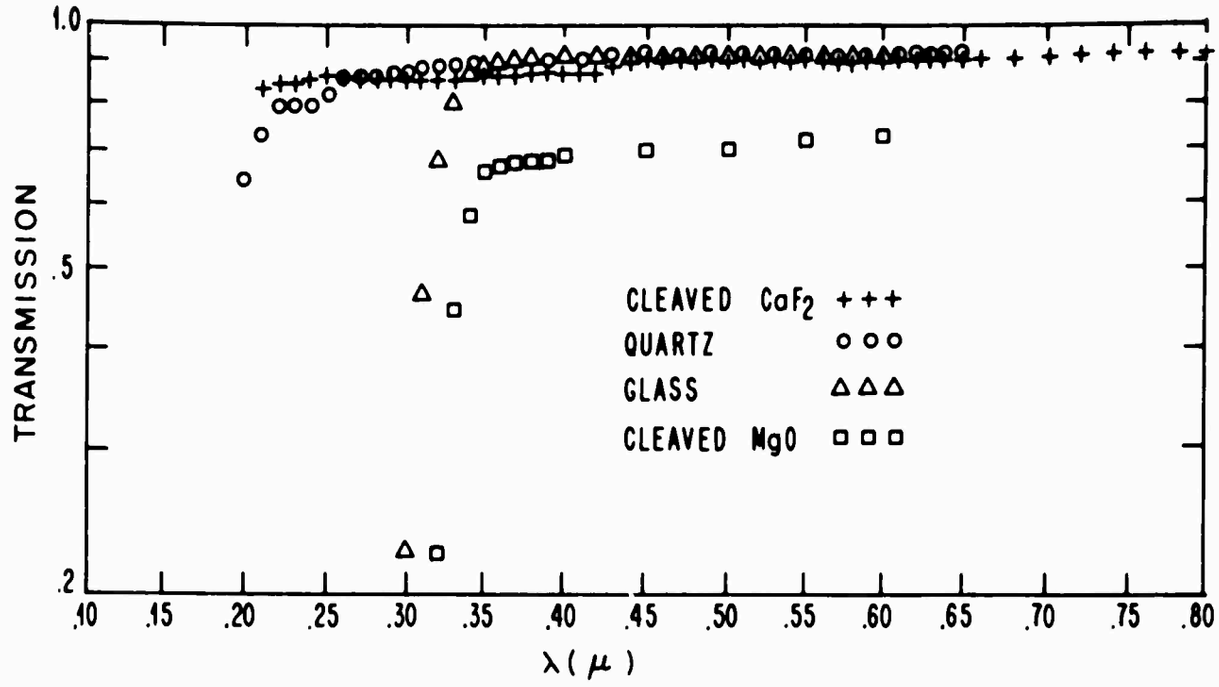

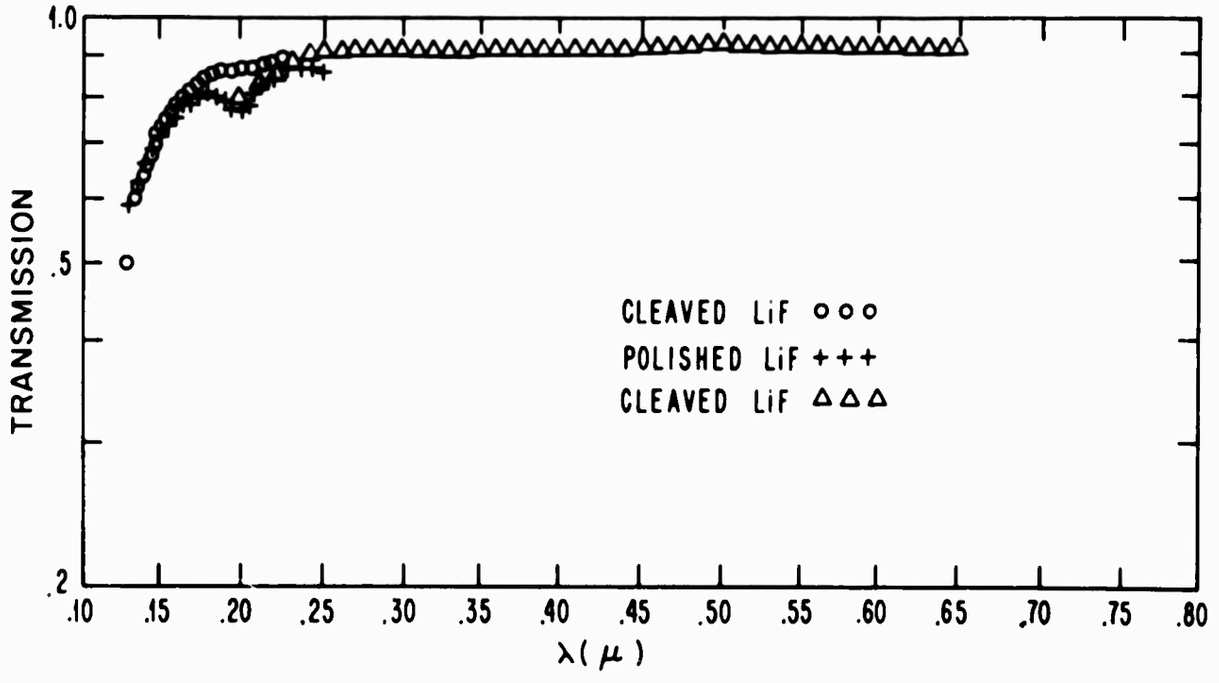

FIG 3-4 TRANSMISSION SPECTRA OF VARIOUS SUBSTRATE MATERIALS.

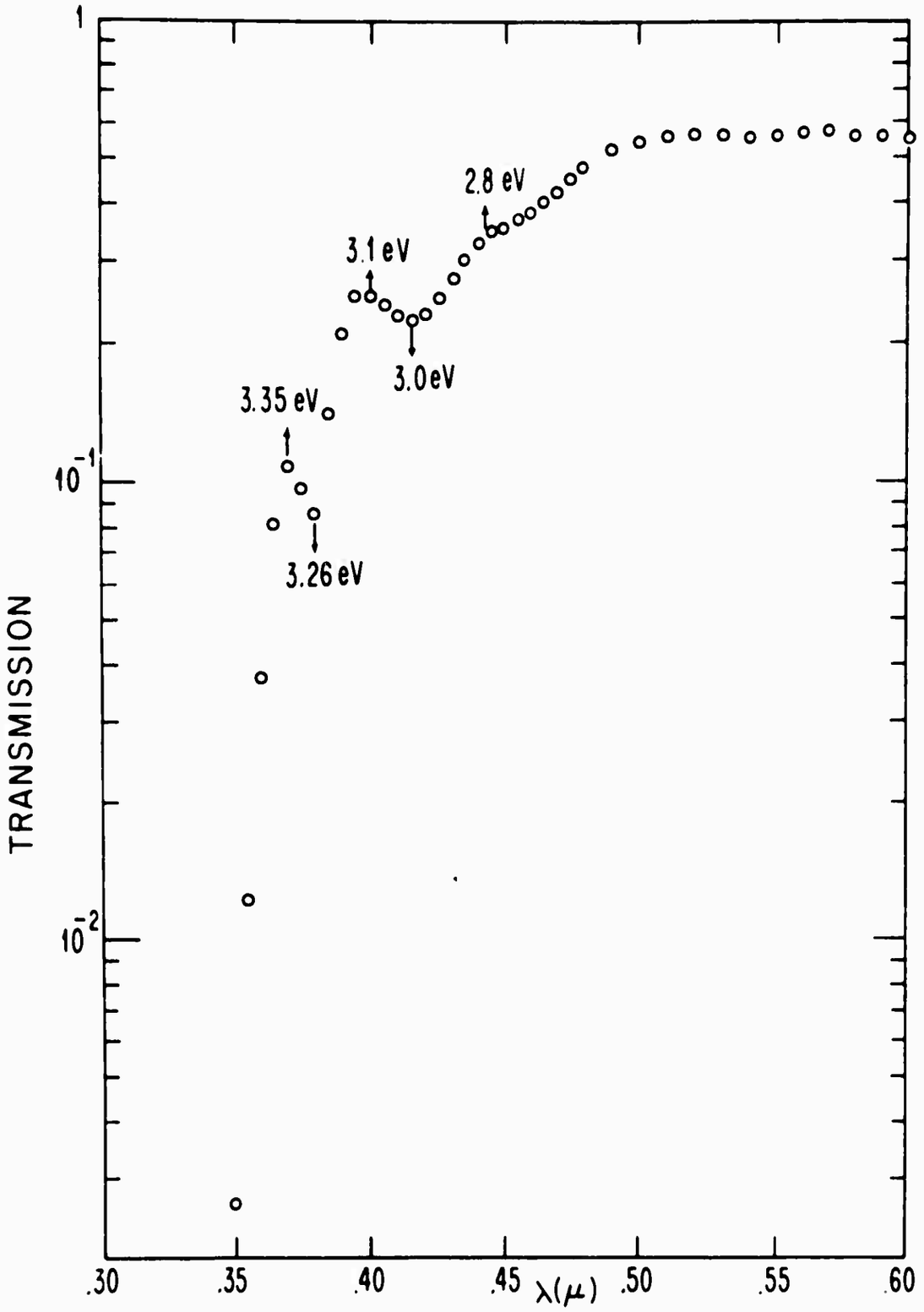

FIG. 3-5 TRANSMISSION SPECTRUM OF A NiO FILM GROWN BY VAPOR DEPOSITION ON A MgO SUBSTRATE

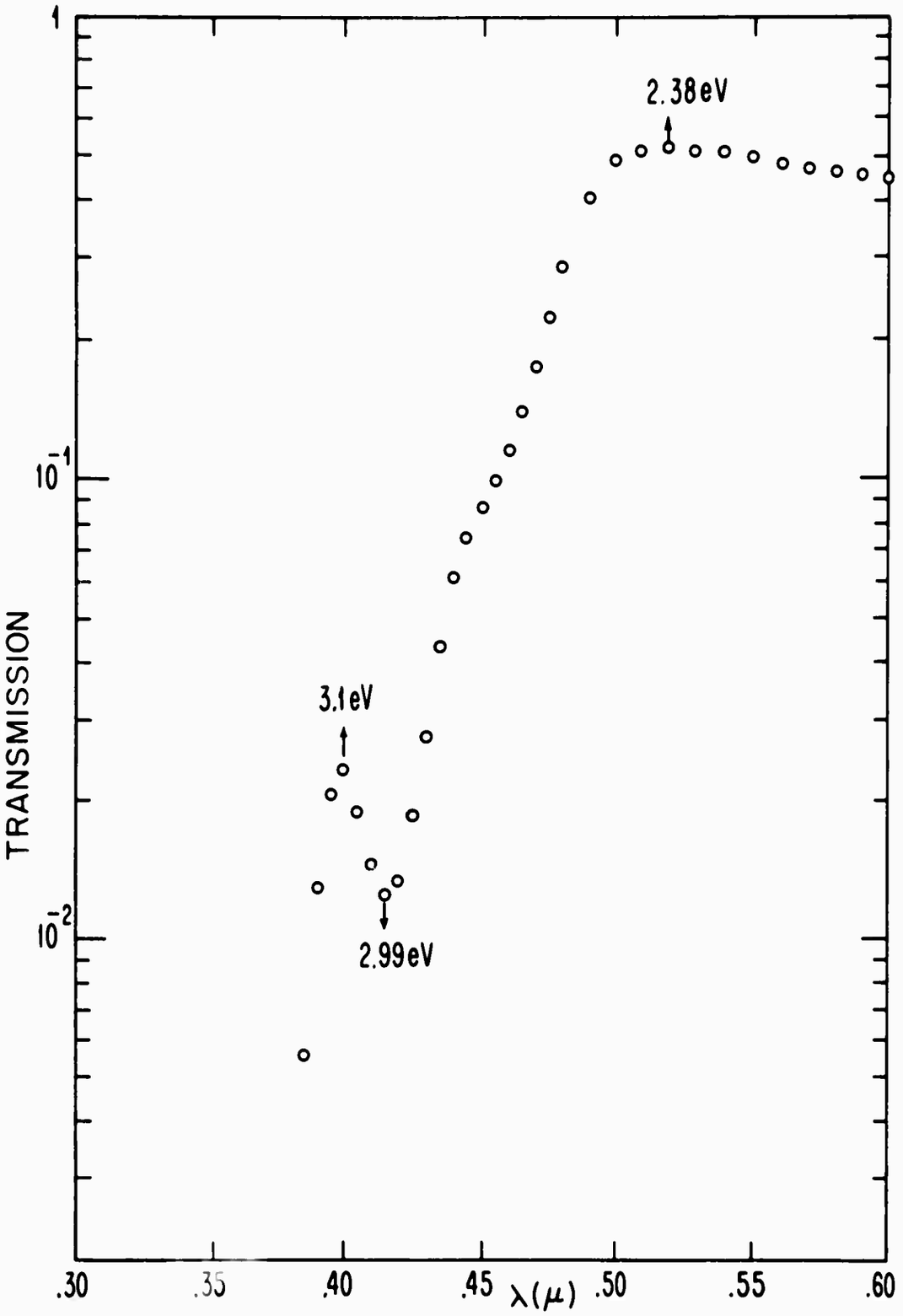

FIG. 3-6 TRANSMISSION SPECTRUM OF A NiO FILM GROWN BY VAPOR DEPOSITION ON A MgO SUBSTRATE.

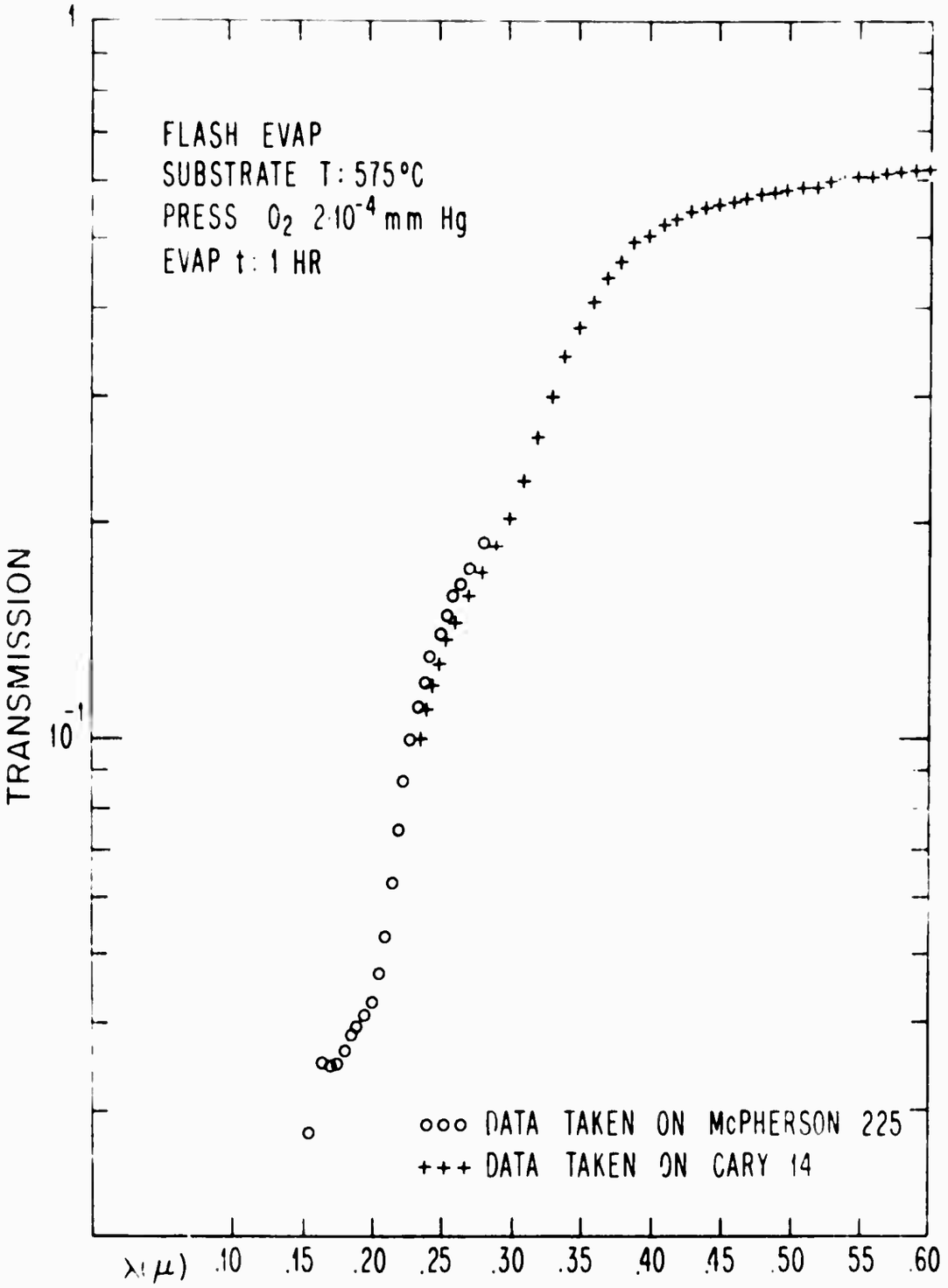

FIG 3-7 TRANSMISSION SPECTRUM OF A FILM GROWN ON LiF BY FLASH EVAPORATING NiO POWDER IN AN O_2 ATMOSPHERE OF $2 \cdot 10^{-4}$ mm Hg.

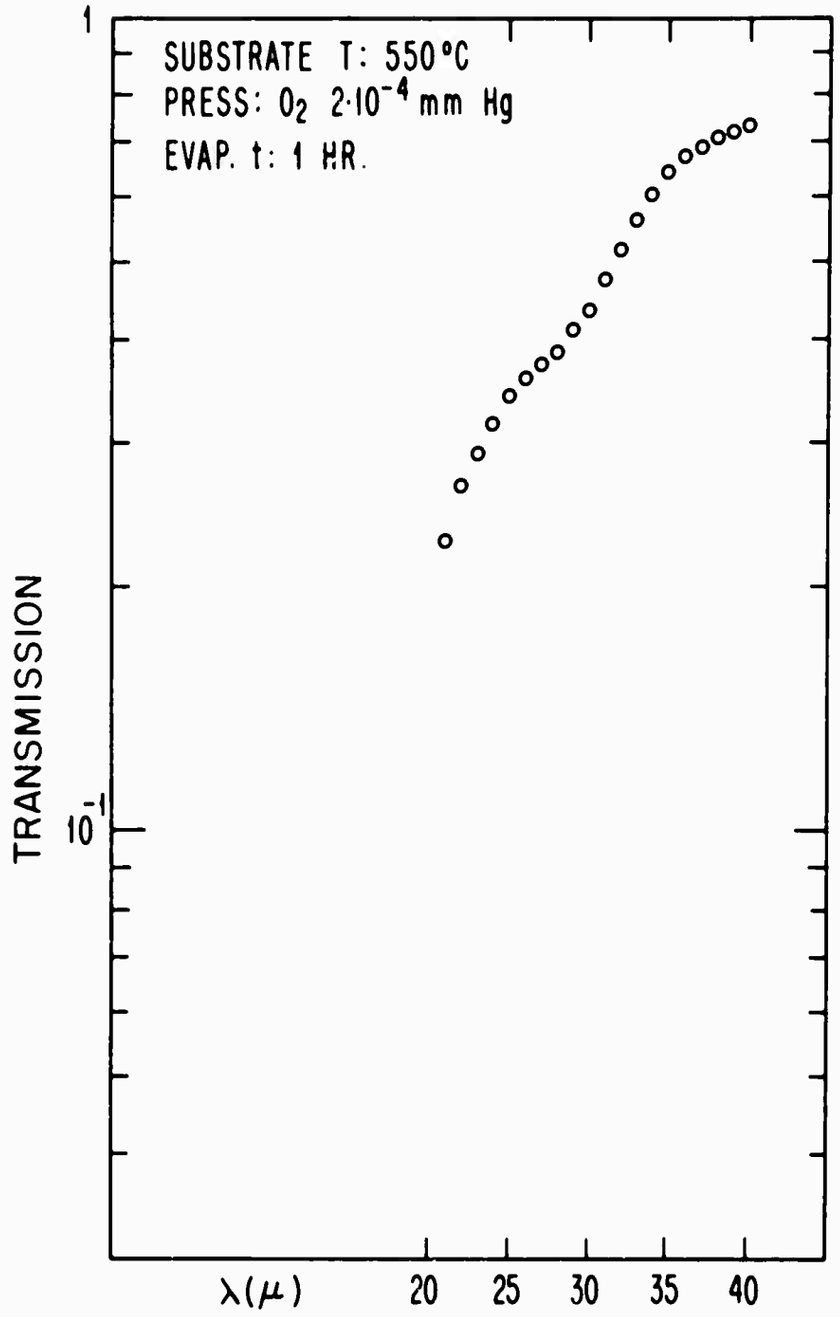

FIG. 3-8 TRANSMISSION SPECTRUM OF A LiF SUBSTRATE AFTER BEING EXPOSED TO A TUNGSTEN BOAT HEATED TO 1850°C FOR ONE HOUR IN O_2 AT $2 \cdot 10^{-4}$ mm Hg.

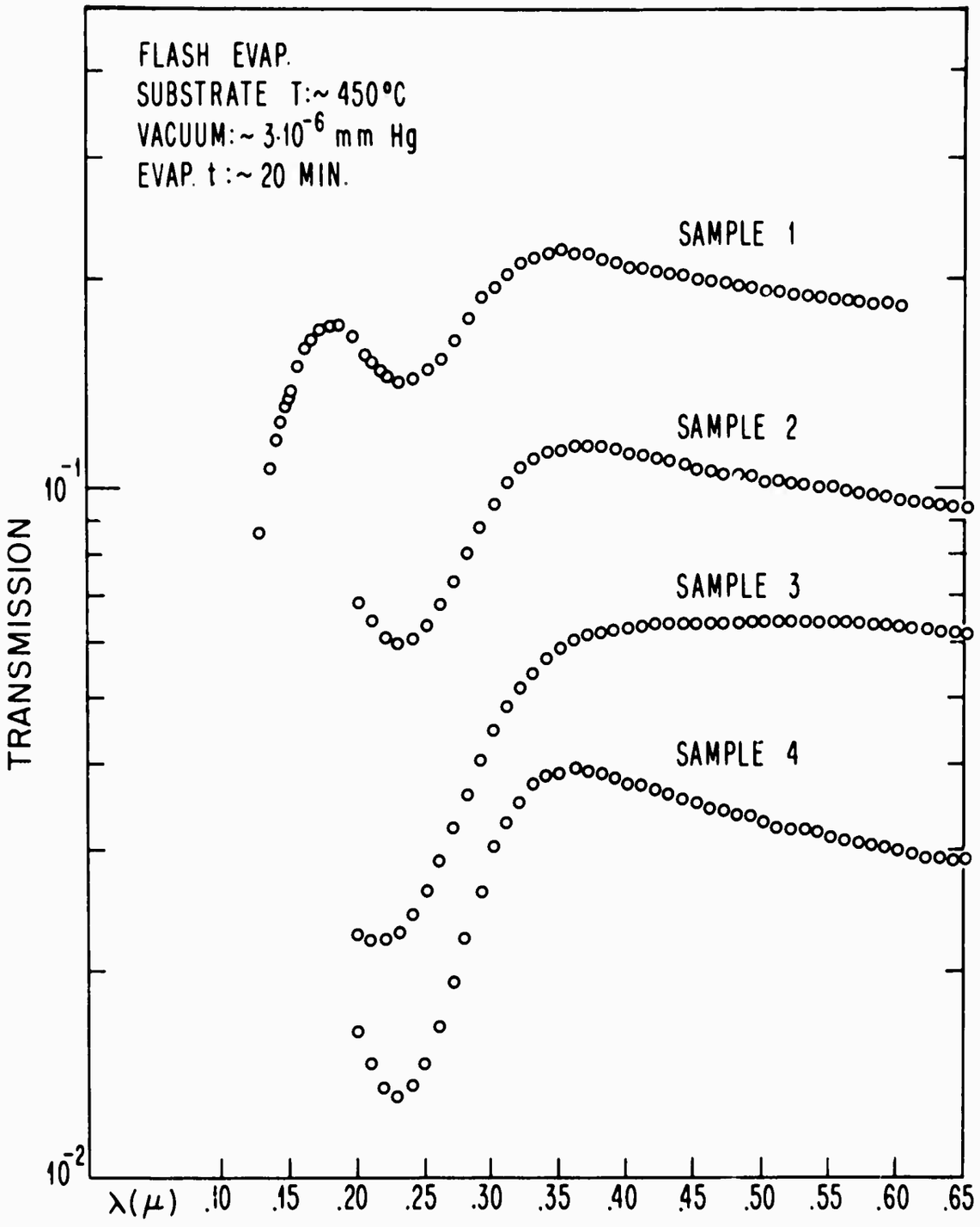

FIG 3-9 TRANSMISSION SPECTRA OF SEVERAL FILMS GROWN ON LiF BY FLASH EVAPORATING Ni POWDER IN A VACUUM OF ~ $3 \cdot 10^{-6}$ mm Hg.

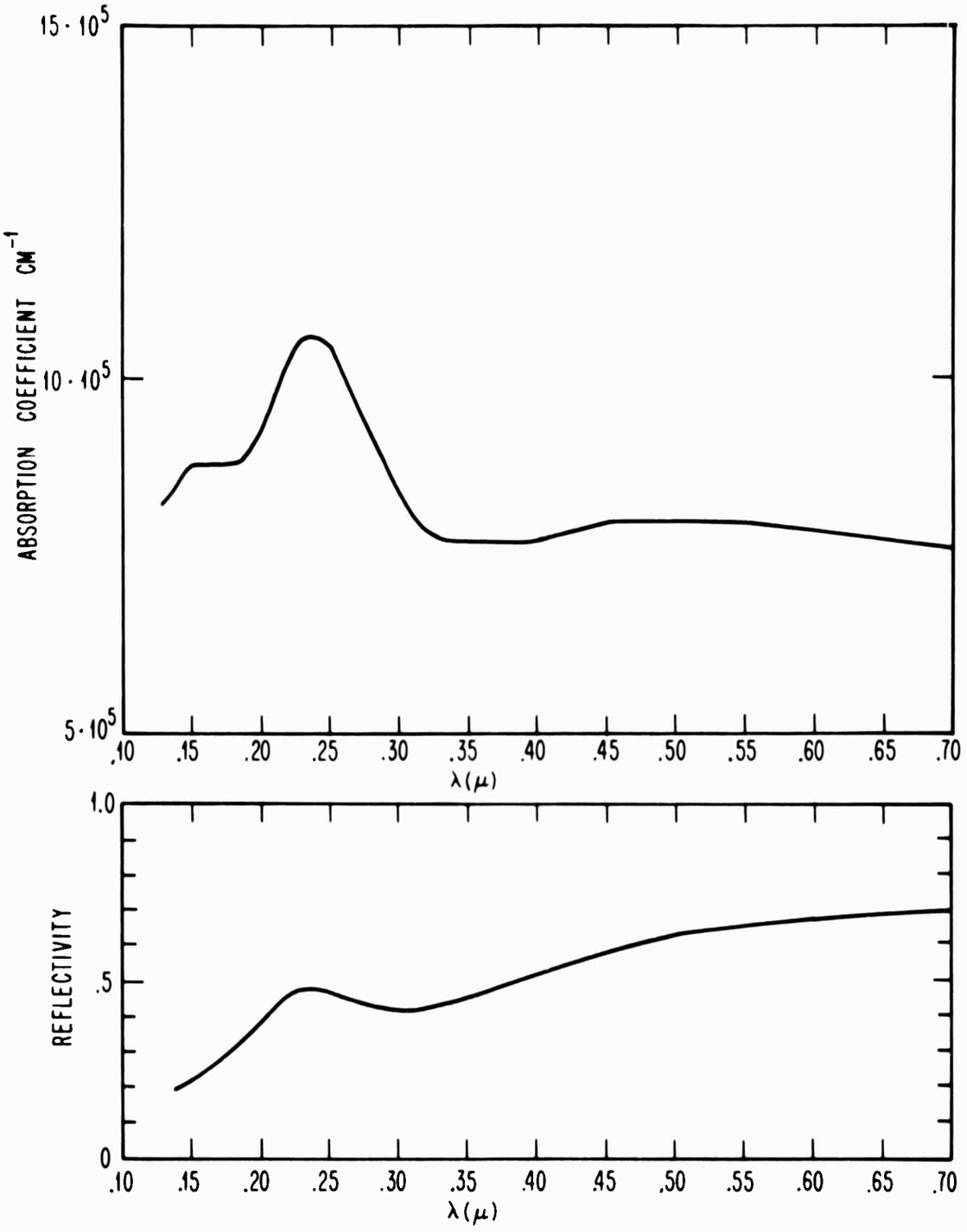

FIG. 3-9A ABSORPTION COEFFICIENT AND REFLECTIVITY OF Ni FROM REF 4

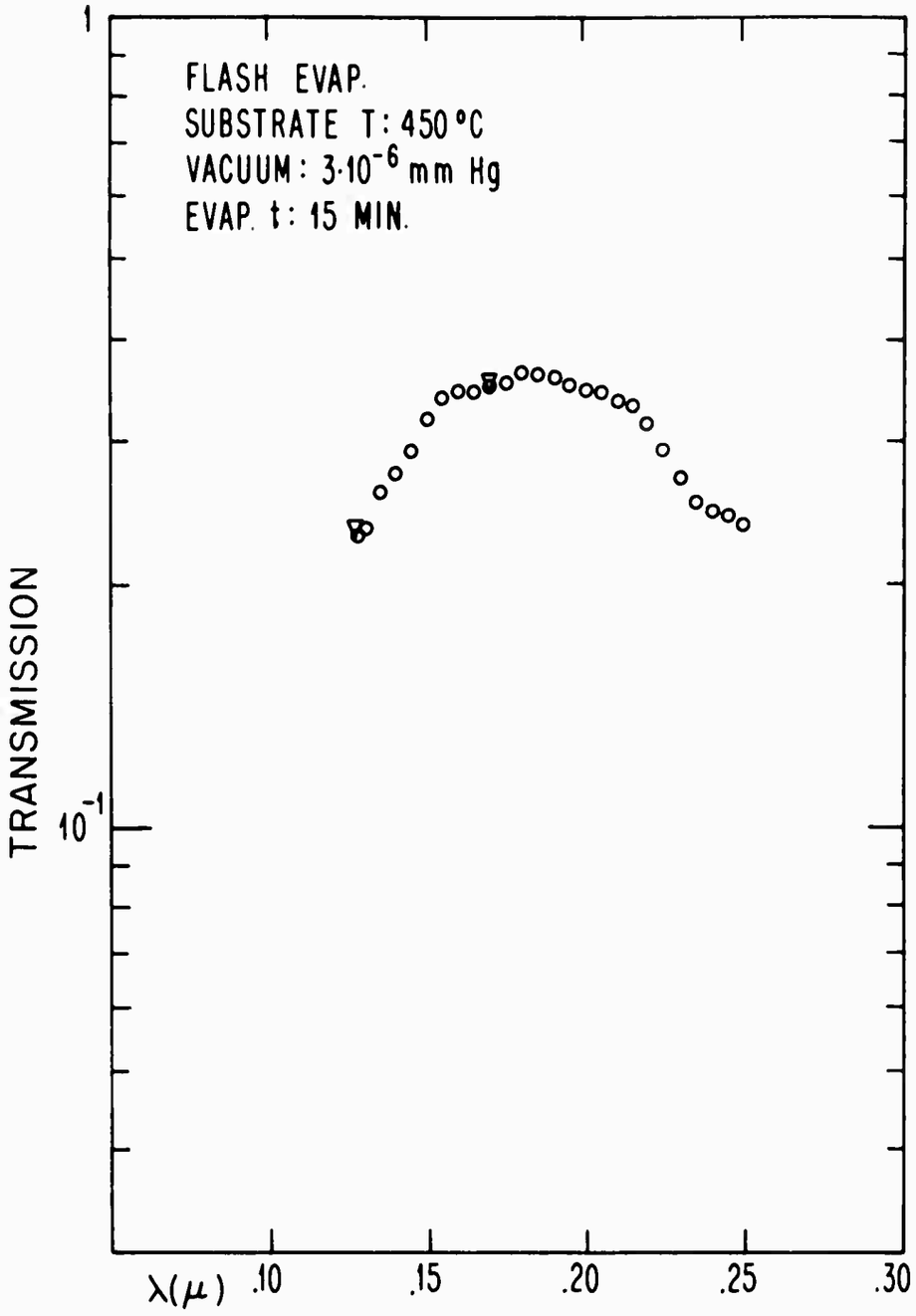

FIG. 3-10 TRANSMISSION SPECTRUM OF A FILM GROWN ON LiF BY FLASH EVAPORATING NiO POWDER IN A VACUUM OF $3 \cdot 10^{-6}$ mm Hg.

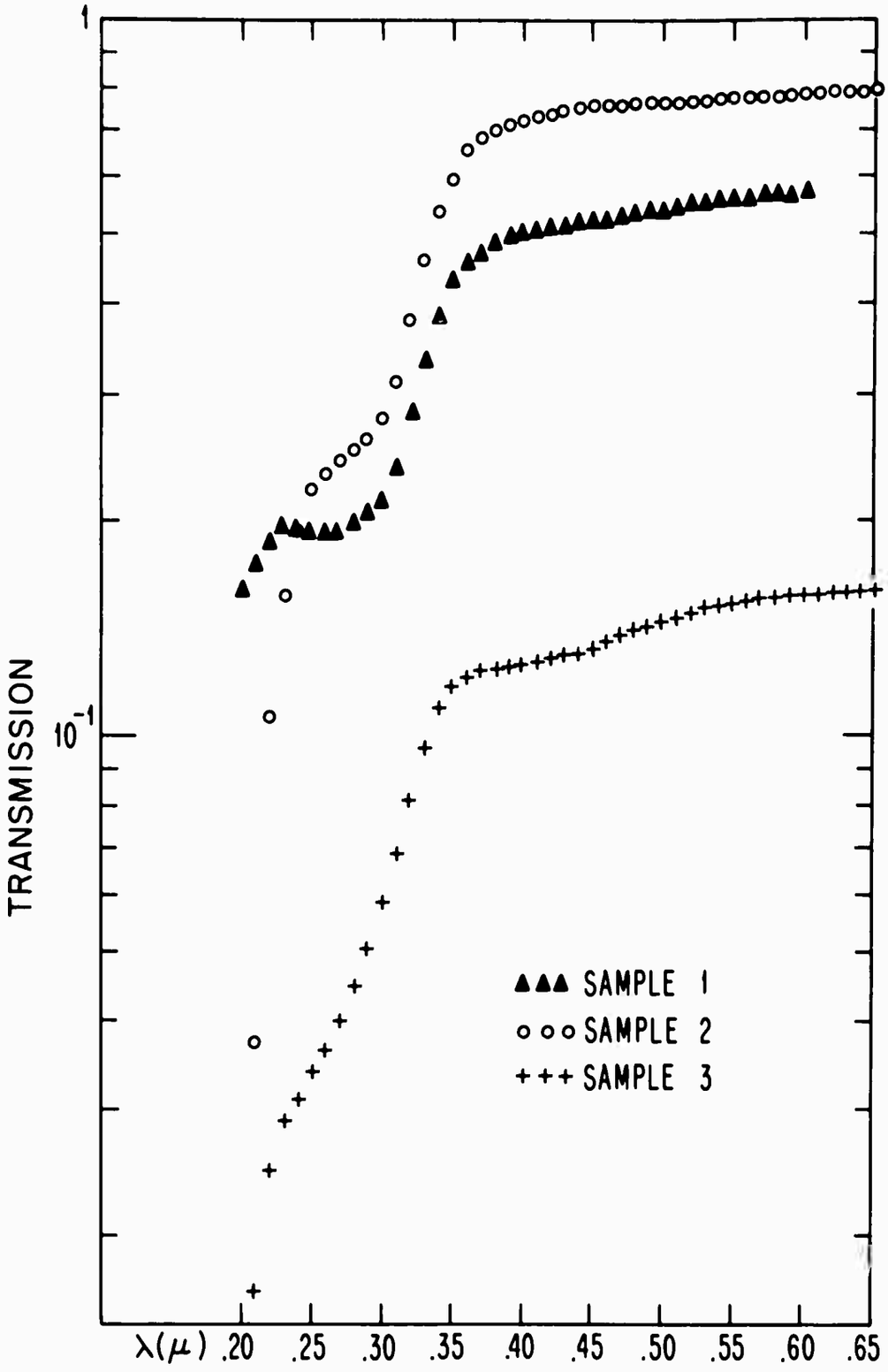

FIG. 3-11 TRANSMISSION SPECTRA OF SAMPLES 1 THROUGH 3 OF FIG. 3-9 AFTER OXIDATION. SAMPLE 1 WAS OXIDIZED FOR TWO HOURS AT 550°C IN O_2 AT $2 \cdot 10^{-4}$ mm Hg AND SAMPLES 2 AND 3 WERE OXIDIZED FOR THREE HOURS AT 300°C IN O_2 AT ROOM PRESSURE.

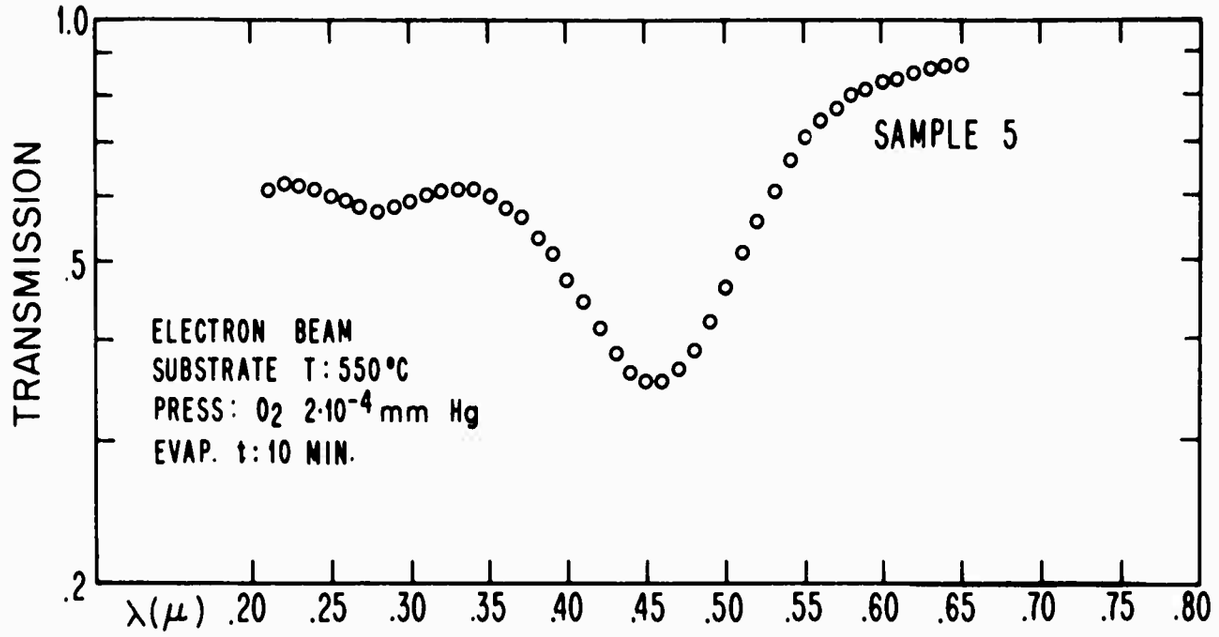

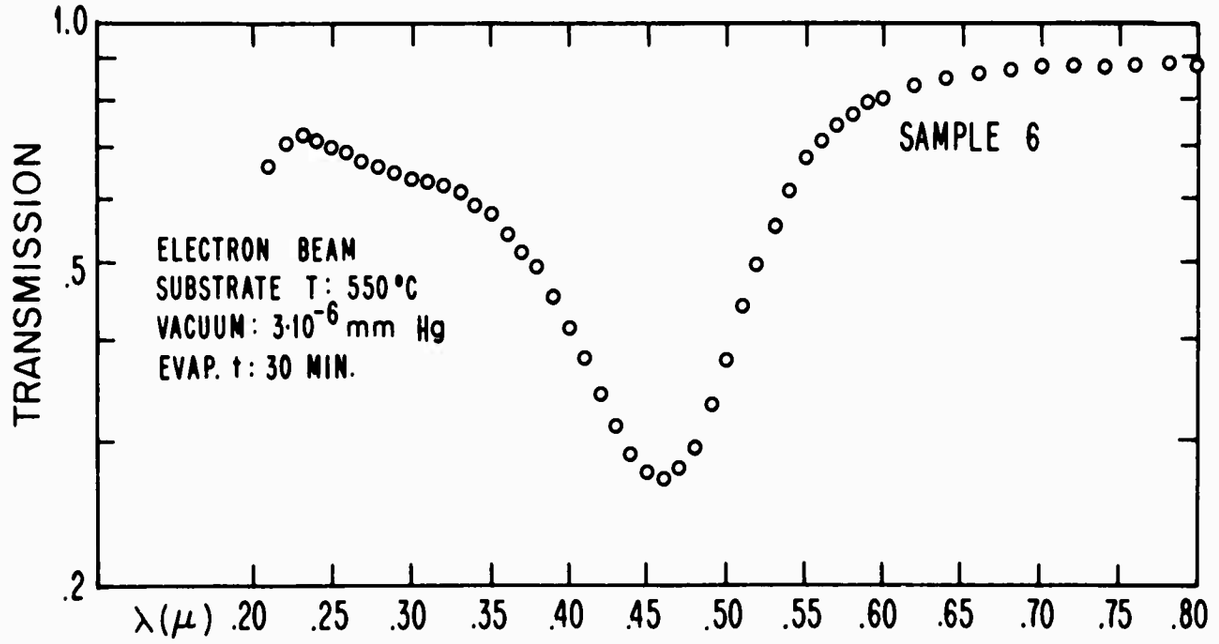

FIG. 3-12 TRANSMISSION SPECTRA SHOWING COLOR CENTER ABSORPTION ENCOUNTERED WITH LiF SUBSTRATES WHEN USING ELECTRON BEAM EVAPORATION.

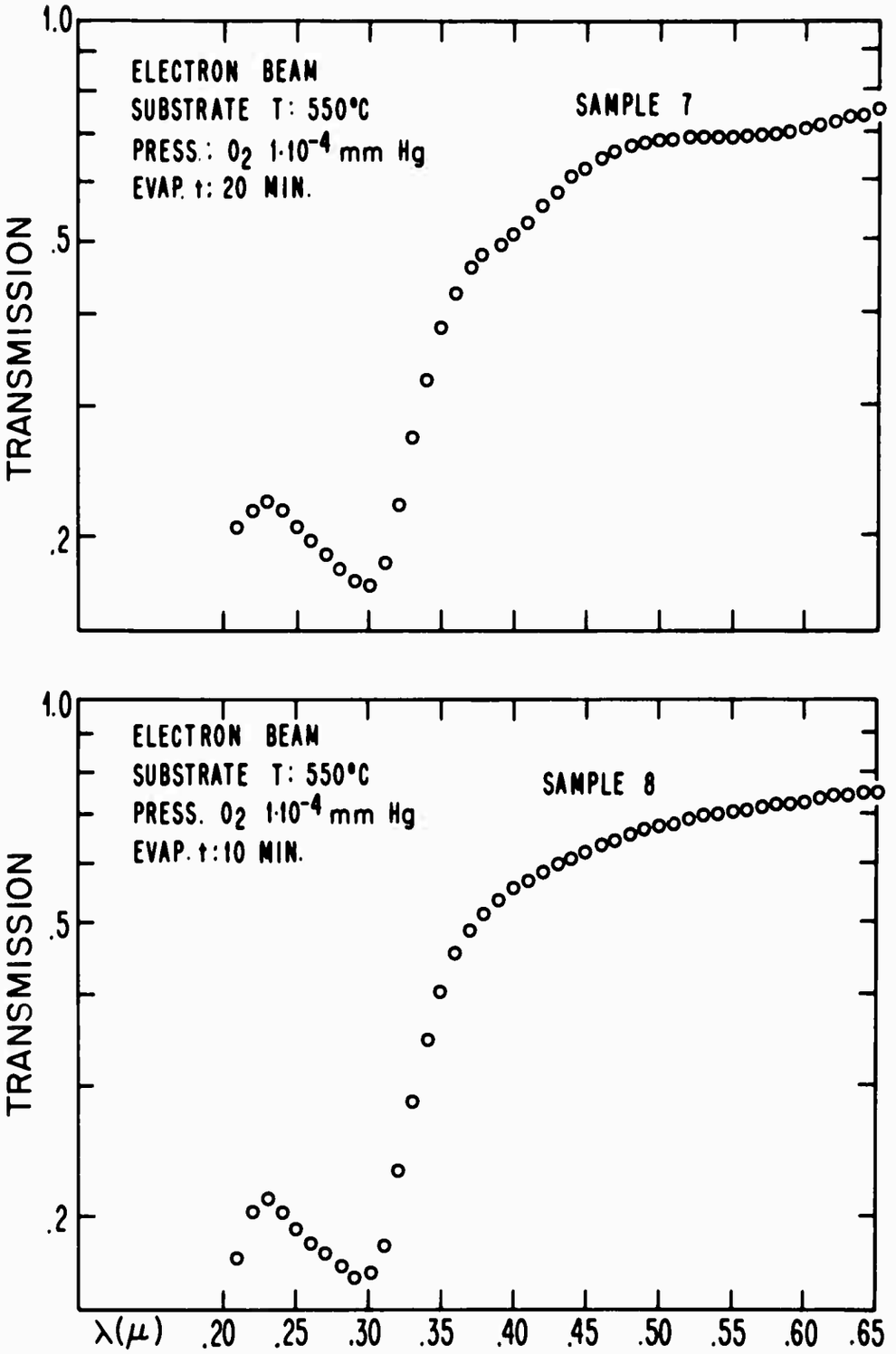

FIG. 3-13 TRANSMISSION SPECTRA OF TWO FILMS GROWN ON CaF_2 BY ELECTRON BEAM EVAPORATION OF Ni IN AN O_2 ATMOSPHERE OF $1 \cdot 10^{-4}$ mm Hg.

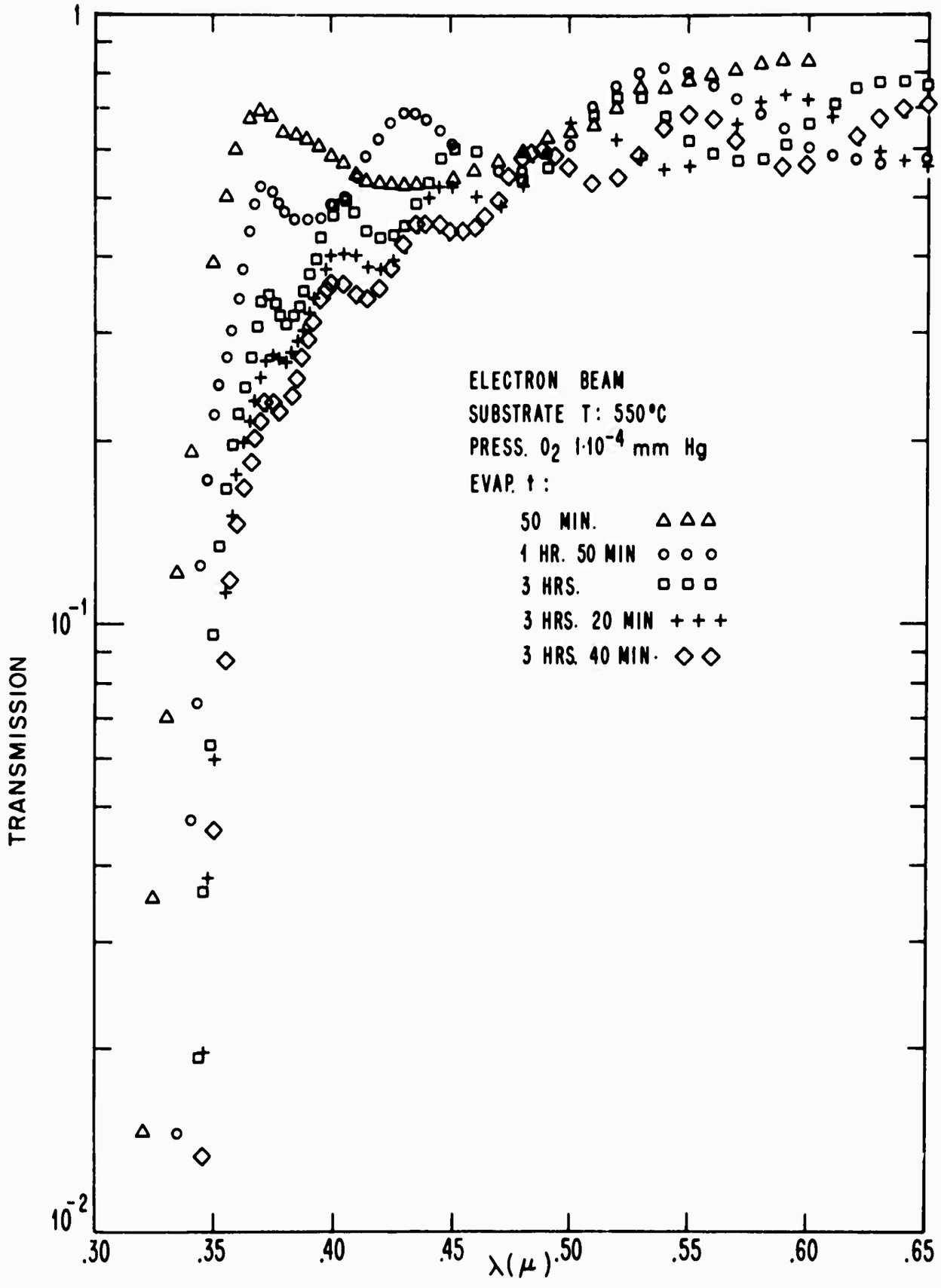

FIG. 3-14 TRANSMISSION MEASUREMENTS MADE BETWEEN SUCCESSIVE EVAPORATIONS ONTO THE SAME CaF_2 SUBSTRATE. THE EVAPORATIONS WERE MADE USING THE ELECTRON BEAM TO EVAPORATE Ni IN AN O_2 ATMOSPHERE OF $1 \cdot 10^{-4}$ mm Hg.

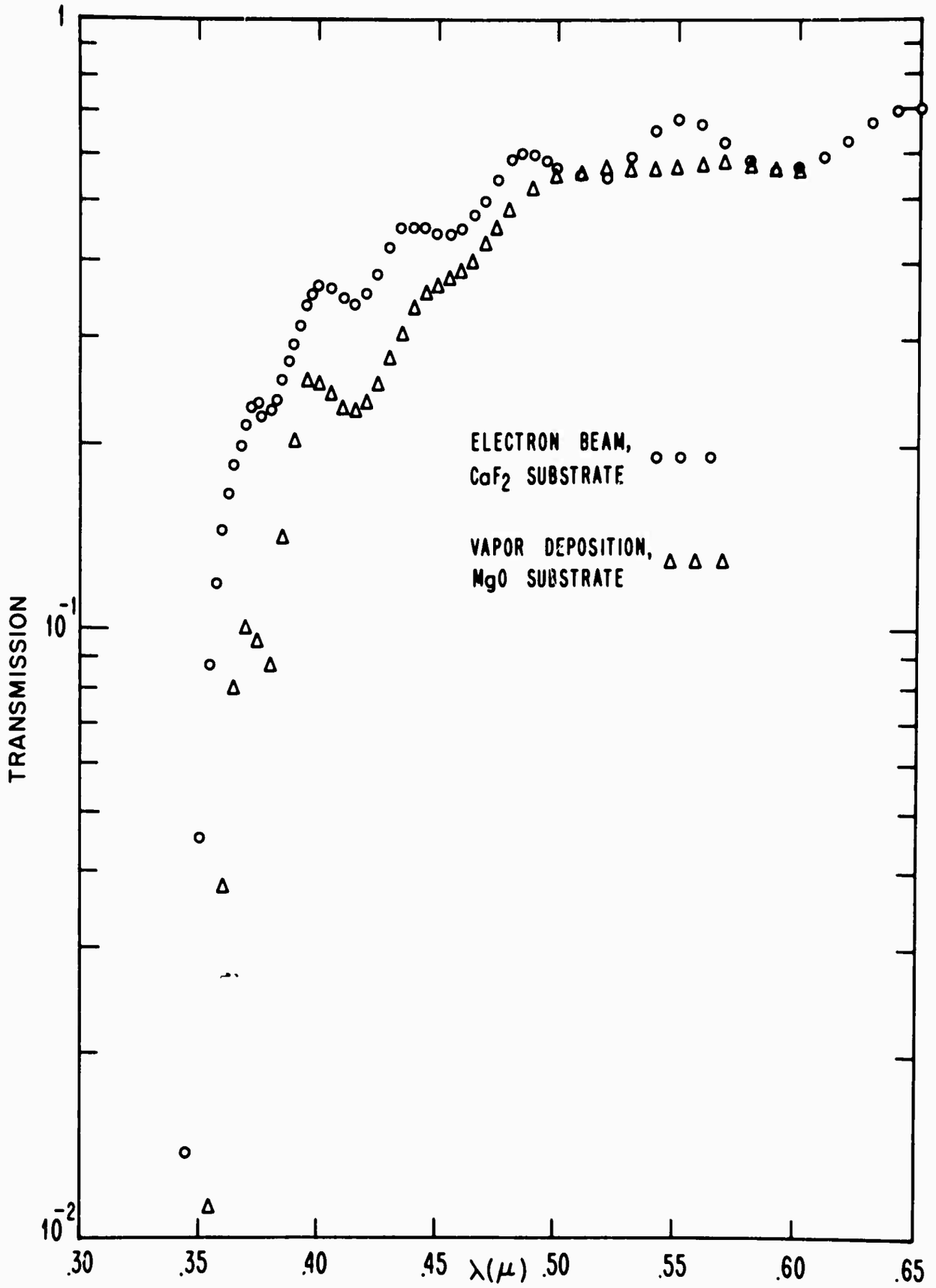

FIG. 3-15 COMPARISON OF TRANSMISSION SPECTRA OF A FILM GROWN ON MgO BY VAPOR DEPOSITION WITH THAT OF THE THICKEST FILM OF FIG. 3-14.

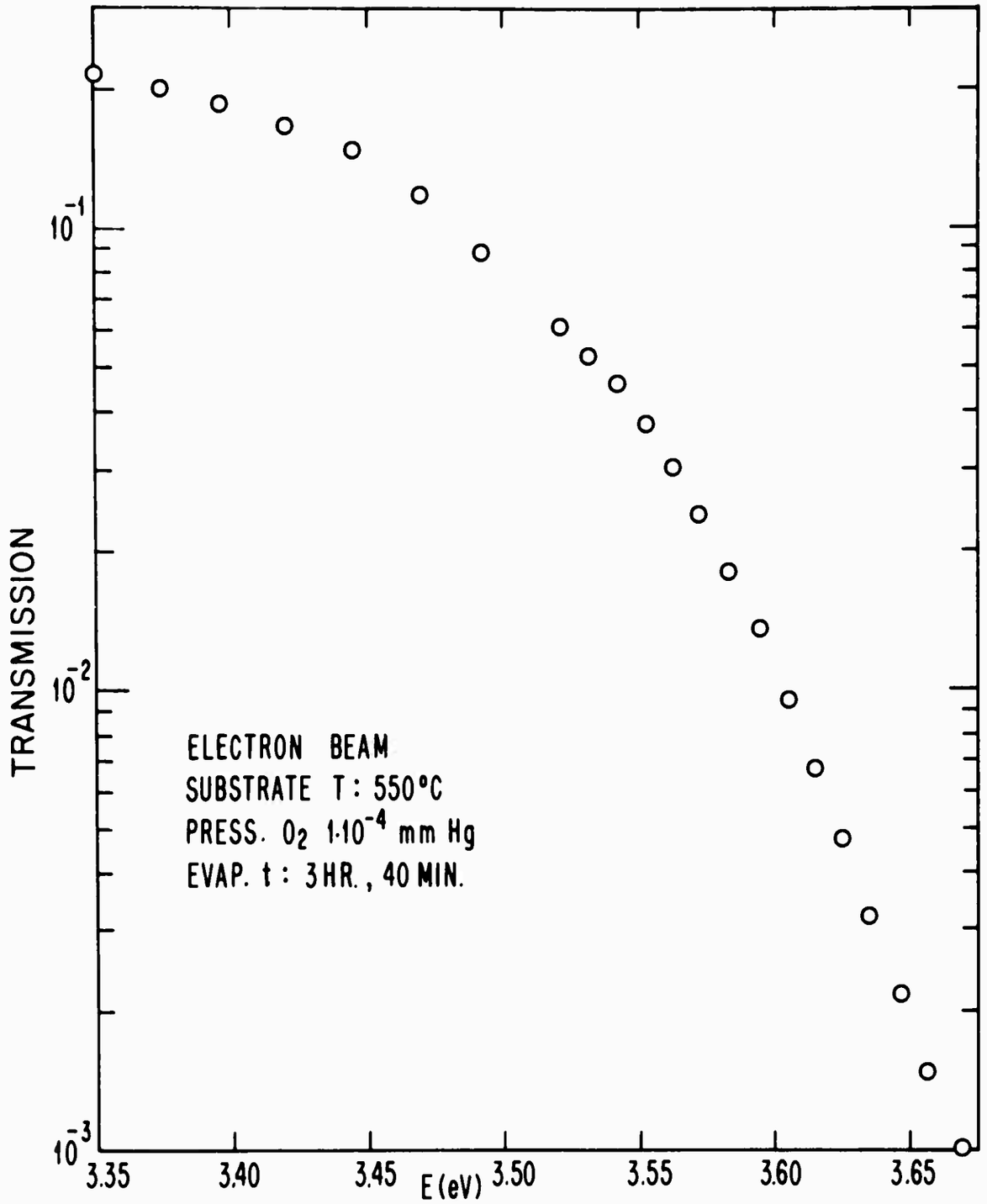

FIG. 3-16 TRANSMISSION SPECTRUM OF THE NiO EDGE OF THE THICKEST FILM IN FIG. 3-14 PLOTTED ON AN EXPANDED ENERGY SCALE.

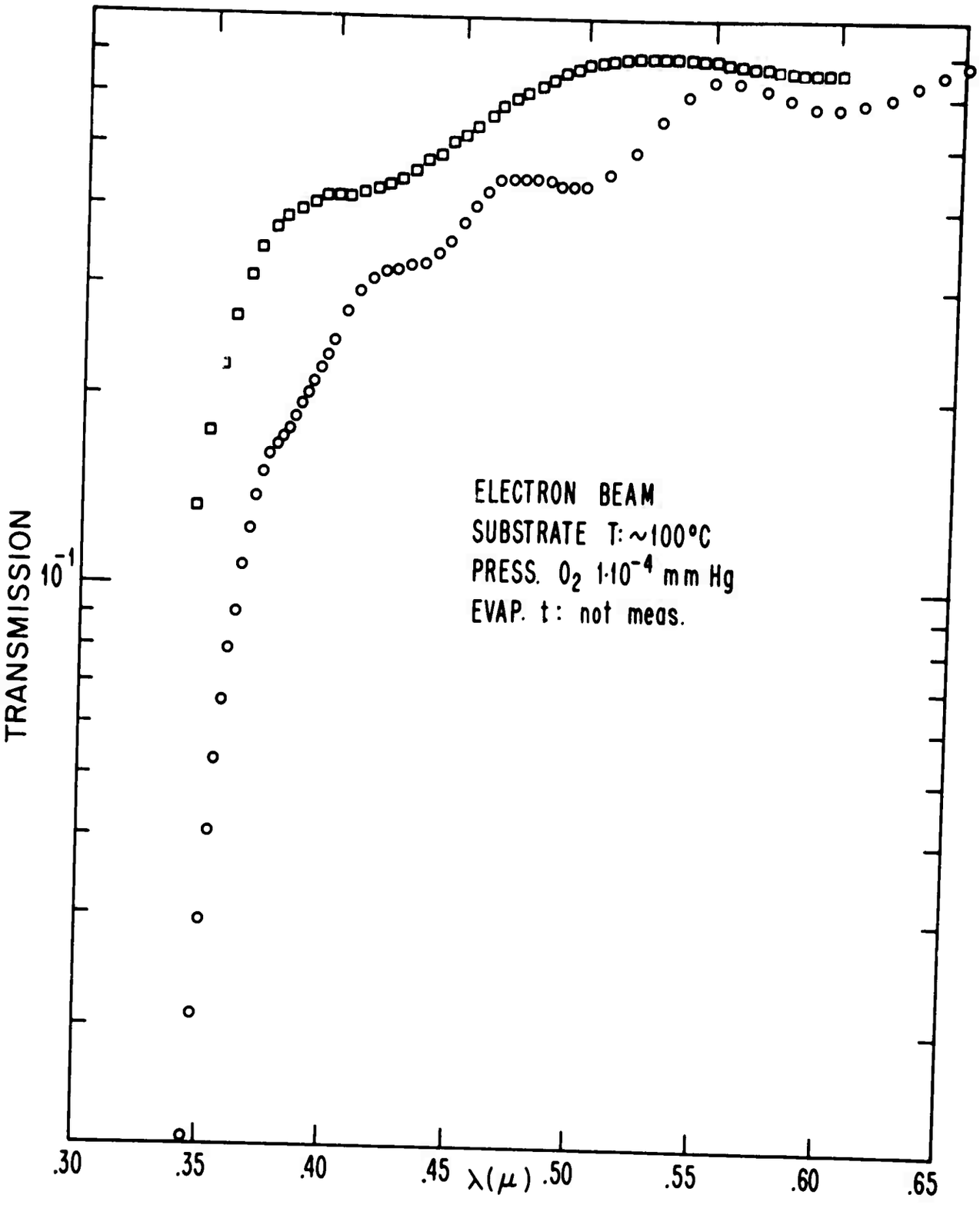

FIG. 3-17 TRANSMISSION SPECTRA OF TWO FILMS GROWN ON GLASS MICROSCOPE SLIDES BY ELECTRON BEAM EVAPORATION OF Ni IN AN O_2 ATMOSPHERE OF $1 \cdot 10^{-4}$ mm Hg.

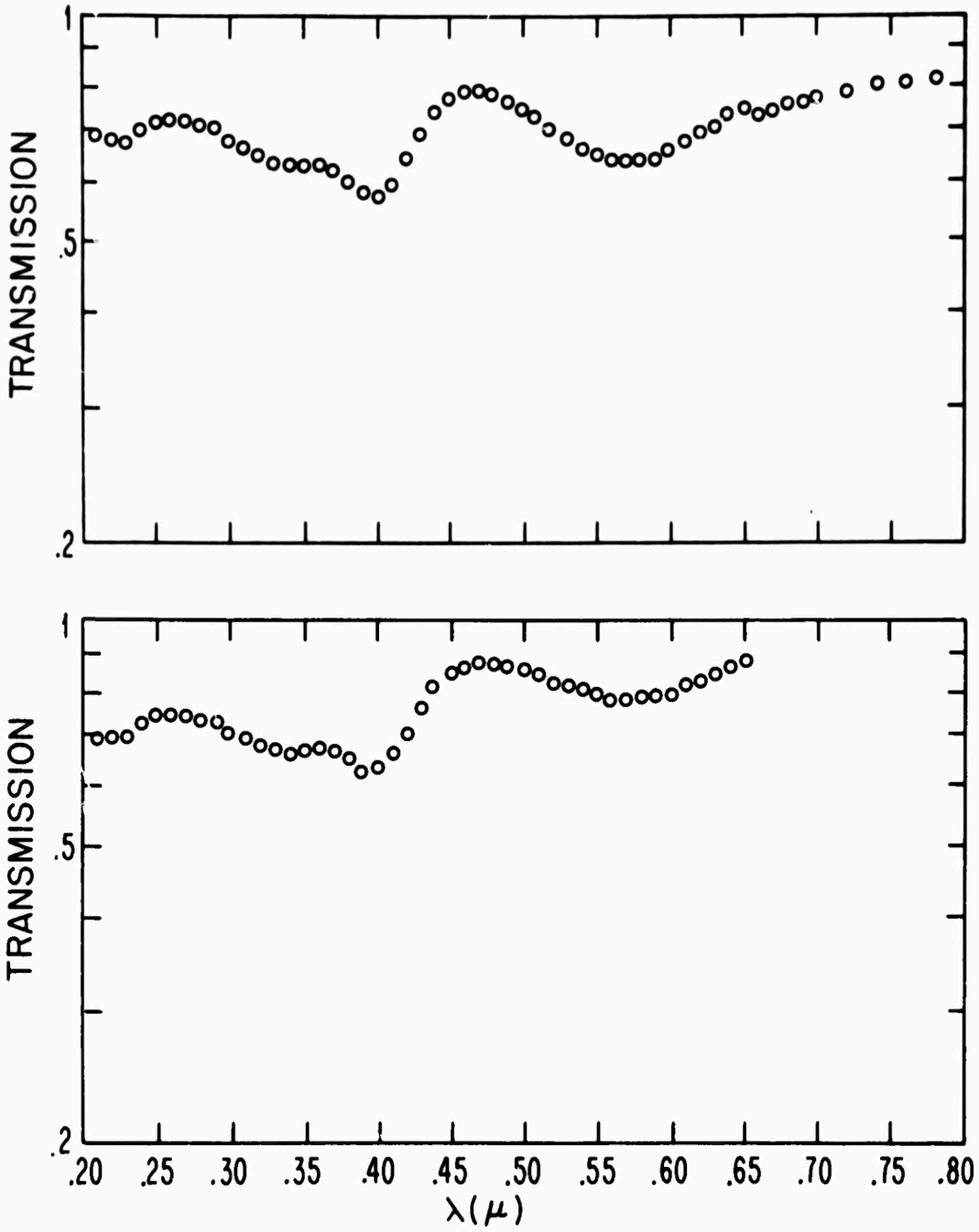

FIG. 3-18 THE UPPER CURVE SHOWS THE TRANSMISSION OF A CaF_2 SUBSTRATE WHICH WAS HEATED TO 550°C WHILE THE ELECTRON BEAM GUN WAS TURNED ON THE Ni SOURCE AT A LOW INTENSITY. THE LOWER CURVE SHOWS THE TRANSMISSION OF THE SAME CaF_2 AFTER ANNEALING IN O_2 AT $1 \cdot 10^{-4}$ mm Hg FOR FIFTEEN MINUTES.

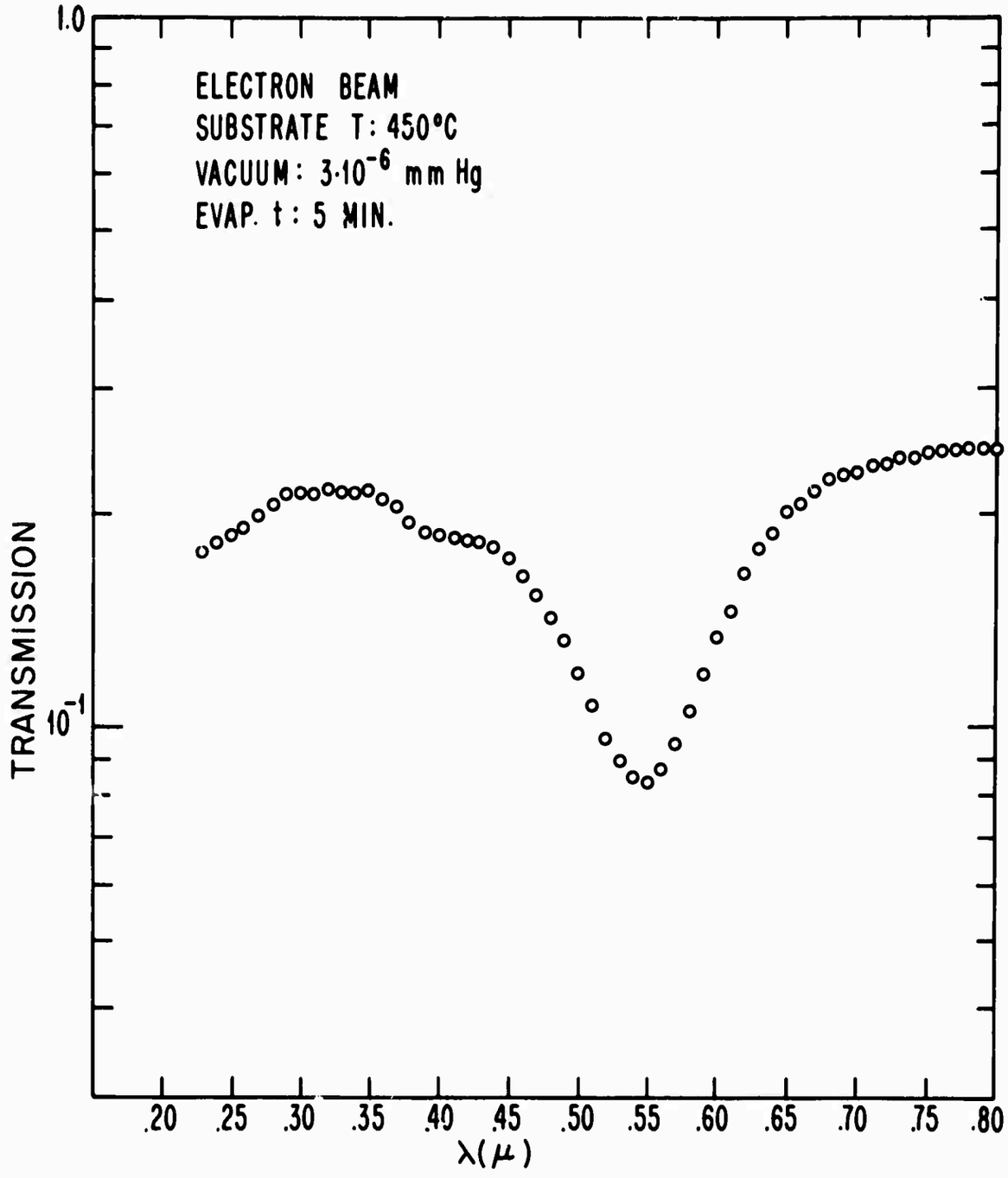

FIG. 3-19 TRANSMISSION SPECTRUM OF A FILM GROWN ON CaF_2 BY ELECTRON BEAM EVAPORATION OF Ni IN A VACUUM OF $3 \cdot 10^{-6}$ mm Hg.

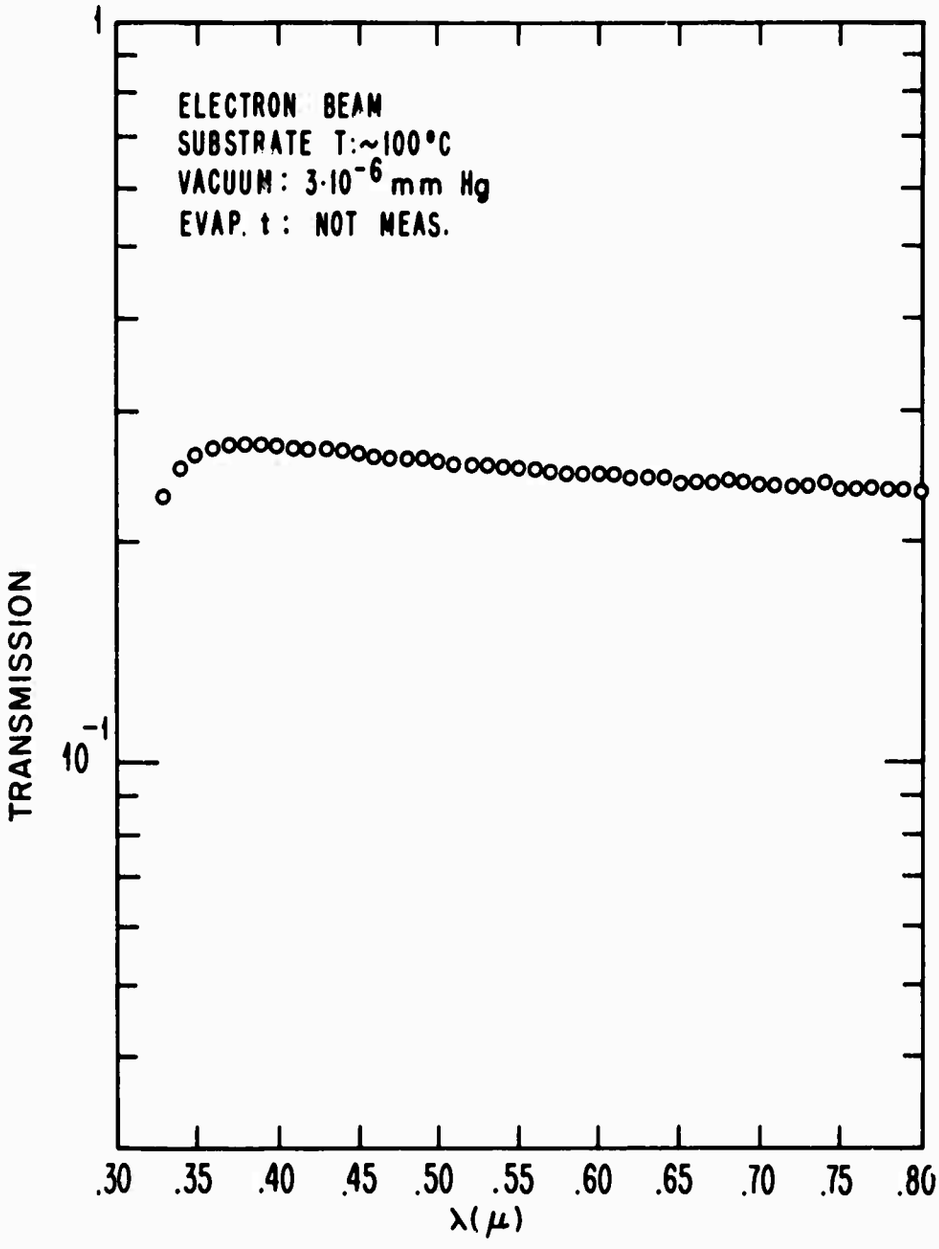

FIG. 3-20 TRANSMISSION SPECTRUM OF A FILM GROWN ON GLASS BY ELECTRON BEAM EVAPORATION OF Ni IN A VACUUM OF $3 \cdot 10^{-6}$ mm Hg.

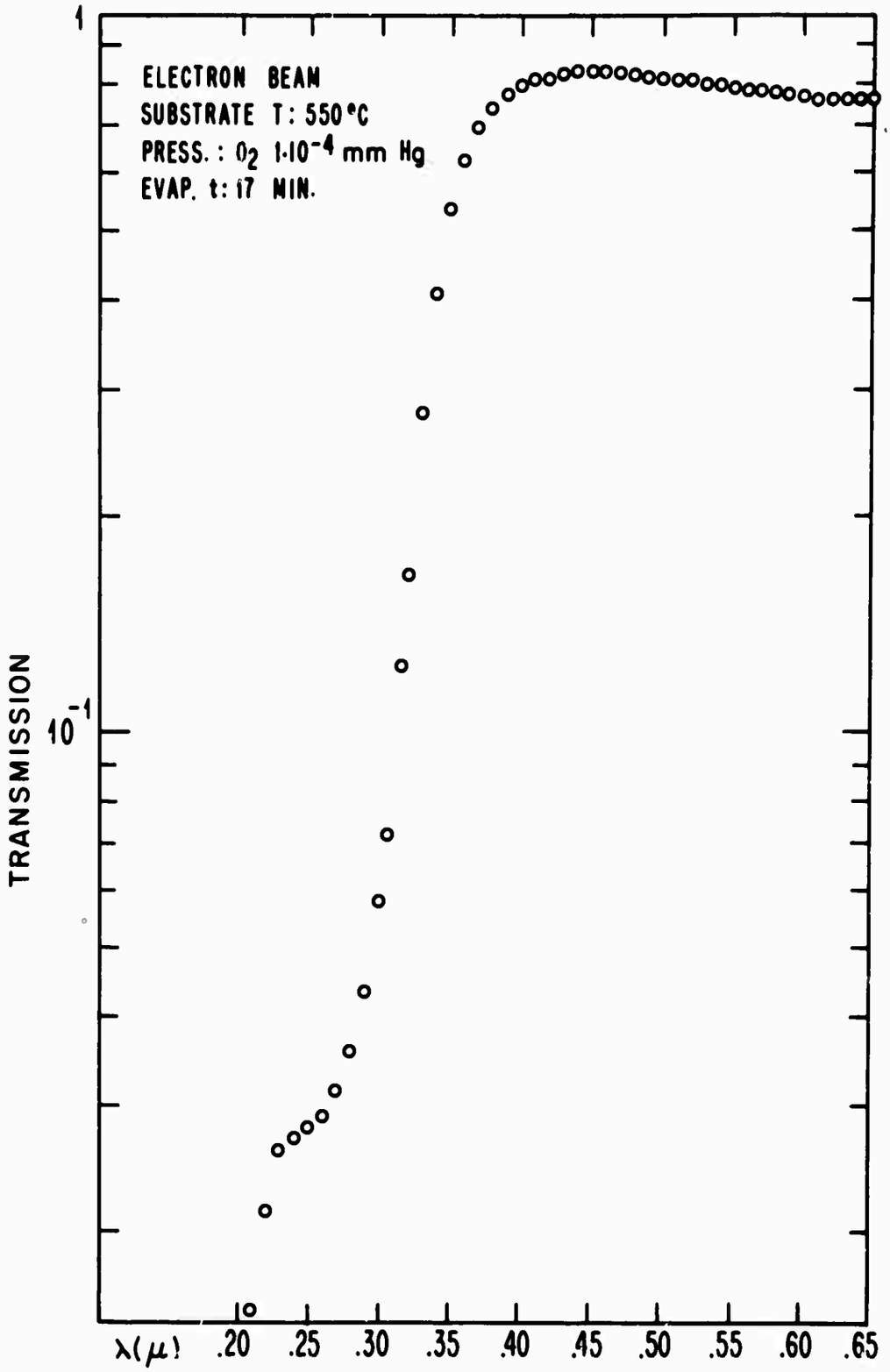

FIG. 3-21 TRANSMISSION SPECTRUM OF A FILM GROWN ON QUARTZ BY ELECTRON BEAM EVAPORATION OF Ni IN AN O_2 ATMOSPHERE OF $1 \cdot 10^{-4}$ mm Hg.

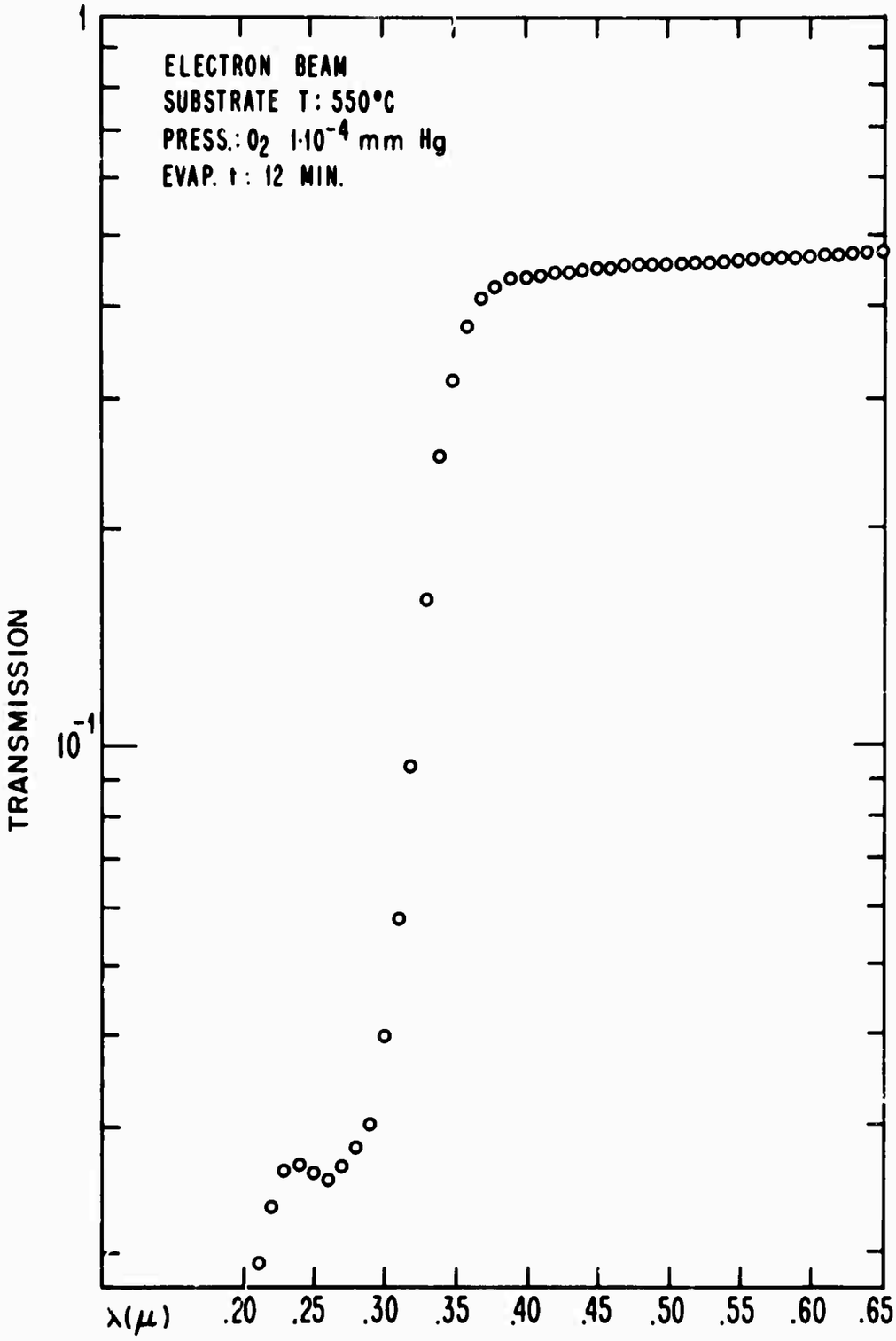

FIG. 3-22 TRANSMISSION SPECTRUM OF A FILM GROWN ON BaF_2 BY ELECTRON BEAM EVAPORATION OF Ni IN AN O_2 ATHOSPHERE OF $1 \cdot 10^{-4}$ mm Hg.

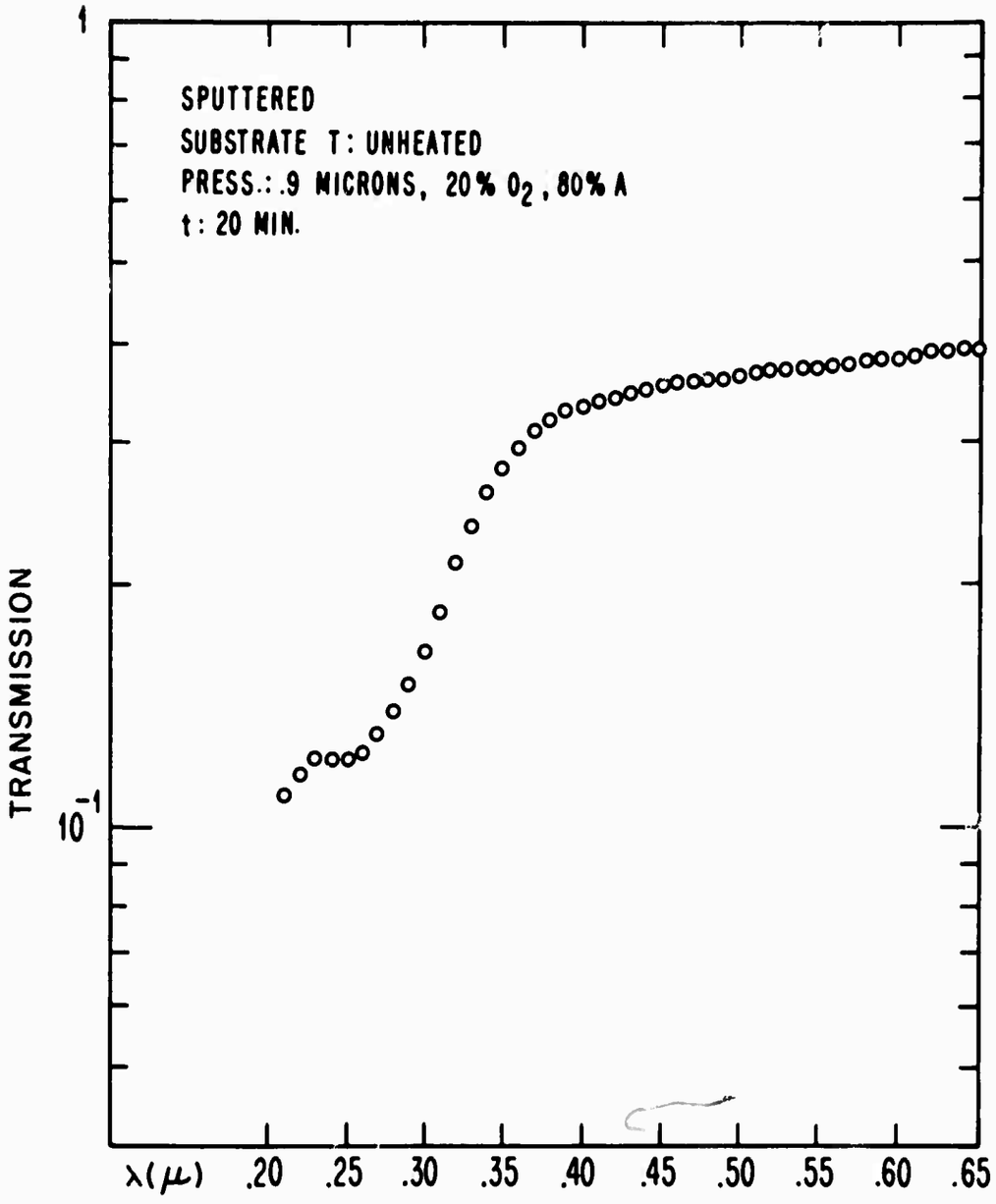

FIG. 3-23 TRANSMISSION SPECTRUM OF A FILM GROWN ON CaF_2 BY SPUTTERING OF Ni IN A 20% O_2, 80% A ATMOSPHERE.

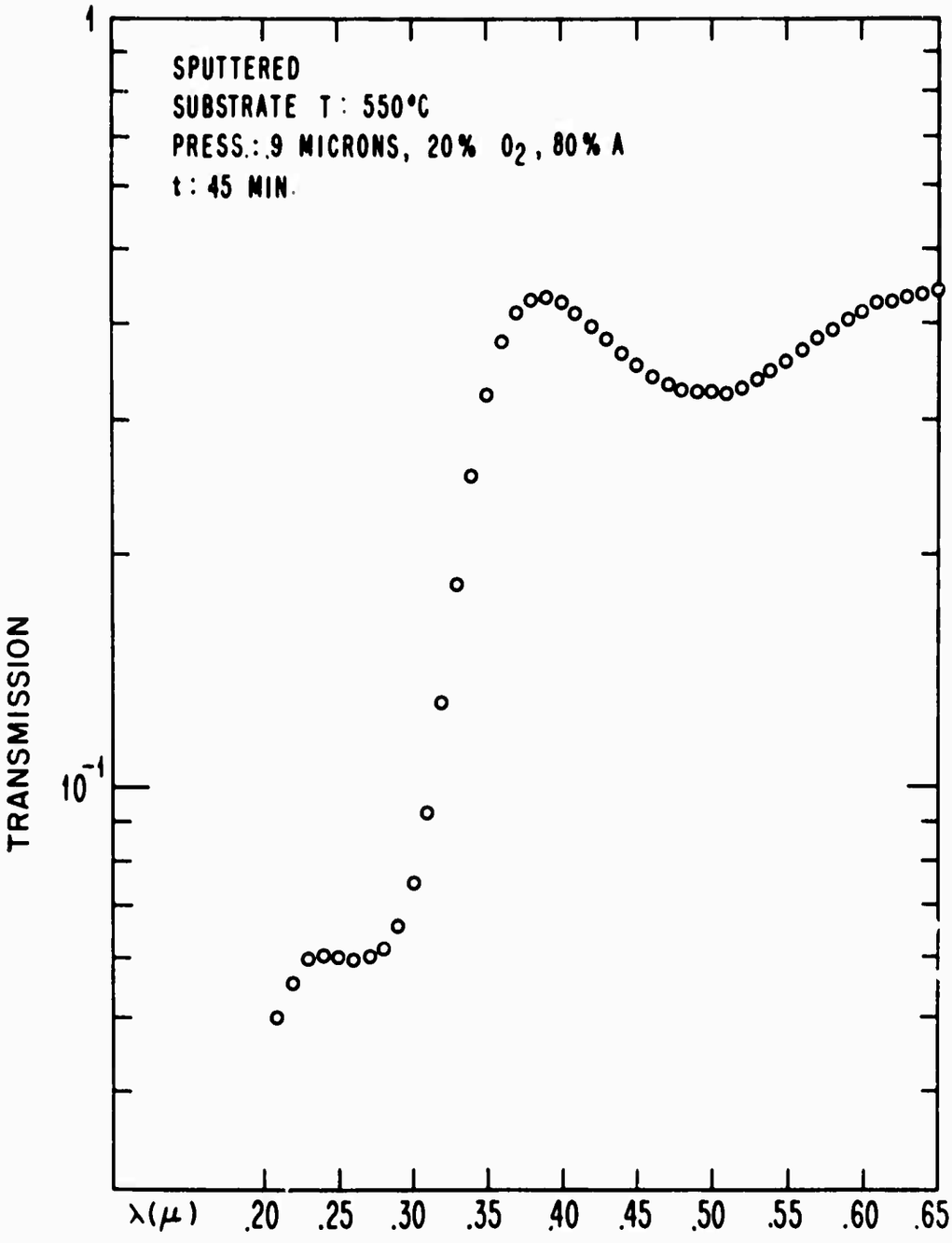

FIG. 3-24 TRANSMISSION SPECTRUM OF A FILM GROWN ON LiF BY SPUTTERING OF Ni IN A 20% O_2, 80% A ATMOSPHERE

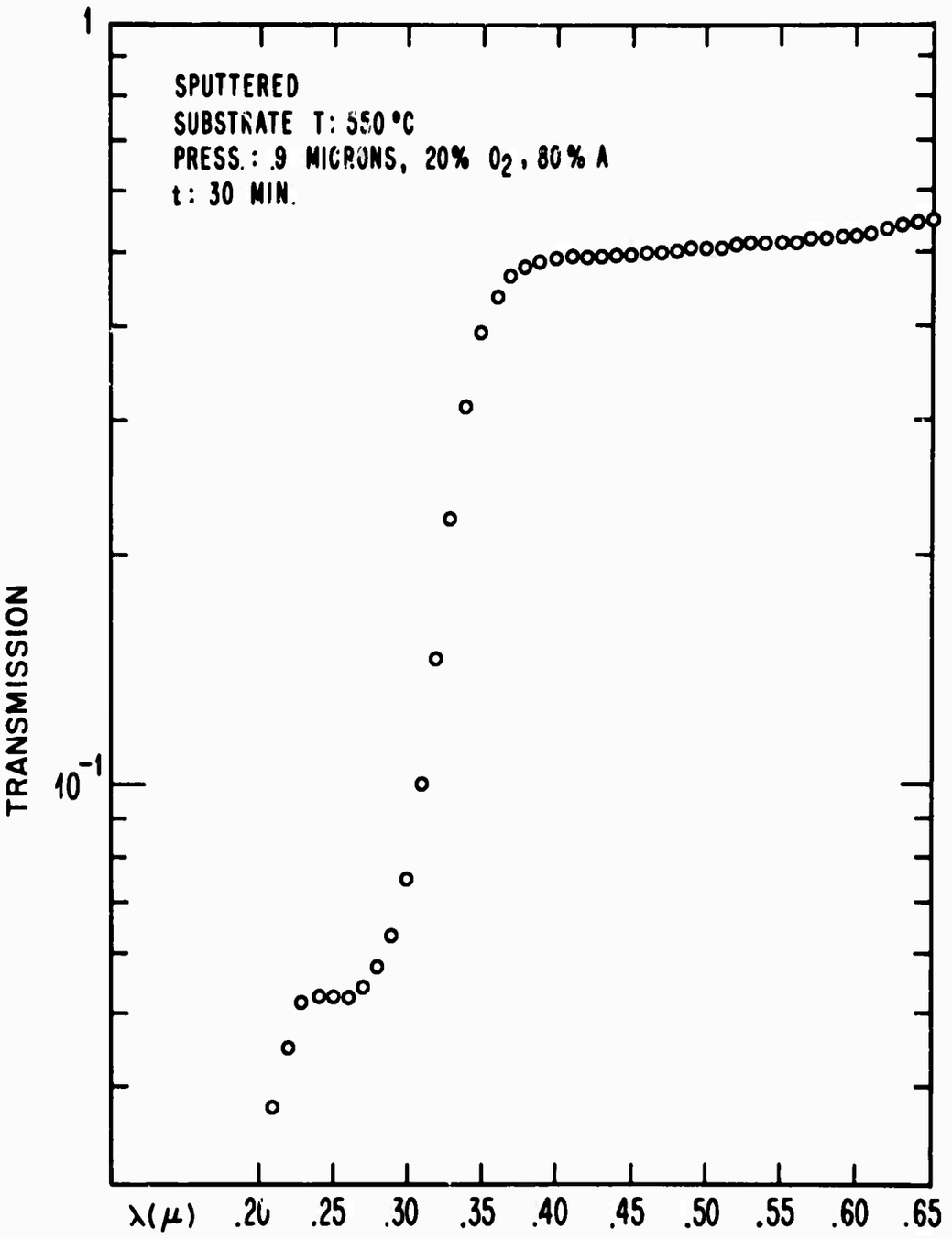

FIG. 3-25 TRANSMISSION SPECTRUM OF A FILM GROWN ON QUARTZ BY SPUTTERING OF Ni IN A 20% O_2, 80% A ATMOSPHERE.

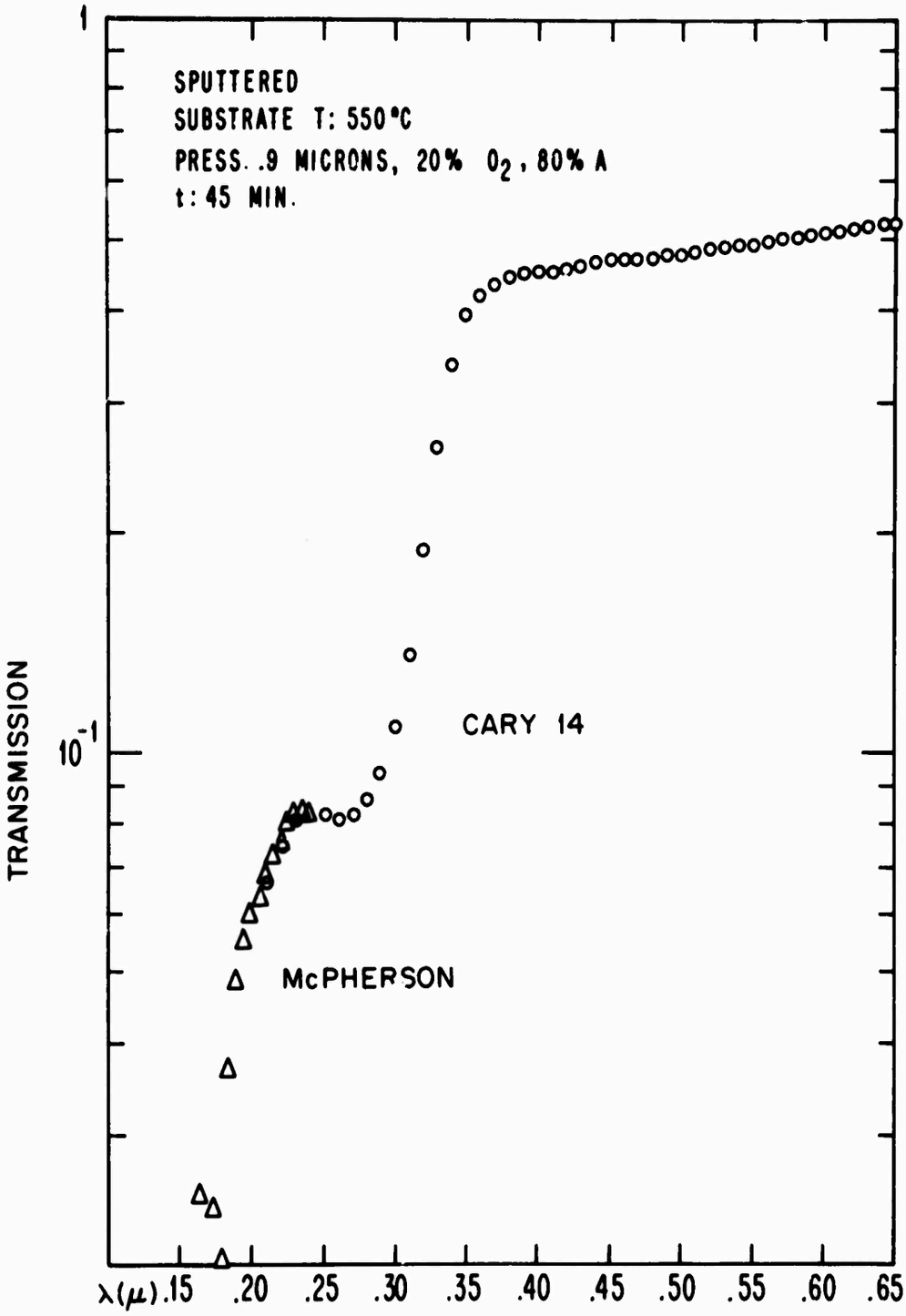

FIG. 3-26 TRANSMISSION SPECTRUM OF A FILM GROWN ON CaF_2 BY SPUTTERING OF Ni IN A 20% O_2, 80% A ATMOSPHERE.

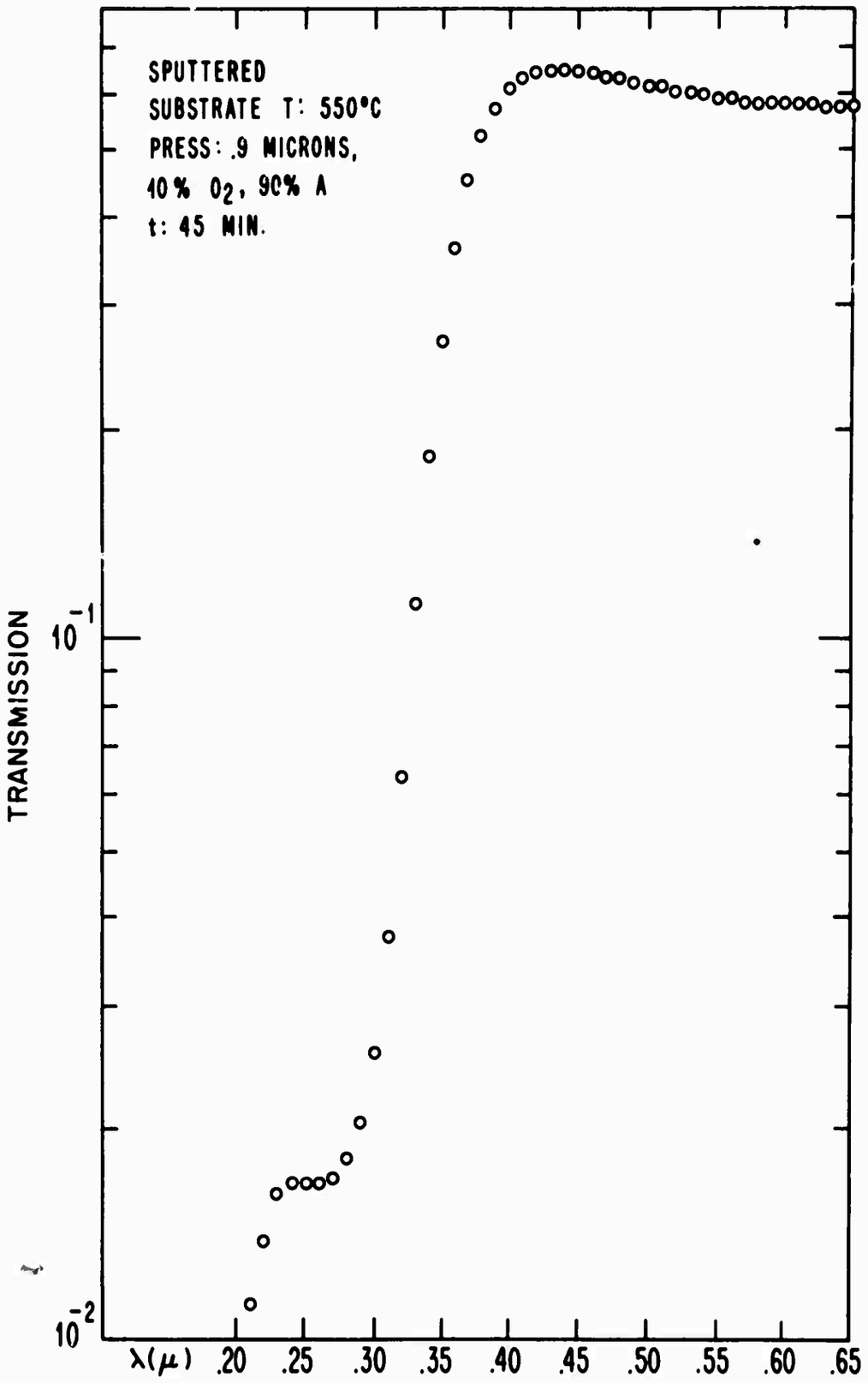

FIG. 3-27 TRANSMISSION SPECTRUM OF A FILM GROWN ON QUARTZ BY SPUTTERING Ni IN A 10% O_2, 90% A ATMOSPHERE.

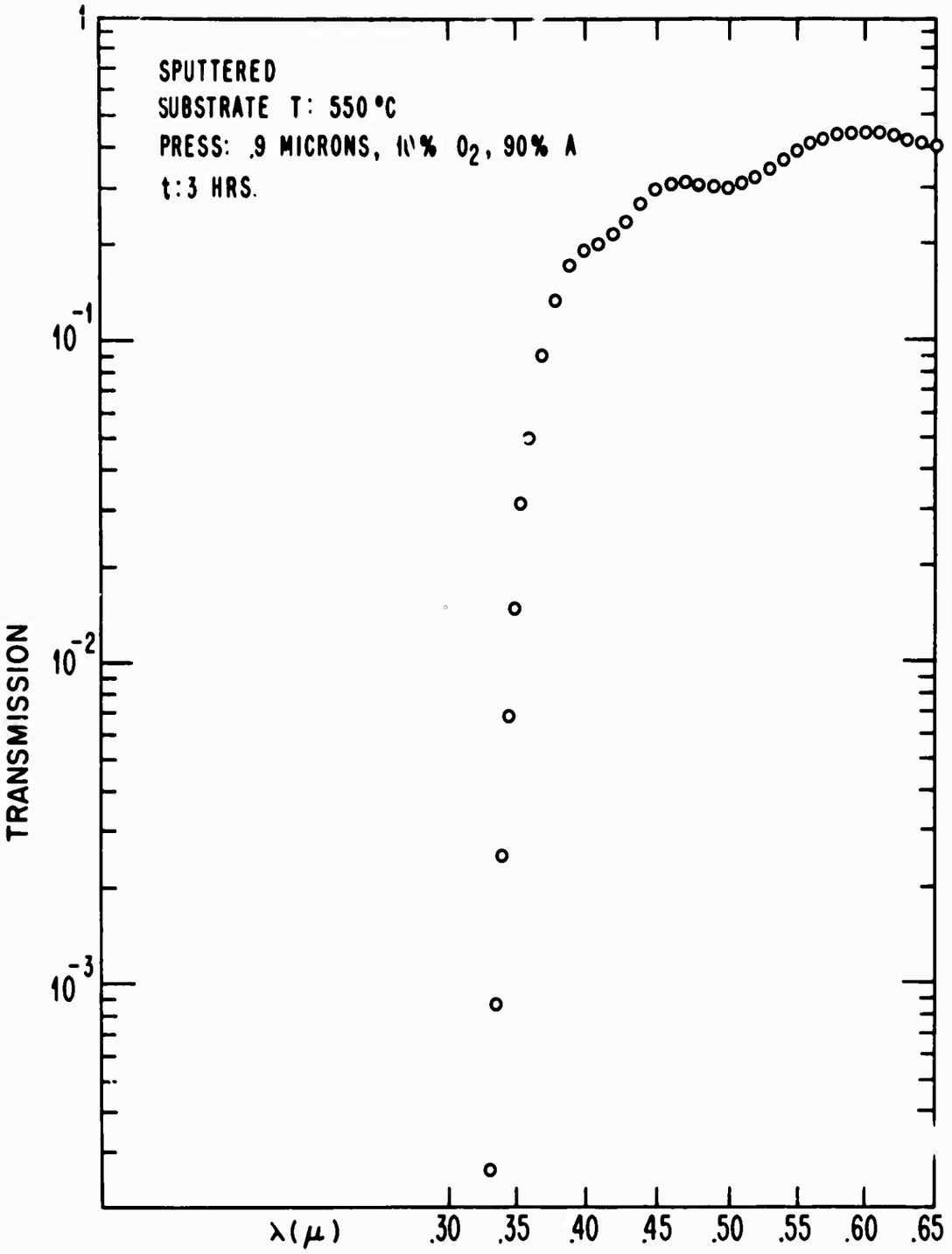

FIG. 3-28 TRANSMISSION SPECTRUM OF A FILM GROWN ON QUARTZ BY SPUTTERING Ni IN A 10% O_2, 90% A ATMOSPHERE.

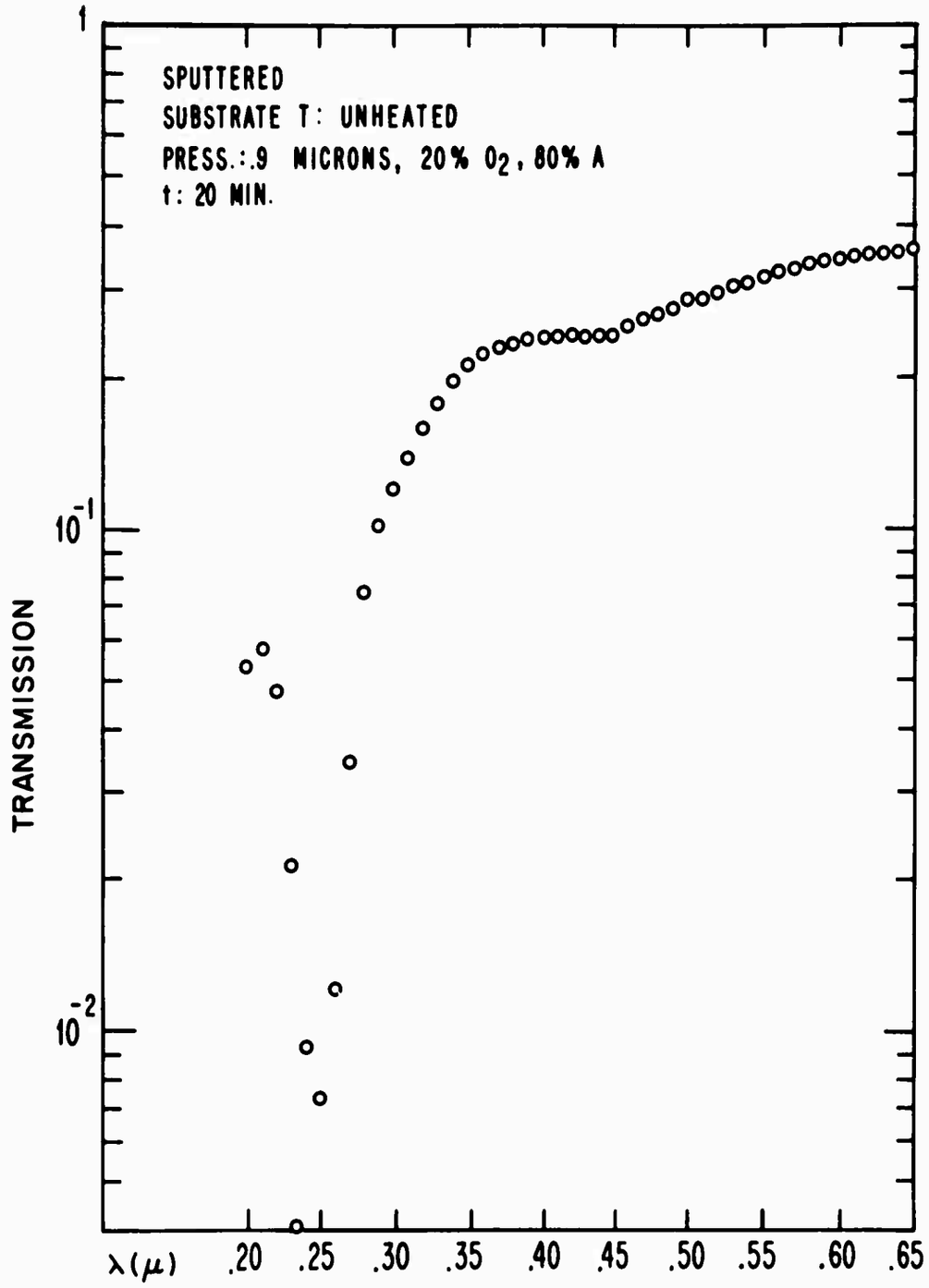

FIG. 3-29 TRANSMISSION SPECTRUM OF A FILM GROWN ON LiF BY SPUTTERING Ni IN A 20% O_2, 80% A ATMOSPHERE.

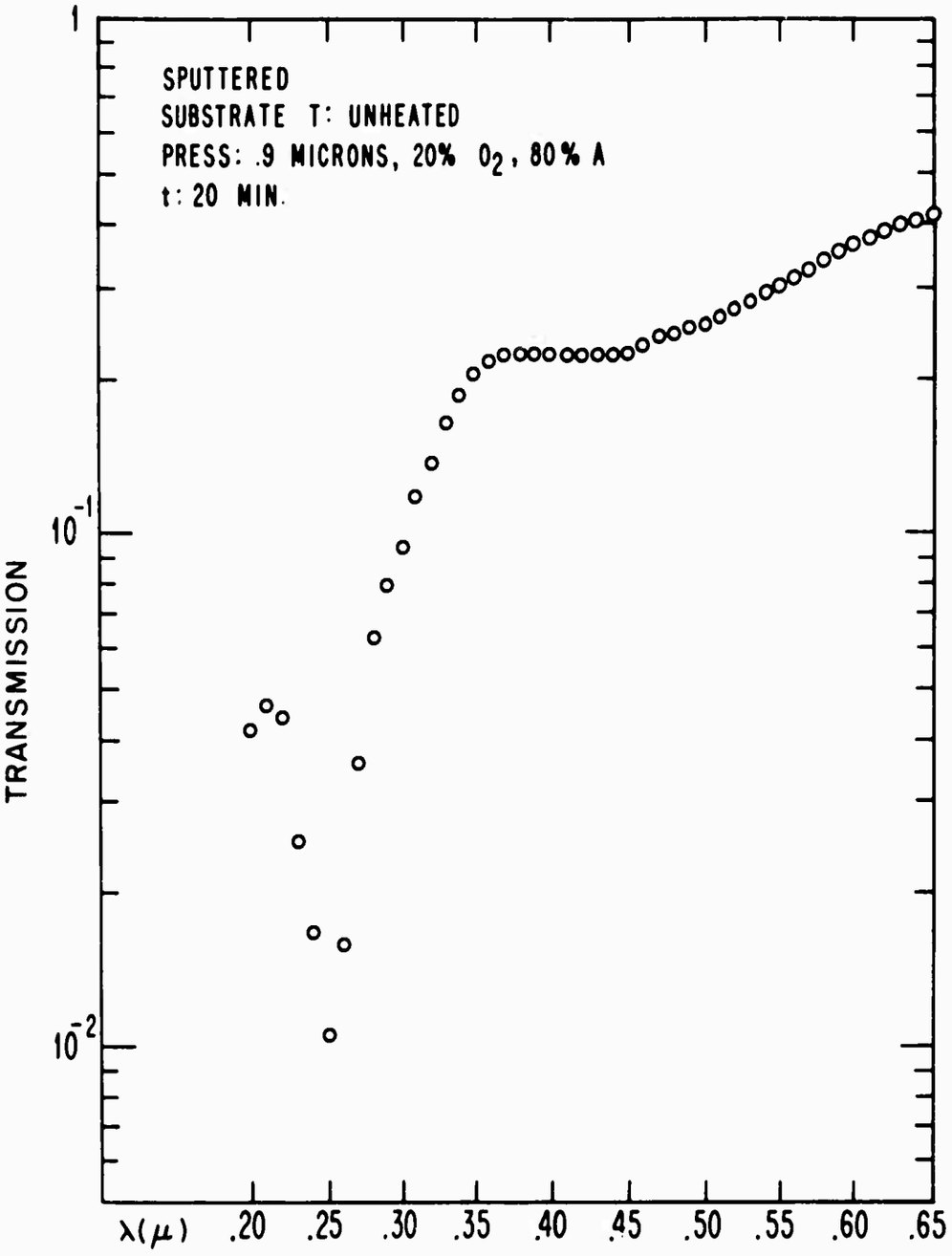

FIG. 3-30 TRANSMISSION SPECTRUM OF A FILM GROWN ON LiF BY SPUTTERING Ni IN A 20% O_2, 80% A ATMOSPHERE.

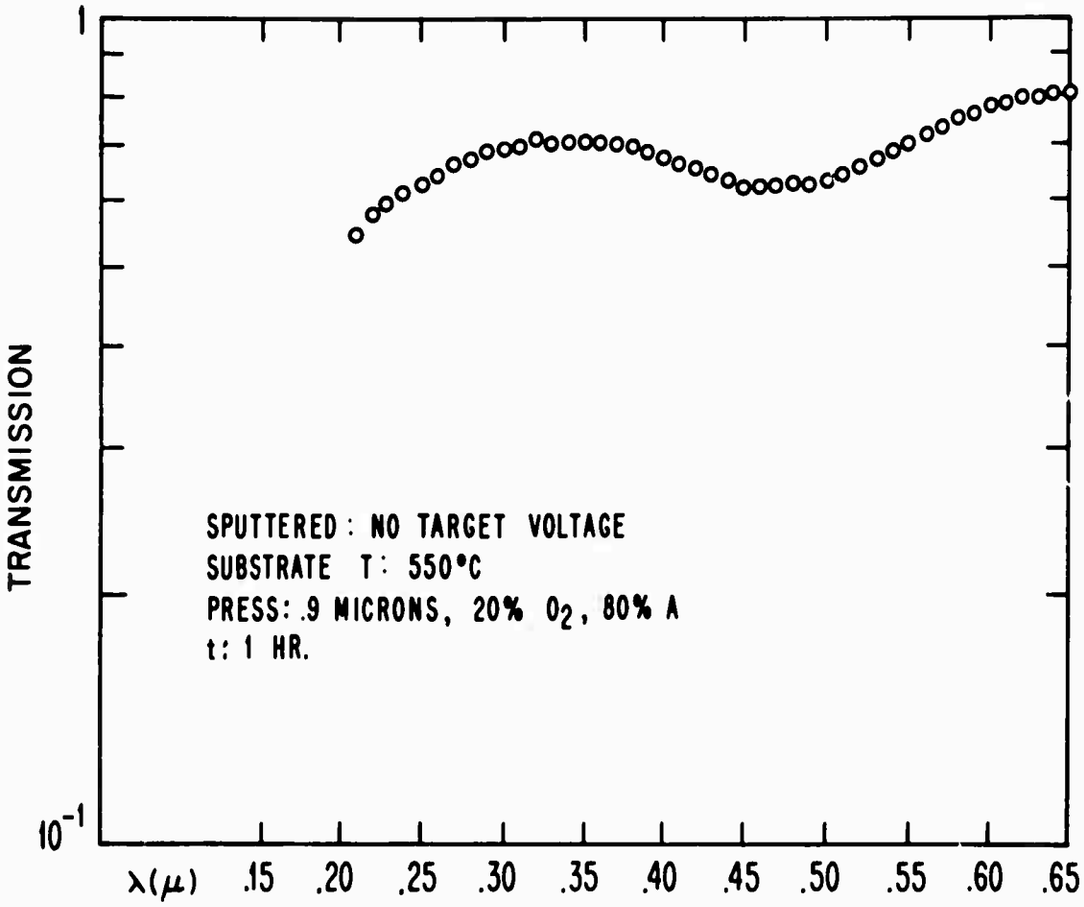

FIG. 3-31 TRANSMISSION SPECTRUM OF A LiF SUBSTRATE PLACED IN THE SPUTTERING UNIT PLASMA AND HELD AT 550°C FOR ONE HOUR WITH THE TARGET VOLTAGE AT ZERO.

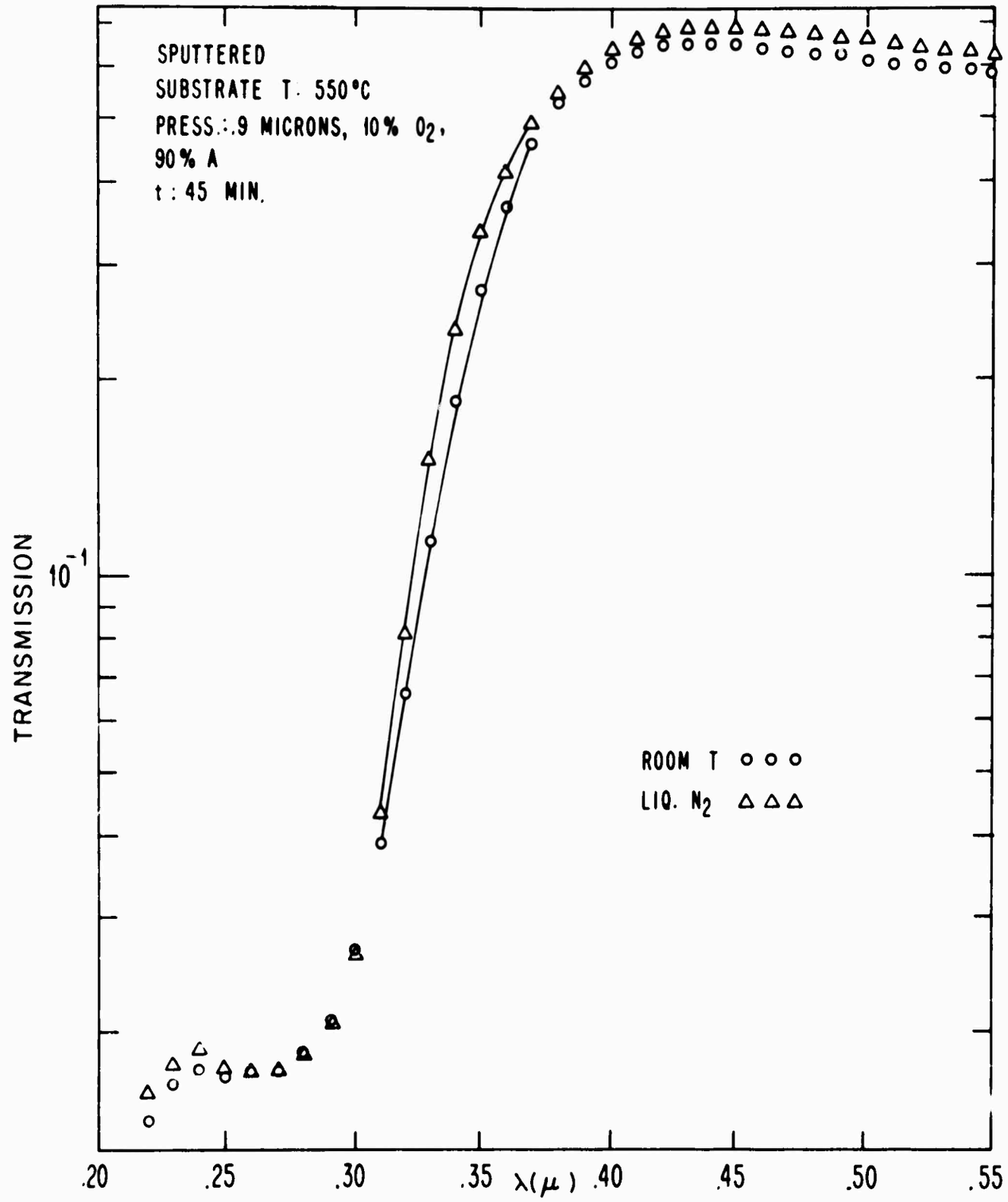

FIG 3-32 TEMPERATURE SHIFT OF ABSORPTION EDGE OF NiO FILM GROWN ON QUARTZ BY SPUTTERING Ni IN A 10% O_2, 30% A ATMOSPHERE.

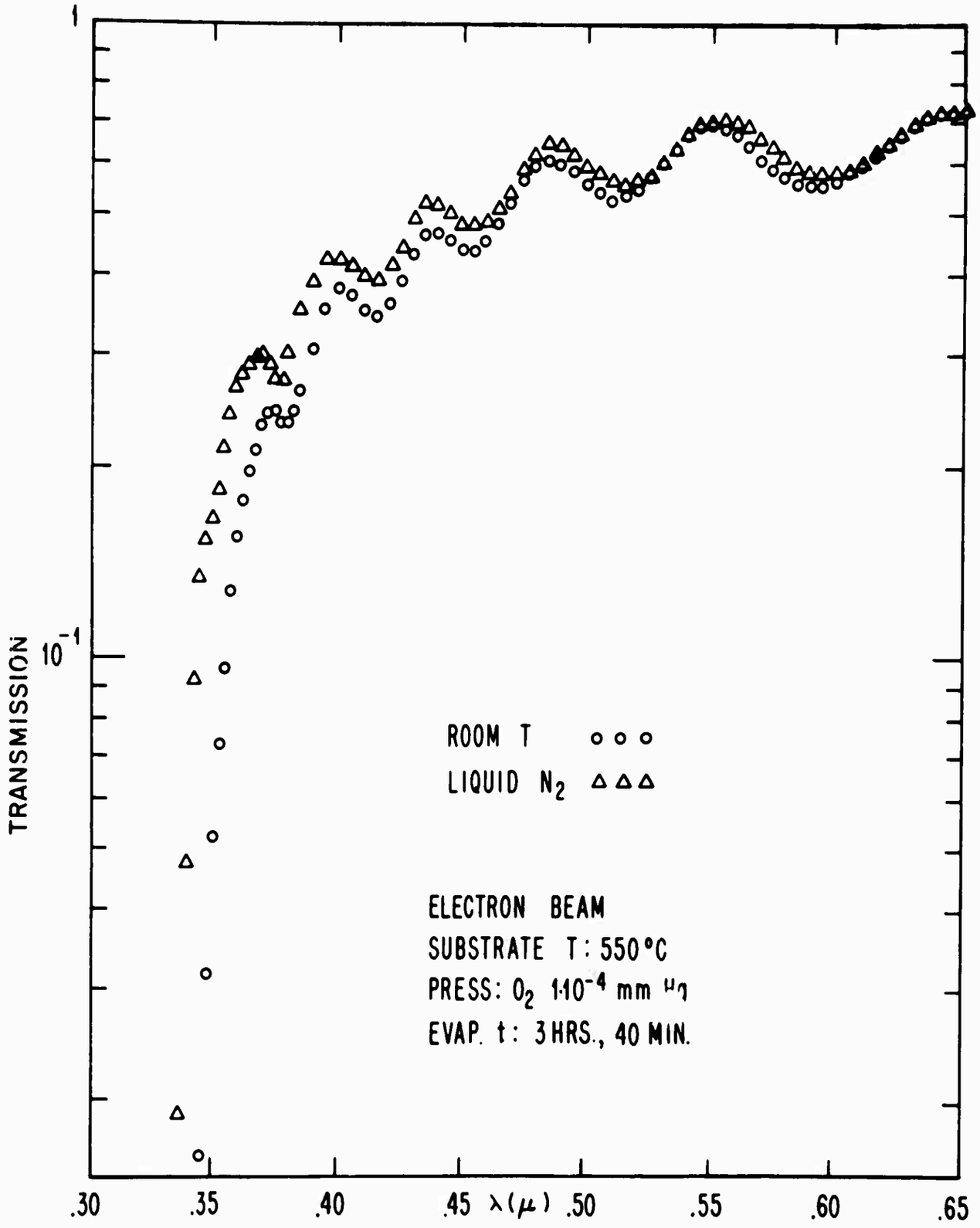

FIG. 3-33 TEMPERATURE SHIFT OF ABSORPTION EDGE OF NiO FILM GROWN ON CaF_2 BY ELECTRON BEAM EVAPORATION OF Ni IN AN O_2 ATMOSPHERE OF $1{\cdot}10^{-4}$ mm Hg.

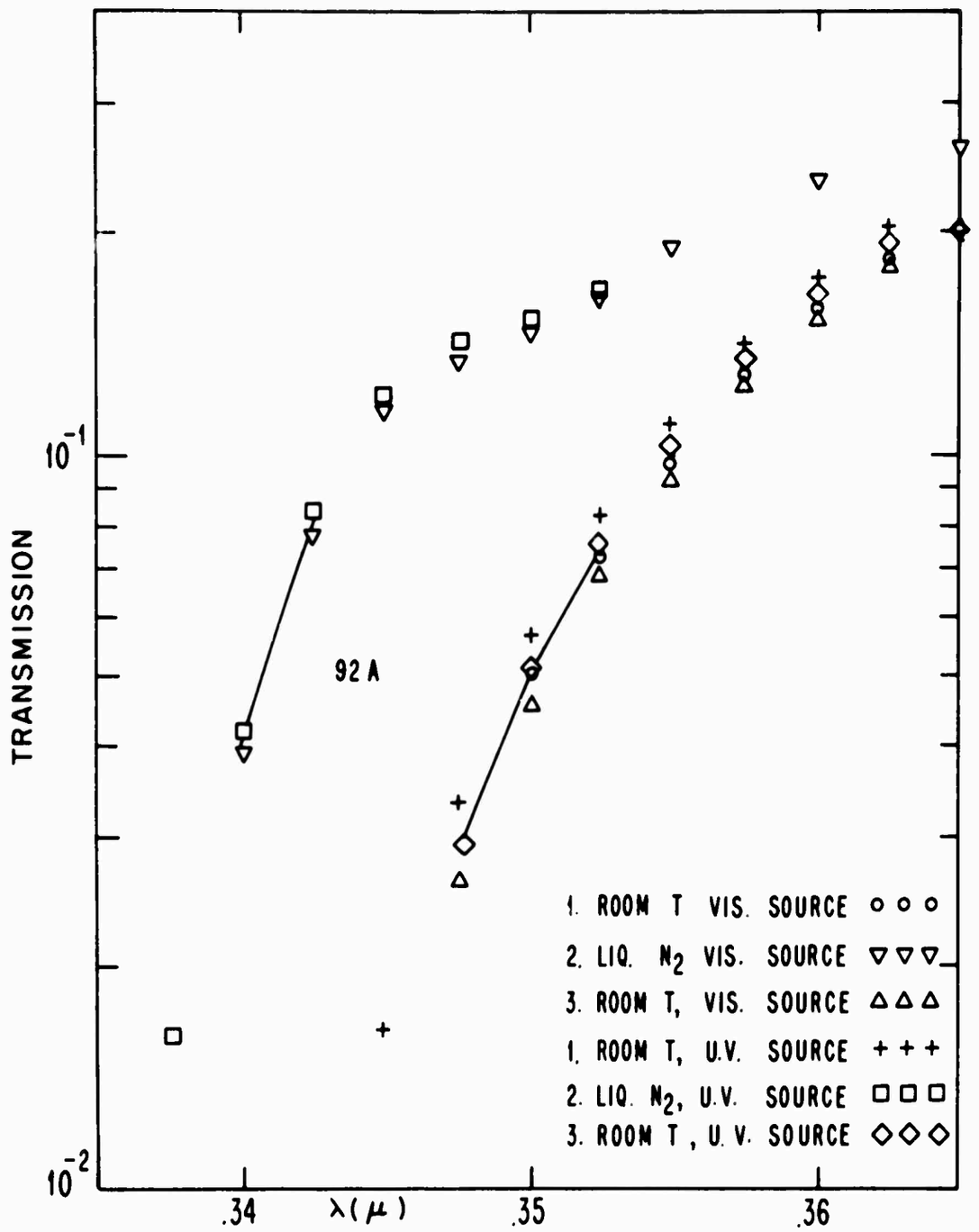

FIG. 3-34 A SECOND MEASUREMENT OF THE TEMPERATURE SHIFT OF THE FILM OF FIGS. 3-14 AND 3-33 INCLUDING A CHECK FOR HYSTERESIS.

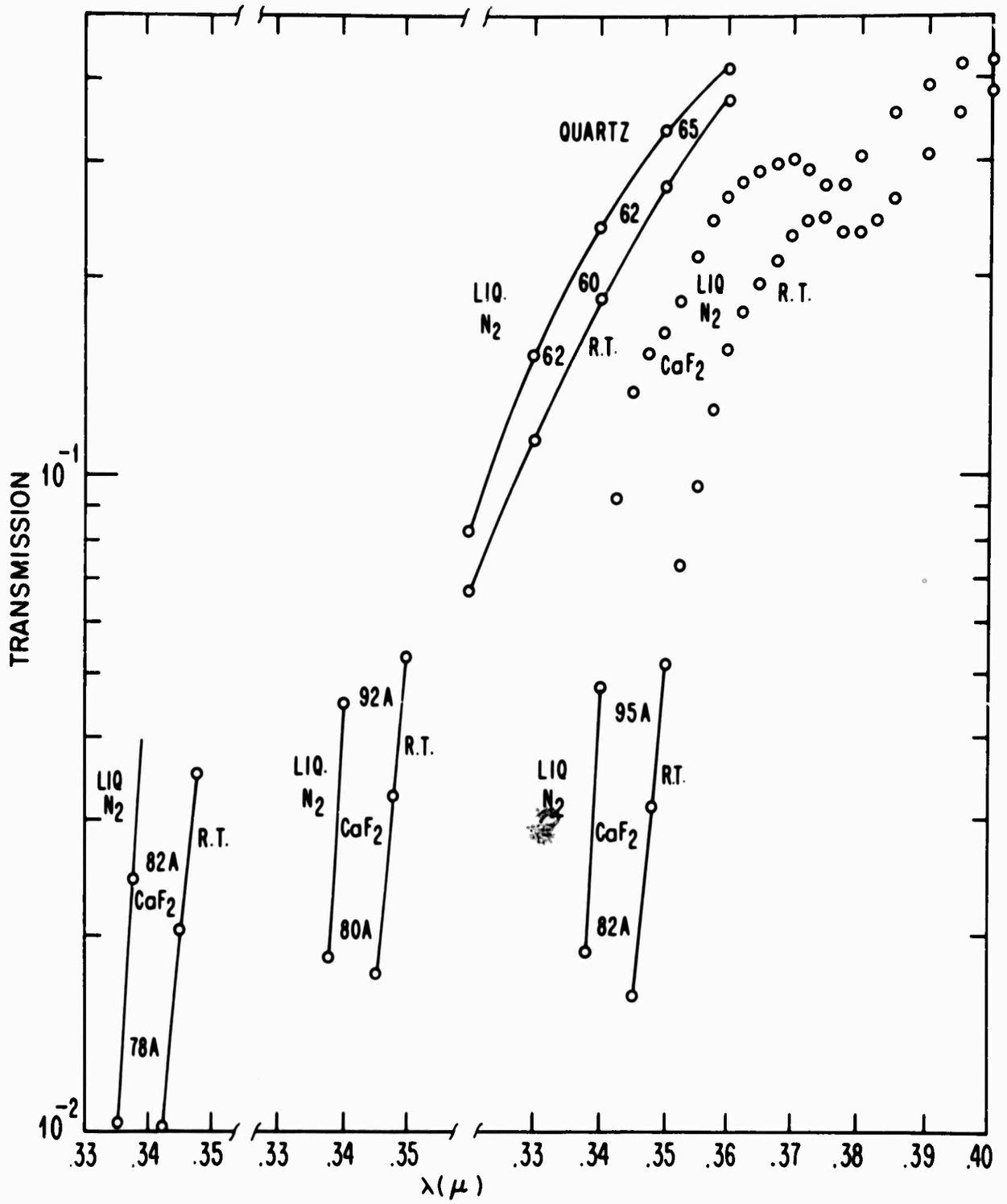

FIG. 3-35 TEMPERATURE SHIFTS OF THE FILMS IN FIGS. 3-32 AND 3-33 SHOWN ON AN EXPANDED SCALE.

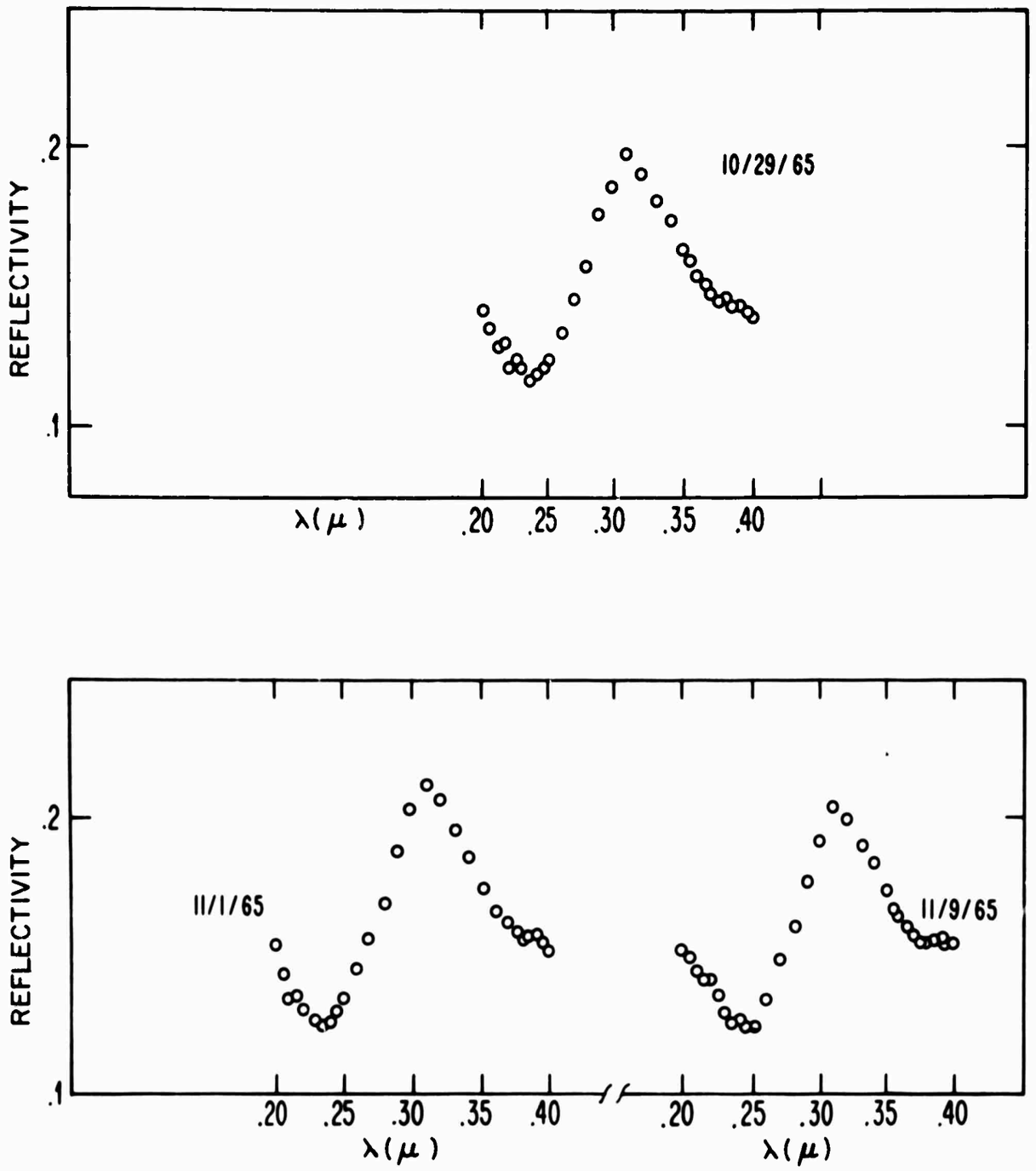

FIG. 3-36 REFLECTIVITY SPECTRA OF THREE FILMS OF NiO GROWN ON MgO SUBSTRATES BY VAPOR DEPOSITION. THE MEASUREMENTS WERE TAKEN WITH THE JARRELL ASH EQUIPMENT (REF. 1).

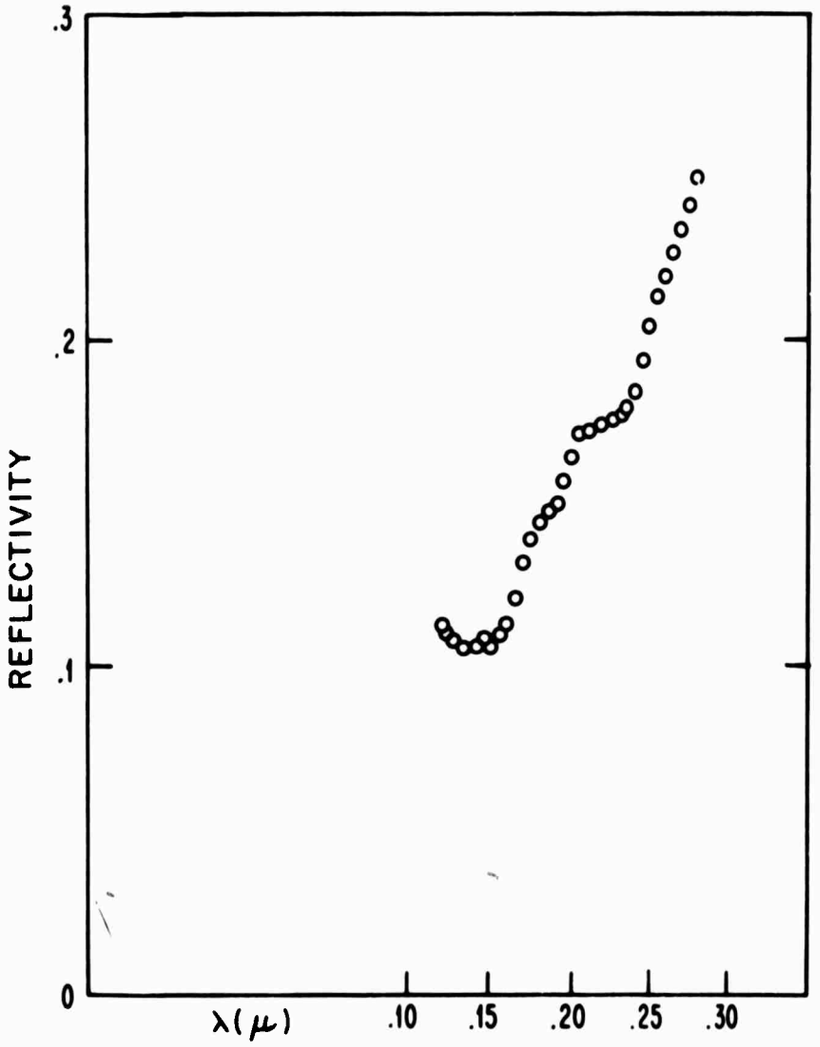

FIG. 3–37 REFLECTIVITY SPECTRUM OF A NiO FILM GROWN ON A MgO SUBSTRATE BY VAPOR DEPOSITION. THE MEASUREMENTS WERE MADE WITH THE MCPHERSON MODEL 225 VACUUM ULTRAVIOLET SPECTROMETER (FIG. 3-1).

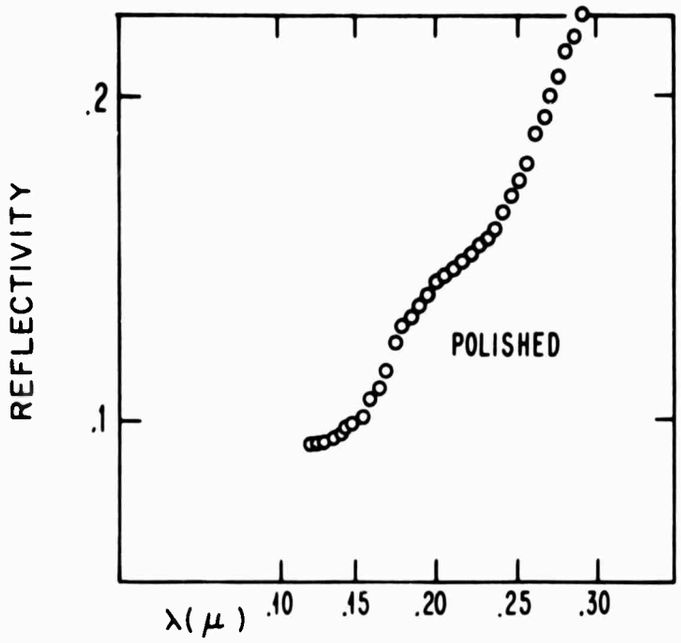

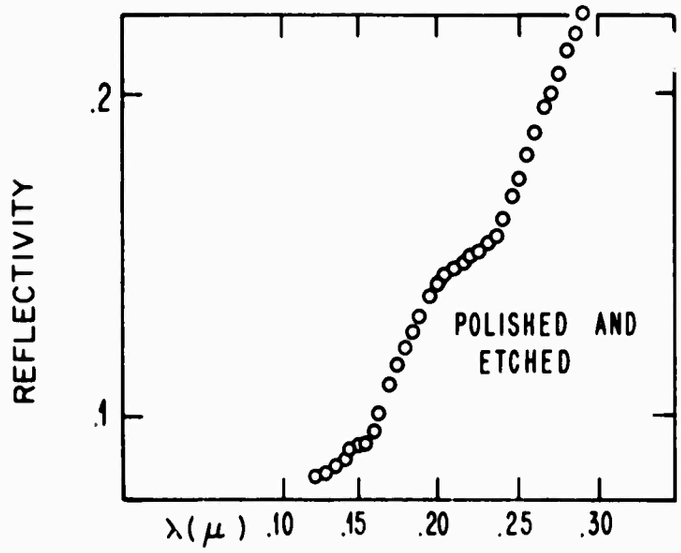

FIG. 3-38 REFLECTIVITY SPECTRA OF BULK NiO. THE UPPER CURVE SHOWS THE REFLECTIVITY OF A POLISHED SAMPLE AND THE LOWER CURVE THE REFLECTIVITY OF A POLISHED AND ETCHED SAMPLE. THE MEASUREMENTS WERE MADE WITH THE MCPHERSON MODEL 225 VACUUM ULTRA-VIOLET SPECTROMETER (FIG. 3-1).

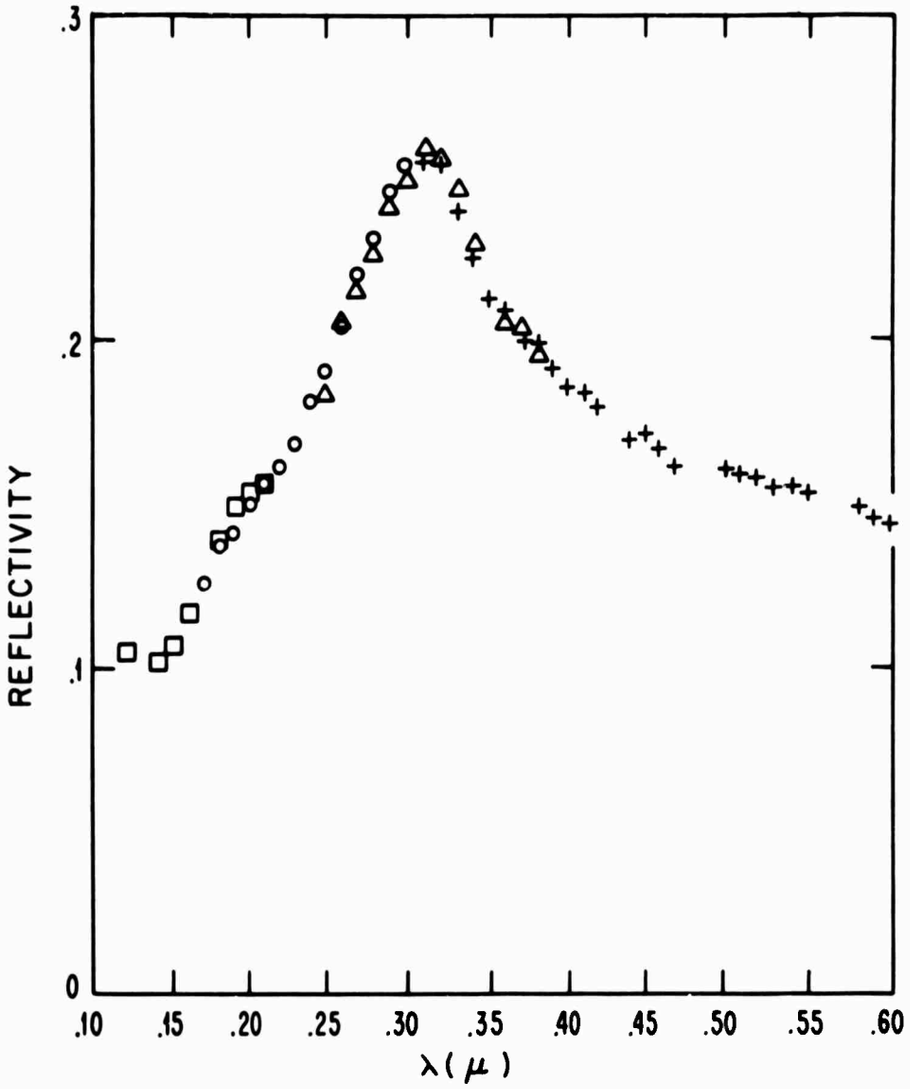

FIG. 3-39 REFLECTIVITY SPECTRUM OF BULK NiO OVER THE WAVELENGTH RANGE OF 1250 TO 6000 A. THE SAMPLE IS THE SAME AS THAT OF FIG. 3-38 AND THE SURFACE IS THE POLISHED AND ETCHED SURFACE OF FIG. 3-38. THE MEASUREMENTS WERE MADE WITH THE MCPHERSON MODEL 225 VACUUM ULTRAVIOLET SPECTROMETER (FIG. 3-1). DIFFERENT FILTERS WERE USED IN DIFFERENT WAVELENGTH REGIONS WITH OVERLAP BETWEEN THE REGIONS. A SEPARATE SYMBOL HAS BEEN USED IN THE FIGURE TO DESIGNATE DATA OBTAINED WITH EACH FILTER.

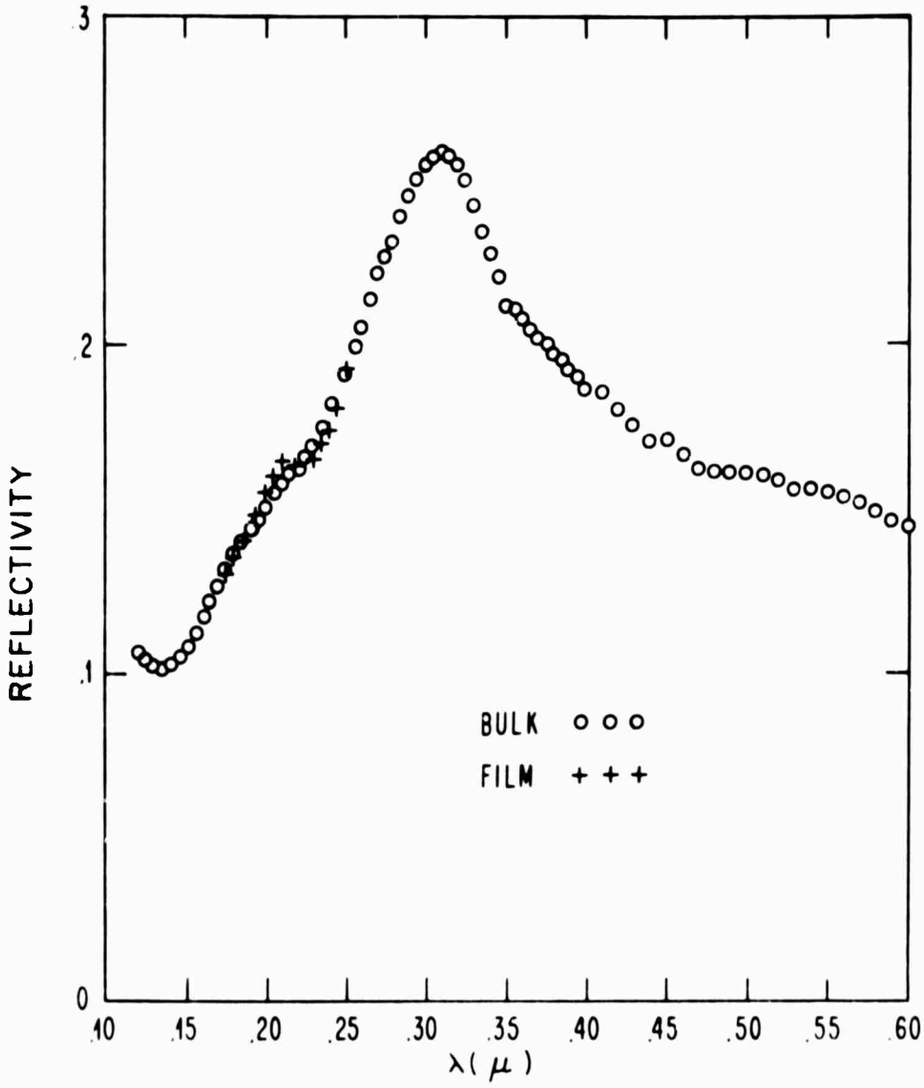

FIG. 3-40 REFLECTIVITY DATA USED IN THE KRAMERS KRONIG ANALYSES OF FIGS. 3-41 AND 3-42. THE BULK DATA IS THAT OBTAINED BY DRAWING A REASONABLY SMOOTH CURVE THROUGH THE VALUES PLOTTED IN FIG. 3-39. ALL GAPS IN DATA WERE FILLED IN BY EXTRAPOLATION TO PROVIDE VALUES FOR THE COMPUTER PROGRAM USED IN THE ANALYSIS. THE FILM DATA SHOWN BETWEEN 1800 AND 2500 A WAS OBTAINED BY ADJUSTING THE VALUES OF FIG. 3-37 TO AGREE WITH THE BULK VALUES AT ~1800 AND ~2500 A.

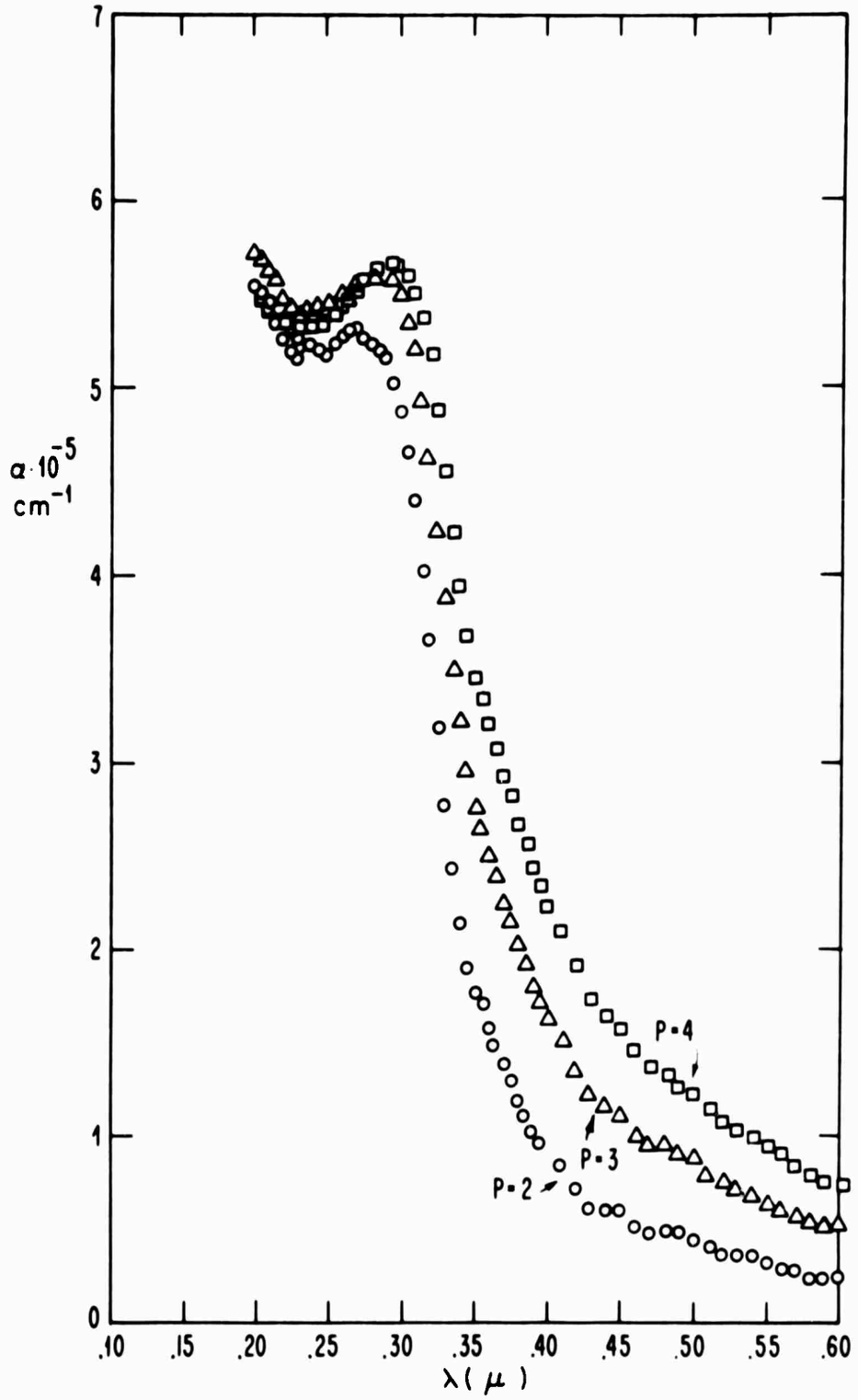

FIG. 3-41 THE ABSORPTION CONSTANT OBTAINED BY A KRAMERS KRONIG ANALYSIS OF THE BULK NiO REFLECTIVITY DATA SHOWN IN FIG. 3-40. THE ABSORPTION CONSTANT IS SHOWN FOR THREE EXTRAPOLATION PARAMETERS, P•2, 3 AND 4 (SEE APPENDIX 1).

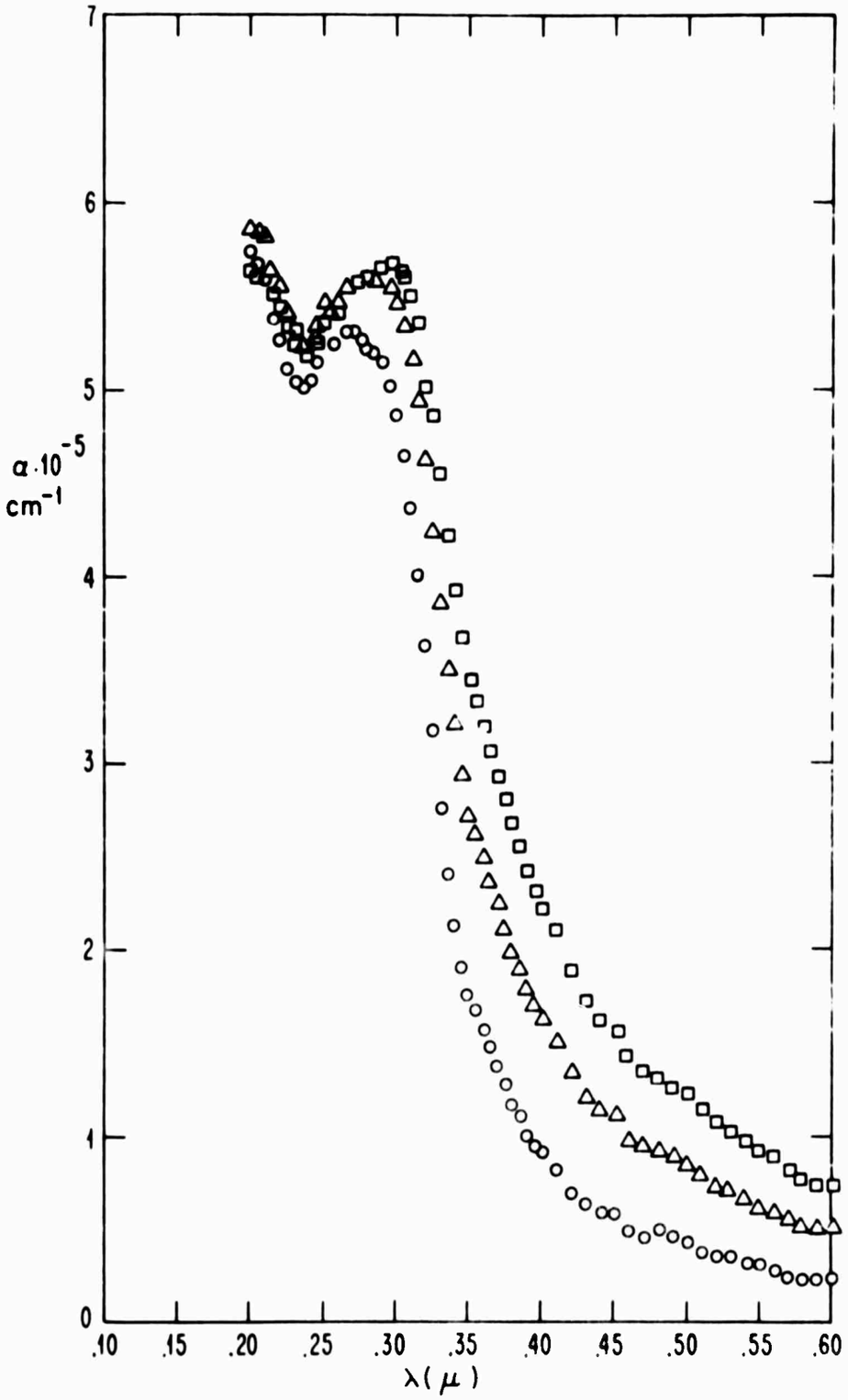

FIG. 3-42 THE ABSORPTION CONSTANT OBTAINED BY A KRAMERS KRONIG ANALYSIS OF THE BULK NiO REFLECTIVITY DATA MODIFIED TO AGREE WITH NiO FILM RESULTS BETWEEN 1800 AND 2500 A. THE DATA USED ARE SHOWN IN FIG. 3-40. THE ABSORPTION CONSTANT IS SHOWN FOR THREE EXTRAPOLATION PARAMETERS, P=2, 3, AND 4 (SEE APPENDIX 1).

Chapter Three

BIBLIOGRAPHY

1. P. M. Grant, Technical Report No. HP-14, Gordon McKay Laboratory Division of Engineering and Applied Physics, Harvard University, 1965.

2. C. E. Rossi, Technical Report No.HP-17, Gordon McKay Laboratory, Division of Engineering and Applied Physics, Harvard University, 1967.

3. R. Newman and R. M. Chrenko, Phys. Rev. 114, 1507 (1959).

4. H. Ehrenreich, H. R. Phillipp, and D. J. Olechna, Phys. Rev. 131, 2469 (1963).

5. W. P. Doyle and G. A. Lonergan, Disc. Faraday Soc. No. 26, 27-33 (1958).

6. C. H. Reiling and E. B. Hensley, Phys. Rev. 112, 1106, (1958).

7. L. Holland, Vacuum Deposition of Thin Films (John Wiley and Sons, Inc., New York, 1960).

Chapter Four

CONCLUDING STATEMENTS AND SUGGESTED FURTHER WORK ON NiO

In Chapter One we have given a brief review of the experimental work performed on the transport and optical properties of NiO. The early models for the NiO transport were for the most part based on the assumption of thermally activated hopping of holes where the activation energy occurred in the mobility. The most recent data, however, points strongly to a model where the activation energy is due to activation of carriers and the transport occurs in a narrow band. It is fairly clear that early transport data were strongly affected by sample perfection and purity and that many workers were misled in their interpretations by phenomena such as grain boundary effects. It is now fairly clear (Reference 36 in Chapter One) that the transport in so-called pure NiO is determined by impurities and/or imperfections up to temperatures as high as room temperature. Adler (Reference 47 of Chapter One) suggests the possibility that all observed transport data up to this time may be due to impurities and intrinsic conduction may not as yet have been observed in NiO. As possible evidence for this suggestion Adler quotes the optical results contained in References 39 and 55 of Chapter One. The optical results indicate an energy gap of $\sim$4 eV which is considerably higher than values obtained from recent transport experiments.

It appears from a perusal of the transport results that considerable emphasis should be placed on the preparation of high quality pure single crystals for use in any future transport experiments on NiO in order to reduce the extraneous effects.

The optical results from thin NiO films described in Chapter Three as well as the results of References 39 and 55 of Chapter One are consistent with a model of absorption by crystal field split 3d levels up to ∿3.3 eV (3700 angstroms). At ∿3.3 eV (3700 angstroms) the absorption of our films increases rapidly to an apparent maximum at about 4.8 eV (2600 angstroms) and then increases again near 5.4 eV (2300 angstroms). The absorption constant derived from our measured reflectivity supports the behavior of the absorption inferred from the transmission of the NiO thin films. Our optical results all indicate structure near the absorption edge either due to two nearby band transitions or a transition to an exciton state followed by a band transition at a higher energy. One possibility is the transition between the oxygen 2p levels and an exciton below the 4s band at about 4.8 eV followed by a transition to the 4s band. Other possibilities also exist and our results are certainly not conclusive as to the precise transitions involved.

It would be interesting to measure the NiO resistivity and thermoelectric power versus temperature at various pressures and the optical spectrum of NiO films as a function of pressure to determine if any relation exists between the transport activation energy and the optical spectrum. Only high quality NiO single crystals should be used in the transport measurements for the reasons discussed earlier in this section. It would also be interesting to compare the effect of pressure on the optical spectrum of NiO with the effect of pressure on the optical spectrum of MgO. The effect on the MgO spectrum should be similar except for the effects caused by the presence of d levels in NiO. Optical measurements such as those reported in Chapter Three

should be extended into the ultraviolet to higher energies. The reflectivity measurements can be reasonably easily extended although some care should be taken in the choice of samples. NiO films epitaxially grown on MgO by vapor deposition may be the best choice for reflectivity measurements since the sample surface probably is of a better quality than any surface which can presently be obtained from bulk samples. Extending transmission measurements to higher energies may be a bit more difficult since the substrates become less transparent in the vacuum ultraviolet and have a definite cutoff at about 1040 angstroms (LiF). However, with high quality LiF substrates it should be possible to make transmission measurements to 1040 angstroms. Various suggestions for improving the quality and purity of NiO thin films were made in Chapter Two and will not be repeated here.

Appendix

KRAMERS KRONIG PROGRAM

A. Description of the Program

A computer program was written to analyze reflectivity through the use of the Kramers Kronig relation where

$$n = \frac{(1-R)}{1 + R - 2\sqrt{R}\cos\theta}$$

$$k = \frac{2\sqrt{R}\sin\theta}{1 + R - 2\sqrt{R}\cos\theta}$$

$$\alpha = \frac{4\pi k}{\lambda}$$

$$\theta(E) = \frac{E}{\pi}\int_0^{\infty} [\ell n\, R(E') - \ell n\, R(E)]\,(E^2 - E'^2)^{-1}\, dE'$$

where n is the index of refraction

k is the extinction coefficient

R is the reflectivity

α is the absorption constant

λ is the wavelength

θ is the phase.

The computer program computes the integrand at each discrete energy for which measured reflectivity data is available. The integral is then approximated by multiplying the average value of the integrand between each adjacent pair of energies by the difference ΔE between the energies and summing the result (trapezoidal rule). The integral

between the two energies adjacent to the energy where E = E' is taken as the average of the integrand at the two adjacent energies times the energy difference.

Above the energy E_{max} where reflectivity data is not available the reflectivity spectrum is approximated by $R_{max}\left(\frac{E_{max}}{E}\right)^P$ where R_{max} is the value of reflectivity at E_{max} and P is an adjustable parameter. The integration of the phase integral from E_{max} to ∞ is

$$\frac{1}{2\pi}\,\ell n\frac{R(E)}{R(E_{max})}\;\ell n\frac{E_{max}+E}{|E_{max}-E|}+\frac{P}{\pi}\sum_n(2n+1)^{-2}\left(\frac{E}{E_{max}}\right)^{2n+1}$$

The sum is computed to 50 terms in the program.

The usual procedure is to adjust P to give values of k which agree with the values obtained by transmission in the region of low absorption.

A complete Fortran listing of the program is given on page A-6. The input is reflectivity as a function of either energy in electron volts or wavelength in microns. The program prints the following out at each data point:

wavelength in microns

energy in eV

reflectivity as a fraction

absorption constant in inverse microns

index of refraction n

extinction coefficient k

phase theta

B. Instructions for Preparation of Input to the Kramers Kronig Analysis Program

All input is in Format E 10.5 -- i.e. each ten columns contain one input value. Note that if a card contains only two pieces of input data there will be no values except in the first twenty columns.

Card 1 contains a 0. somewhere in the first 10 columns if input reflectivity is a function of energy and 1. if a function of wavelength.

The next set of cards contains the reflectivity values as a function of either energy or wavelength depending on the value input on card 1. Up to 500 values of reflectivity can be input. Each card contains two values. The energy or wavelength is in the first field of 10 columns and the reflectivity in the second. The energy is in electron volts and wavelength in microns. Reflectivity is input as a fraction. The cards must be arranged in order of increasing energy or decreasing wavelength. The second card (first reflectivity card) always contains the reflectivity to be used at 0 energy. A card follows the last card containing a reflectivity to designate the end of reflectivity data. The first two fields of this card contain the value -1.0.

The next card contains a -1.0 in the first field of 10 columns.

The next set of cards contains the values of the extrapolation parameters P, one per card in the first field of 10 columns. The end of P data is designated by a card containing the value - 10000. in the first field. Up to 10 P values may be input for one problem.

Sample

Computer Card Column	1 2 3 4 5 6 7 8 9 10	11 12 13 14 15 16 17 18 19 20
Card 1 contains a 1. to designate reflectivity is input as a function of wavelength (or a 0. to designate reflectivity is input as a function of energy).	1 .	
Card 2 contains the reflectivity at 0 energy (infinite wavelength) in the second 10 columns. The value in the first 10 columns is inconsequential.	0 .	. 3
The next set of cards contains the wavelength in microns (or energy in electron volts) in the first 10 columns with the corresponding reflectivity in the second 10 columns. The cards are arranged in order of decreasing wavelength (or increasing energy) 500 data points are allowed.	1 . . . . . . 5 . . . . . 3 . . . . . . 2 . . . . . 1 3	. 3 . 4 . 5 . 4 . 3 5

	1 2 3 4 5 6 7 8 9 10 11 12 13 14 15 16 17 18 19 20
These two cards always follow the cards containing reflectivities.	- 1 . - 1 .
The next cards contain the P values. 10 values are allowed	2 . . . . . 3 . . . . . 4 .
This card follows the cards containing the P values.	- 1 0 0 0 0.

```
      DIMENSION  E(501), R(501), THI(21),  P(11),  Y1(500),
     1THA(500), ON(500), OK(500), ALF(500),W(500)
      READ (5,1) D1
    1 FORMAT (E10.5)
      READ (5,2) E(1),R(1)
    2 FORMAT (2E10.5)
      DO 3  I=2, 501
      READ (5,5) E(I), R(I)
    5 FORMAT (2E10.5)
      II=I-1
      IF (E(I).EQ.-1.) GO TO 7
      IF (D1.EQ.1.) E(I) = 1.23946/E(I)
    3 CONTINUE
    7 RMAX = R(II)
      EMAX = E(II)
      E(1) =0.
      I2 =II-1
      DO 9  I=1,21
      READ (5,8) THI (I)
    8 FORMAT (E10.5)
      IF (THI(I) .EQ.-1.) GO TO 10
      THIMX = THI(I)
    9 CONTINUE
   10 DO 12 I=1,11
      READ (5,11) P(I)
   11 FORMAT (E10.5)
      IF (P(I) .EQ. -10000.) GO TO 13
      PMAX = P(I)
   12 CONTINUE
   13 I3 = 0
   14 I3 =I3 +1
      WRITE (6,15) P(I3)
   15 FORMAT (1H1, 5H P = , 1PE15.4///)
      WRITE (6,16)
   16 FORMAT (1H ,15H  WAVELENGTH   ,15H      ENERGY    ,
     115H  REFLECTIVITY ,15H      ALPHA      ,15H       N         ,
     215H       K        ,15H      THETA      //)
      LINES = 0
      DO 42 J=2,500
      DO 21 I=1,500
      IF(E(I) .EQ. E(J)) GO TO 17
      Y1(I) = (ALOG (R(I))-ALOG(R(J)))/(E(J)**2-E(I)**2)
      GO TO 19
   17 Y1(I) = .5*((ALOG(R(I-1))-ALOG(R(J)))/(E(J)**2-E(I-1)**2)
     1+(ALOG(R(I+1))-ALOG(R(J)))/(E(J)**2-E(I+1)**2))
      Z1=Y1(J)
   19 IF (I.EQ.II) GO TO 23
   21 CONTINUE
   23 DO 25 I=1,500
      Y1(I)=(Y1(I)+Y1(I+1))*(E(I+1)-E(I))*.5
      IF (I.EQ.I2) GO TO 27
```

```
   25 CONTINUE
   27 THA(J) = 0.
      Y1(J-1)=Z1*(E(J)  - E(J-1))
      Y1(J) = Z1*(E(J+1) - E(J))

      DO 29 I=1,500
      THA(J) = THA(J)+Y1(I)*E(J)/3.1416
      IF (I.EQ.12) GO TO 31
   29 CONTINUE
   31 Y=ABS(EMAX-E(J))
      THA(J) =THA(J)+(1./6.2832)*ALOG(R(J)/RMAX)
     1*ALOG((EMAX+E(J))/Y)
      Z=0.
   32 DO 33 I=1,50
      Z=Z+1.
      THA(J)=THA(J)+(P(I3)*((2.*Z-1.)**(-2))*(E(J)/EMAX)**(2*I-1))/
     13.1416
   33 CONTINUE
      CN(J)=(1.-P(J))/(1.+R(J)-2.*SQRT(R(J))*COS(THA(J)))
      OK(J)=(2.*SQRT(R(J))*SIN(THA(J)))/(1.+R(J)-2.*SQRT(R(J))*
     1COS(THA(J)))
      W(J) = 1.23946/E(J)
      ALF(J) = 4.*3.1416*OK(J)/W(J)
      LINES = LINES + 2
      WRITE(6,35) W(J), E(J), R(J), ALF(J), CN(J),
     1OK(J),THA(J)
   35 FORMAT(1H0,1P7E15.4)
      IF (LINES.LT.20)  GO TO 41
      WRITE (6,37)  P(I3)
   37 FORMAT(1H1,5H P = ,1PE15.4///)
      WRITE (6,39)
   39 FORMAT(1H ,15H  WAVELENGTH   ,15H      ENERGY     ,
     115H  REFLECTIVITY ,15H      ALPHA      ,15H         K        ,
     215H         K        ,15H      THETA      //)
      LINES=0
   41 IF (J.EQ.12) GO TO 43
   42 CONTINUE
   43 IF (P(I3).EQ.PMAX) GO TO 45
      GO TO 14
   45 RETURN
      END
```

ACKNOWLEDGEMENTS

I would like to thank the National Science Foundation, the Office of Naval Research, and the Advanced Research Projects Agency for giving me research assistantship aid while at Harvard.

I would like to thank Professor William Paul for his advice during the course of this research. He suggested the original topics and through numerous discussions made my research work an experience which has contributed greatly to my scientific education. He further spent considerable time and effort in reading and commenting on the written description of my research.

James Inglis and Albert Manring have aided in machining apparatus. David MacLeod, in discussions, has made numerous contributions to the sample preparation. He also aided in clearing up many of the final experimental details and in preparing the manuscript and drawings.

Many discussions with Dr. Paul Grant and Dr. Rudolph Ludeke contributed greatly to my education as well as to the research work.

Dr. Peter Melz and Mr. Fred Kahn were quite helpful in completing some of the final experimental measurements. Mr. Larry Ladd also aided in some of the final details necessary to complete a final report on the research.

I would like also to thank my wife, Kathy, for handling the details of the typing, aiding in data reduction, and aiding in the preparation of drawings.

DOCUMENT CONTROL DATA - R & D

Security classification of title, body of abstract and indexing annotation must be entered when the overall report is classified

1 ORIGINATING ACTIVITY (Corporate author)
Division of Engineering and Applied Physics
Harvard University
Cambridge, Massachusetts

2a. REPORT SECURITY CLASSIFICATION
Unclassified

2b. GROUP

3 REPORT TITLE

THE PREPARATION OF NiO THIN FILMS FOR USE IN OPTICAL MEASUREMENTS IN THE VISIBLE AND ULTRAVIOLET

4 DESCRIPTIVE NOTES (Type of report and, inclusive dates)
Interim technical report

5 AUTHOR(S) (First name, middle initial, last name)
Charles E. Rossi

6 REPORT DATE
October 1968

7a. TOTAL NO OF PAGES
164

7b. NO OF REFS
86

8a. CONTRACT OR GRANT NO
N00014-67-A-0298-0012 and ARPA SD-88

b. PROJECT NO

c.

d.

9a. ORIGINATOR'S REPORT NUMBER(S)
Technical Report No. HP-18
Technical Report No. ARPA-29

9b. OTHER REPORT NO(S) (Any other numbers that may be assigned this report)

10 DISTRIBUTION STATEMENT
Reproduction in whole or in part is permitted by the U. S. Government.
Distribution of this document is unlimited.

11 SUPPLEMENTARY NOTES

12 SPONSORING MILITARY ACTIVITY
Office of Naval Research

13 ABSTRACT

In this report, several methods for producing nickel oxide films for use in optical experiments are discussed including an indication of the significant problems encountered with each method. Electron reflection diffraction measurements indicate that films grown by electron beam evaporation of nickel in an oxygen atmosphere and by reactive sputtering on CaF_2 and LiF have at least some degree of crystalline order. Transmission spectra between 2000 angstroms and 6000 angstroms are presented for films grown by both electron beam evaporation and reactive sputtering. The spectra appear to be consistent with one another as well as with the spectra of epitaxial NiO films grown on MgO by vapor deposition. The spectra are, however, at least in some cases, distorted by color centers introduced in the substrate during film deposition. Two films have been used to provide information on the shift of the NiO absorption edge with temperature, the results being $-2.9.10^{-4}$ eV/°C and $-4.2.10^{-4}$ eV/°C respectively. A Kramers Kronig analysis of the reflectivity of bulk NiO has been made and shows that the absorption constant derived from the reflectivity data.

14 KEY WORDS	LINK A		LINK B		LINK C	
	ROLE	WT	ROLE	WT	ROLE	WT
NiO Thin Films						
Optical Measurements						
Electron Reflection Diffraction Measurements						
Electron Beam Evaporation						
Reactive Sputtering						